BOOK of ABSTRACTS

MIC Festival 2022
Success by imaging: How to lift my research to the next level

09.06.2022

Van Swieten Saal, Medical University of Vienna

Medical Imaging Cluster
mic@meduniwien.ac.at

MIC Festival 2022
Success by imaging: How to lift my research to the next level

The 4th MIC Festival "*Success by imaging: How to lift my research to the next level"* combines imaging expertise in technology and application and is targeting scientists from various disciplines. The event will be initiated by a keynote lecture followed by scientific presentations of the nodes. A "Multi-Cluster Round Table" discussion will bring together representatives from all MedUni Vienna clusters. A highlight lecture will present "How biomedical image informatics can support multi-modal imaging across scales" for driving research forward. Finally, all MIC nodes invite you to participate in the poster session, displaying the newest achievements in medical imaging research. The Festival will be an "in-person" event.

Program Highlights:

- Keynote lecture by Niki Popper (TU Vienna)
- "Multi-Cluster Round Table"
- Highlight lecture by Katja Bühler (VRVis)
- Thematic poster-tours and poster awards
- Rapid-Fire-Pitch and poster presentation

Timeline:

2 March | Registration Open
28 March | Opening Late-Breaking Abstract Submission
15 April | Deadline Late-Breaking Abstract Submission
13 May | Deadline Submission of e-posters and poster teaser slide
29 May | Registration Deadline
9 June | MIC Festival 2022

Scientific Committee

Wolfgang J. Weninger (Speaker), Pascal Baltzer, Marcus Hacker, Georg Langs, Rupert Lanzenberger, Cecile Philippe, Ursula Schmidt-Erfurth, Tatjana Traub-Weidinger

Organization Committee and Contact

Claudia Kuntner-Hannes, Wolfgang Birkfellner, Roxane Licandro, Ursula Schmidt-Erfurth, Wolfgang Wadsak, Ute Weber-Woisetschläger

mic@meduniwien.ac.at

ABSTRACT SUBJECT AREAS | MIC Festival 2022

- Telemedicine
- Development of Imaging Probes
- Preclinical Imaging
- Quantitative Clinical Imaging
- Microscopy, and Advanced Optical Imaging
- Image Computing, Analysis, and Visualisation
- Image Guided Therapy and Theranostics

SUBMISSIONS

We have received 63 submissions in the 7 subject areas. Each abstract was reviewed by 3 independent reviewers and scored according to the criteria: clarity of the question/methodology, presentation of results, and topicality/relevance.

Reviewers:

Theresa Balber
Hrvoje Bogunovic
Bianca Burger
Gregor Dovjak
Michael Figl
Joachim Friske
Marion Gröger
Andreas Hahn
Gilbert Hangel
Lena Hirtler
Claudia Kuntner-Hannes
Rupert Lanzenberger
Rainer A. Leitgeb
Roxane Licandro
Severin Mairinger
Irena Pashkunova-Martic
Matthias Perkonigg
Cecile Philippe
Ivo Rausch
Ernst Schwartz
Philipp Seeböck
Daniel Sobotka
Athena Taymourtash
Wolf-Dieter Vogl
Thomas Wanek

We want to thank the reviewers for their commitment!

SPONSORS

Gold Sponsor

SIEMENS Healthineers

Silver Sponsors

Dedalus

Elekta

Bronze Sponsors

ATOMED

BAYER

DSD PHARMA GmbH
Diagnostics.Solutions.Diversity.

HERMES MEDICAL SOLUTIONS

THQ MEDICAL PRODUCTS

PROGRAM

09:00 **Welcome:** M. Müller (Rector, MedUniVienna); W. Weninger (MIC)

09:10 **Keynote Lecture:** Chair: G. Langs
Success by science? N. Popper (TU Wien)

09:50 **Success by imaging technology:** Chairs: C. Philippe, M. Hacker

09:50 *Understanding molecular mechanisms for theranostic applications in nuclear medicine using imaging probes* (W. Wadsak, M. Mitterhauser)

10:10 *Unconventional optical microscopy modalities with medical diagnostic and prognostic potential* (K. Elsayad)

10:20 *AI and imaging - the glue that links modalities* (G. Langs, W. Birkfellner)

10:30 **Promotional film MIC**

10:40 **Coffee Break** (exhibition)

11:00 **Multi-Cluster-Roundtable:** Moderation: H. Redl
„Together makes us stronger!“

R. Valenta (Immunology), J. Widder (Cancer Research and Oncology), D. Pollak (Medical Neuroscience), I. Lang (Cardiovascular Medicine), W. Weninger (Medical Imaging)

12:00 **Lunch and Postersession**

12:00 **Posterwalk 1**: Chairs: W. Wadsak, M. Mitterhauser
Development of Imaging Probes & Preclinical Imaging
Posterwalk 2: Chairs: W. Birkfellner, T. Helbich
Image Computing, Analysis and Visualisation

12:30 **Posterwalk 3**: Chairs: R. Leitgeb, G. Heilemann
Image Guided Therapy and Theranostics & Microscopy and Advanced Optical Imaging
Posterwalk 4: Chairs: T. Beyer, R. Kain
Quantitative Clinical Imaging & Telemedicine

13:00 **Success by imaging application:** Chairs: P. Baltzer, R. Lanzenberger

13:00 *Deuterium Metabolic Imaging - the new frontier in Molecular Imaging* (W. Bogner)

13:10 *Telemedicine in the retina: A pioneering role* (G. Reiter)

13:20 *Theranostics - Quo vadis?* (A. Haug)

13:30 *Hybrid OCT and Photoacoustic capsule endoscopy for oesophageal imaging* (Q. Li)

13:35 *Deep learning-based monitoring of geographic atrophy on OCT in the FILLY phase II clinical trial* (J. Mai)

13:40 *Eye motion surveillance system for noninvasive ocular particle therapy* (M. Regodic)

13:45 *PET Study on the characterization of an APP/Tau rat model of Alzheimer's disease* (S. Mairinger)

13:50 *Implementing Virtual Microscopy for Academic Education in Pathology at the Medical University of Vienna* (M.C. Koeller)

14:00 **Coffee Break** (exhibition)

14:20 **Highlight Lecture:** Chair: C. Kuntner-Hannes
“How biomedical image informatics can support multi-modal imaging across scales” (K. Bühler, VRVis)

14:50 **Promotional film MIC**

15:00 **Farewell and Poster award:** M. Fritz (Vice Rector, MedUniVienna), W. Weninger

CONTENT

Rapid Fire Pitch

RFP1 Hybrid OCT and Photoacoustic capsule endoscopy for esophageal imaging

Qian Li[1], Zakiullah Ali[2], Christian Zakian[2], Jerome Gloriod[3], V Ntziachristos[2], Wolfgang Drexler[1]

[1] Center for Medical Physics and Biomedical Engineering, Medical University of Vienna, Vienna, Austria
[2] Institute of Biological and Medical Imaging, Helmholtz Zentrum München, Neuherberg, Germany
[3] Statice, Besançon, France

Disclosure statement: Nothing to disclose

Keywords: Multimodal imaging, endoscopic capsule, oesophageal imaging.

Objective
Oesophageal cancer remains the sixth deadliest form of cancer. Presently the white light endoscopy (WLE) is employed to survey the oesophagus for dysplasia. However, WLE provides only a poor contrast of the tissue surface without insights of the structure and the microvasculature within the lumen wall.
To overcome the limitations of WLE, a novel multimodal oesophageal endoscopic capsule combining optical coherence imaging (OCT) and photoacoustic imaging (PAI) is designed and evaluated. The OCT part is designed to provide an 'optical biopsy' on the oesophagus. PAI provides vascular information from the surface to deeper tissue.

Methods and Materials
A distal scanning endoscopic probe is designed for 360° side-view imaging of the oesophageal lumen surface. OCT and PAI excitation light paths are intrinsically integrated into the capsule through a double clad fiber coupler. A double-clad-fiber-based GRIN lens then delivers the multimodal excitation light on the tissue. A motor rotates within the capsule to realize the 360° imaging.

Results
Phantom imaging demonstrates that the two modalities are intrinsically co-registered and provide complementary information. *Ex vivo* pig oesophagus imaging demonstrates that the capsule is suited for imaging oesophagus. *In vivo* human oral cavity imaging shows both the structural information of the mouth mucosa and the vascular network within the mucosa. An *ex vivo* study on resected samples from patients further show the clinical potential of the multimodal probe.

Conclusion
A novel multimodal oesophageal endoscopic capsule is and the multimodal imaging results show its complementary power and indicate its clinical potential for detecting oesophageal dysplasia.

Funding Sources:
This study receives funding from the European Union's Horizon 2020 research and innovation programme under grant agreement No 732720 (ESOTRAC).

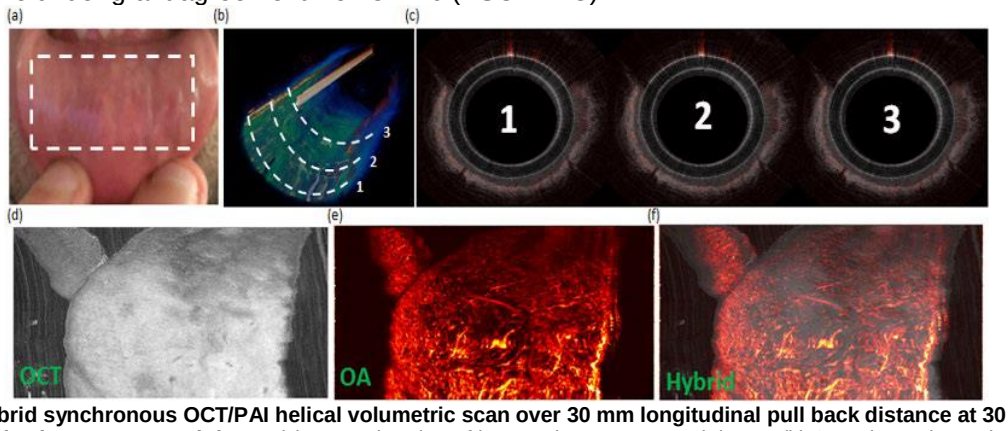

Figure: Hybrid synchronous OCT/PAI helical volumetric scan over 30 mm longitudinal pull back distance at 30 Hz frame rate of *in vivo* human mucosal tissue (a) Imaged region of interest human mucosal tissue. (b) 3D volumetric render of hybrid OCT-PAI data (c) OCT-PAI B-scans acquired at arbitrary locations during the pull-back scan. (d-f) Maximum intensity projection images of OCT, PAI and hybrid respectively.

RFP2 Deep learning-based monitoring of geographic atrophy on OCT in the FILLY phase II clinical trial

Julia Mai[1]; Dmitrii Lachinov[1]; Sophie Riedl[1]; Gregor S. Reiter[1]; Wolf-Dieter Vogl[1]; Hrvoje Bogunovic[1]; Ursula Schmidt-Erfurth[1]

[1] Department of Ophthalmology and Optometry, Medical University of Vienna, Vienna, Austria

Disclosure statement: USE: Genentech, Heidelberg Engineering, Kodiak, Novartis, Roche, RetInSight: Consultancy ; Apellis: Grant; HB: Heidelberg Engineering, Apellis: Grant

Keywords: deep learning, OCT, geographic atrophy.

Objective
To develop an automated deep learning (DL) based image segmentation algorithm to delineate and measure geographic atrophy (GA) lesions on OCT scans and to monitor GA progression under complement inhibitory treatment.

Methods and Materials
A DL-based image segmentation method using a 3D-to-2D convolutional neural network (CNN) (1) was trained to automatically segment a topographic 2D GA area on a 3D-OCT volume. The algorithm was validated internally on the GA cohort from the Vienna Study Center (VSC) and externally on a subset of patients from the FILLY phase II clinical trial (2). To evaluate the ability of DL-based GA monitoring, the GA growth rate after 1 year from patients in the FILLY trial was calculated and compared between the treatment groups.

Results
In the internal test set 967 OCT volumes from 100 patients from the VSC and in the external test set 226 OCT volumes from 113 patients from the FILLY trial were included. For internal validation, mean DSC was 0.849 ± 0.116. For external validation, mean DSC was 0.897 ± 0.057. Mean DSC for the GA growth area after one year was 0.457 ± 0.165. The DL-based segmentation revealed a significant difference in growth rates after one year between the monthly treated and sham group ($p = 0.014$).

Conclusion
We propose a fully automated image segmentation algorithm to delineate and measure GA lesions on OCT with high accuracy. The results represent an important step towards AI-based monitoring of GA progression and therapeutic response on OCT.

Funding Sources:
The FILLY Phase 2 study was conducted by Apellis Pharmaceuticals and our work was in part supported by an Apellis research grant. The funding organizations had no role in the design and conduct of this research.

References:
1. Lachinov D, Seeböck P, Mai J, Schmidt-Erfurth U, Bogunović H. Projective Skip-Connections for Segmentation Along a Subset of Dimensions in Retinal OCT2021.
2. Liao DS, Grossi FV, El Mehdi D, Gerber MR, Brown DM, Heier JS, et al. Complement C3 Inhibitor Pegcetacoplan for Geographic Atrophy Secondary to Age-Related Macular Degeneration: A Randomized Phase 2 Trial. Ophthalmology. 2020;127(2):186-95.

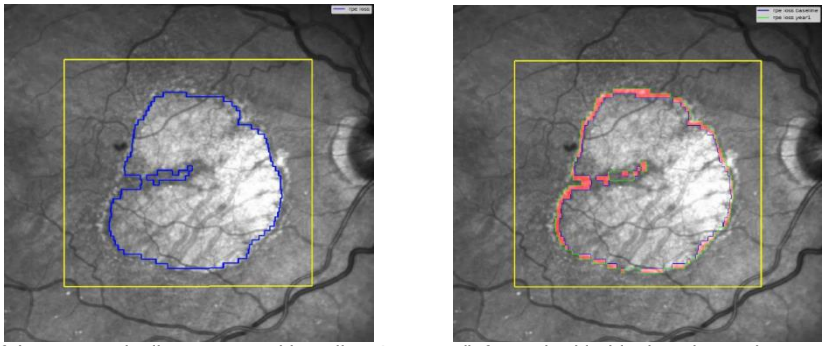

Figure 1: Example of the automatically segmented baseline GA area (left, marked in blue) and growth area after one year (right, marked in red)

RFP3 Eye motion surveillance system for noninvasive ocular particle therapy

Milovan Regodic[1], Andreas Resch[1], Patrick Roisl[2], Markus Stock[2], Dietmar Georg[1]

[1] Department of Radiation Oncology, Medical University of Vienna/AKH, Vienna, Austria
[2] Division of Medical Physics, EBG MedAustron GmbH, Wiener Neustadt, Austria

Disclosure statement: None

Keywords: eye tracking, ocular proton therapy, patient positioning.

Objective

Although relatively rare, uveal melanoma (UM) is the most common primary intraocular tumor in adults. Ocular proton therapy has been widely accepted as a first-line treatment for UM patients, offering preservation of the eyeball and frequently also visual functions. However, in current practice, it requires radio-opaque tantalum clips which are surgically placed onto the sclera of the diseased eye and act as fiducials to verify that the patient's eye position prior to irradiation is the same as the one defined in the treatment plan. The clips are highly invasive and represent treatment-related burdens of ocular proton therapy impairing the patient's quality of life. Here, we propose a non-invasive eye-tracking system (ETS) for fixation and monitoring of the patient's gaze direction during beam delivery as well as to assist during patient positioning.

Methods and Materials

The ETS is attached to the head fixation used in particle therapy. Eye immobilization is achieved by having patients hold their gaze at a fixed light stimulus. A graphical user interface assists during both patient positioning and irradiation (see Figure 1). The pupil center is automatically detected, and in combination with eyeball dimension, serves to calculate angular eye deviations from a reference position. If deviation criteria is exceeded, a gating trigger is sent to the accelerator to interrupt the treatment. First evaluations measure the detection accuracy of the pupil centre in recorded images for eight eye rotations.

Results

The submillimetric mean ± standard deviation accuracy of the pupil detection is 0.58±0.25 mm and 0.38 ± 0.1 mm for horizontal and vertical direction respectively.

Conclusion

Our current system – based on a proven and successful clinical experience in stereotactic photon therapy [1] – was improved and adapted for proton therapy at MedAustron Ion Therapy Center. A working prototype is already at a final development and evaluation stage and follows certain quality standards to ensure compliance with medico-legal requirements.

Funding Sources:

This work was funded by the Austrian Research Promotion Agency (FFG) within the project IMPACTOR.

References:

[1] K. Dieckmann, D. Georg, J. Bogner, M. Zehetmayer, et al. Optimizing Linac-based stereotactic radiotherapy of uveal melanomas: 7 years' clinical experience Int J Rad Oncol Biol Phys (2006), pp. S47-S52.

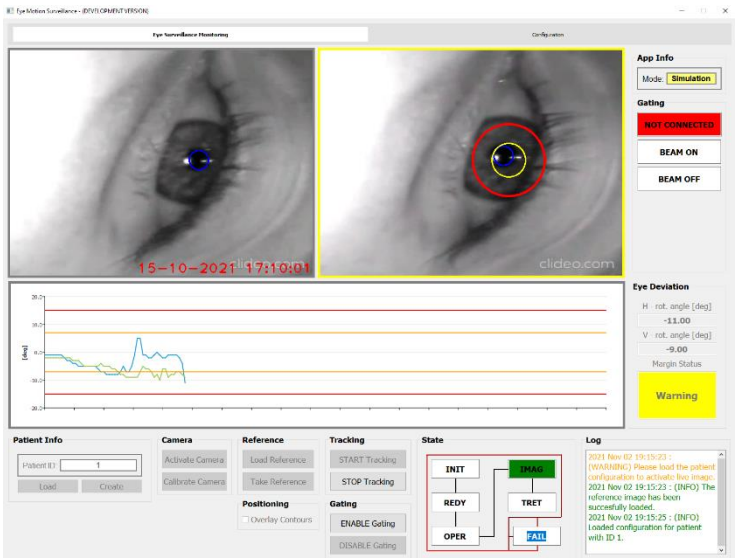

Figure 1: A development version of the eye tracking system.

RFP4 PET Study on the characterization of an APP/Tau rat model of Alzheimer's disease

Severin Mairinger[1, 2], Thomas Filip[1, 3], Jörg Neddens[4], Michael Sauberer[1, 5], Stefanie Flunkert[4], Johann Stanek[1, 5], Thomas Wanek[1, 5], Nobuyuki Okamura[6], Oliver Langer[1, 2, 5], Birgit Hutter-Paier[4], Claudia Kuntner[1, 5]

[1] AIT Austrian Institute of Technology GmbH, Preclinical Molecular Imaging, Seibersdorf, Austria
[2] Medical University of Vienna, Department of Clinical Pharmacology, Vienna, Austria
[3] Medical University of Vienna, Department of Biomedical Research, Vienna, Austria
[4] QPS Austria GmbH, Neuropharmacology, Grambach, Austria
[5] Medical University of Vienna, Department of Biomedical Imaging und Image-guided Therapy, Vienna, Austria
[6] Tohoku Medical and Pharmaceutical University, Division of Pharmacology, Faculty of Medicine, Sendai, Japan

Disclosure statement: Authors JN, SF and BHP are employees of QPS Austria, Austria

Keywords: Alzheimer's disease, rat model, [^{18}F]THK-5317

Objective
To better understand the complex pathomechanisms of Alzheimer's disease, we studied a new transgenic rat animal model generated by crossing of amyloid precursor protein (APP) rats with tau rats using positron emission tomography (PET) scans and immunohistochemical analyses at different ages.

Methods and Materials
APP/Tau rats, generated by crossbreeding male McGill-R-Thy1-APP rats with female hTau-40/P301L rats, aged between 7-21 months were subjected to dynamic [^{11}C]PiB and [^{18}F]THK-5317 scans. For regional brain analysis, anatomical MR images were co-registered with the PET images and additional immunofluorescent labeling (tau, amyloid) was performed. For [^{11}C]PiB data the simplified reference tissue model was used, whereas [^{18}F]THK-5317 data were analysed using a 2-tissue compartment model and Logan graphical analysis.

Results
In APP/Tau rats a positive correlation in the age-dependent increase of cortical and hippocampal amyloid stains and [^{11}C]PIB BPND was observed, whereas tau staining only yielded a trend towards higher levels. [^{18}F]THK-5317 *VT*s in APP/Tau rats showed a significant increase in the striatum and brainstem in 21-month compared to 7-month old animals, whereas significantly higher *VT*s in hippocampus, thalamus and hypothalamus were only found in female animals.
No correlation was found between tau immunofluorescence labeling results and the respective *VT* values.

Conclusion
PET imaging showed an age-related increase in [^{11}C]PiB and [^{18}F]THK-5317 binding in several brain regions in the APP/Tau group. Although a positive correlation was observed for amyloid, rather low human tau and amyloid fibril expression levels were observed, as well as unstable brain pathology questioning the future use of this model.

Funding Sources:
The research leading to these results was funded by the Austrian Research Promotion Agency (FFG) [grant number 853256] awarded to Claudia Kuntner.

RFP5 Implementing Virtual Microscopy for Academic Education in Pathology at the Medical University of Vienna

Koeller Maximilian C.[1], Jentus Maaia-Margo[1], Kaltenecker Christopher[1], Gletthofer Maximilian[1], Kain Renate[1]

[1] Department of Pathology, Medical University of Vienna, Austria

Disclosure statement: The authors declare no conflicts of interest.

Keywords: Medical Education, Virtual Microscopy, Telepathology

Objective
The current COVID 19 epidemic has emphasised the need for digital educational solutions. Digital Pathology is ideally suited to translate conventional state of the art teaching into the digital space[1]. Consequently, the Department of Pathology currently establishes a digital environment that allows a seamless integration into the current curriculum while at the same time providing tools capable of enhancing the learning process of individual students.

Methods and Materials
The requirements of a virtual environment for students, teachers and from an institutional point of view were investigated using literature researches and personal interviews. Based on the findings available solutions were evaluated. Next, a prototype of the most promising software solution was set up and its performance tested in use case scenarios. Subsequently, the technical requirements were adjusted to meet real life conditions in terms of storage size, user number and server speed. Currently, the institutional identity management solution (Shibboleth) and learning management system (Moodle) are integrated and new learning tools are developed.

Results
Mandatory requirements established by students (on demand remote access, interactivity, embedded cross referenced annotations and descriptions), teachers (ease of use, autonomous extension of case collections) and for institutional use (ease of maintenance, long term availability, open source, resource integration, scalability) was met by Cytomine[2] which was consequently chosen.

Conclusion
The implemented solution is designed as a digital platform for interactive learning that will enable (self) evaluation of students' learning progress and the development of didactical methods to increase the recall of pattern recognition and morphological understanding by Machine Learning and Artificial Intelligence Systems.

Funding Sources:
The project is funded by the Austrian Federal Ministry of Education, Science and Research via the - Hochschulraumstrukturmittel Projekt 'Digitale Mikroskopie in der Lehre 2.0'.

References:
1. Hamilton PW, Wang Y, McCullough SJ. Virtual microscopy and digital pathology in training and education. APMIS 2012; 120: 305–15. DOI: 10.1111/j.1600-0463.2011.02869.x
2. Raphaël Marée et al., Collaborative analysis of multi-gigapixel imaging data using Cytomine, *Bioinformatics*, Volume 32, Issue 9, 1 May 2016, Pages 1395–1401, DOI: 10.1093/bioinformatics/btw013

Poster Presentations

P1 Novel neurotropic contrast agents for visualization of peripheral nerves by magnetic resonance imaging (MRI)

Irena Pashkunova-Martic[1,6], Krisztina Manzano-Szalai[2], Joachim Friske[1], Oskar Aszmann[2], Sarah Theiner[3,6], Matthias H. M. Klose[3], Dieter Baurecht[4], Siegfried Trattnig[5], Bernhard K. Keppler[6], Thomas H. Helbich[1]

[1] Department of Biomedical Imaging and Image-guided Therapy, Division of Molecular and Structural Preclinical Imaging, Medical University of Vienna & General Hospital of Vienna, Austria
[2] Department of Surgery, Division of Plastic & Reconstructive Surgery, Medical University of Vienna, Austria
[3] Institute of Analytical Chemistry, Faculty of Chemistry, University of Vienna, Austria
[4] Department of Physical Chemistry, University of Vienna, Austria
[5] Department of Biomedical Imaging and Image-guided Therapy, High Field MR Center, Austria
[6] Institute of Inorganic Chemistry, Faculty of Chemistry, University of Vienna, Austria

Disclosure statement: The authors declare no conflicts of interest.

Keywords: neurotropic contrast medium, modified amino-dextran, magnetic resonance imaging

Objective
Amino-dextrans (AD) conjugated with gadolinium (Gd^{3+}) were developed as neuro-specific contrast agents (CA) for the visualization of the sciatic nerve in rats by magnetic resonance imaging (MRI).

Methods and Materials
AD with 3, 10, and 70 kDa molecular weights were assessed as carrier molecules known to be transported with various speed by axonal microtubules. Detailed physico-chemical characterizations were carried out. For MRI, the paramagnetic Gd^{3+} ion was coupled as a T1 signal enhancer. The well-established linear chelator, diethylenetriaminepentaacetic acid (DTPA), was used and subsequently replaced by the more stable cyclic chelator 1,4,7,10-Tetraazacyclododecane-1,4,7,10-tetraacetic acid (DOTA). In addition, a fluorescently labeled AD-DTPA-Gd was prepared to demonstrate an active transport to the spinal cord by histochemistry. After successful synthesis and characterization, molecular migration of the AD-DTPA-Gd in the *sciatic nerve* of healthy Sprague Dawley rats was monitored by MRI for up to seven days.

Results
Successful synthesis and characterization of three AD, coupled to either DTPA-bisnahydride or to DOTA-NHS ester and finally complexated with paramagnetic Gd^{3+} was carried out. The *ex vivo* and *in vitro* measurements verified contrast uptake and highlighted the rat's sciatic nerve on MRI. This is the first assessment of active uptake and transport of AD-based, nerve-specific contrast agents visualized with MRI and quantified by inductively coupled plasma-mass spectrometry (ICP-MS).

Conclusion
Modified AD-Gd compounds may serve as nerve-specific imaging probes in a completely novel setting for intra-axonal transport. The reported work is the first step toward the development of an agent for MR neurography analogous to MR angiography.

Funding Sources:
This work was generously supported by the University of Vienna (Institute of Inorganic Chemistry) in cooperation with the Medical University of Vienna (Department of Surgery, Division of Plastic & Reconstructive Surgery and the Department of Biomedical Imaging and Image-guided Therapy, Division of Molecular and Structural Preclinical Imaging).

References:
[1] Wessig C, Bendszus M, Stoll G. In vivo visualization of focal demyelination in peripheral nerves by gadofluorine M-enhanced magnetic resonance imaging. Exp Neurol. 2007 Mar;204(1):14-9. doi: 10.1016/j.expneurol.2006.09.022. Epub 2006 Nov 16. PMID: 17112515.
[2] Wessig C, Jestaedt L, Sereda MW, Bendszus M, Stoll G. Gadofluorine M-enhanced magnetic resonance nerve imaging: comparison between acute inflammatory and chronic degenerative demyelination in rats. Exp Neurol. 2008 Mar;210(1):137-43. doi: 10.1016/j.expneurol.2007.10.014. Epub 2007 Nov 4. PMID: 18061168.

P2 Development of small molecule PET-tracers targeting PD-L1

Karsten Bamminger[1,2], Verena Pichler[3], Chrysoula Vraka[1], Lukas Kenner[4,5], Markus Mitterhauser[1,6], Marcus Hacker[1], Wolfgang Wadsak[1,2]

[1] Department of Biomedical Imaging and Image-guided Therapy, Division of Nuclear Medicine, Medical University of Vienna, Vienna, Austria
[2] CBmed GmbH - Center for Biomarker Research in Medicine, Graz, Austria
[3] Department of Pharmaceutical Sciences, Division of Pharmaceutical Chemistry, University of Vienna, Vienna, Austria
[4] Institute of Clinical Pathology, Medical University of Vienna, Vienna, Austria
[5] Ludwig Boltzmann Institute Cancer Research, Vienna, Austria
[6] Ludwig Boltzmann Institute Applied Diagnostics, Vienna, Austria

Disclosure statement: The authors declare that they have no known competing financial interests or personal relationships that could have appeared to influence the work.

Keywords: PD-L1, cancer, positron emission tomography

Objective

Immune evasion is a hallmark of cancer progression[1]. The inhibitory PD-1/PD-L1 immune checkpoint has emerged as a promising new target for anti-cancer immunotherapy. Quantification of tumor PD-L1 expression by immunohistochemistry as a theragnostic biomarker is confronted with intrinsic problems of invasive sampling and heterogeneous PD-L1 expression[2]. Positron emission tomography (PET) with PD-L1 selective tracers could improve *in vivo* quantification of PD-L1, patient stratification and therapy response. This work aims to develop small molecule PET-tracers targeting PD-L1.

Methods and Materials

PD-L1 ligands were synthesized by (i) a ligand-based drug design approach using lead structures of known binding affinity and (ii) *de novo* multi-step synthesis using advantageous substructures. Their chemical structures were fully characterized by ESI-MS, $^{1}H/^{13}C/^{19}F$-NMR and RP-HPLC. Lead structures and ligands physico-chemical parameters were evaluated regarding binding affinity using an HTRF assay, in-solution stability, lipophilicity (log*P*) and cytotoxicity. Two ligands were radiolabelled with carbon-11.

Results

A plethora of new molecules and intermediates were synthesized in high purity. Binding affinities (IC50) for methylated molecules ranged from (i) 430 – 5800 nM and (ii) 6 – 10 nM. Fluoroethylated compounds yielded IC50s of (i) 1200 nM and (ii) 1300 nM. The results of stability, lipophilicity and cell toxicity are comparable to clinically well-established tracers. Radiolabelling showed yields of up to 54% as determined by radio-HPLC.

Conclusion

Novel *de novo* synthesized molecules were superior in terms of binding affinities. Synthesis of further (optimized) ligands, their radiolabelling and applicability as potential PET-tracers are subject to ongoing research.

Funding Sources:

This project is supported by the Austrian Federal Government within the framework of the COMET K1 Centre Programme of the province of Styria and the province of Vienna.

References:

1. Hanahan D, Weinberg RA. Hallmarks of cancer: The next generation. *Cell*, 144(5):646-674, 2011. doi:10.1016/j.cell.2011.02.013.
2. Ilie M, Long-Mira E, Bence C, Butori C, Lassalle S, Bouhlel L, Fazzalari L, Zahaf K, Lalvée S, Washetine K, Mouroux J, Vénissac N, Poudenx M, Otto J, Sabourin JC, Marquette CH, Hofman V, Hofman P. Comparative study of the PD-L1 status between surgically resected specimens and matched biopsies of NSCLC patients reveal major discordances: a potential issue for anti-PD-L1 therapeutic strategies. *Ann. Oncol.*, 27(1):147-153, 2016.

P3 Design, synthesis, and biological evaluation of 4,4'- difluorobenzhydrol carbamates as potential ligands for muscarinic acetylcholine receptors.

Jonas Kilian [1], Marius Ozenil [1], Marlon Millard [2], Mariella Mogeritsch [2], Verena Maisetschläger [2], Wolfgang Holzer [2], Helmut Spreitzer [2], Thierry Langer [2], Wolfgang Wadsak [1,3], Marcus Hacker [1], Verena Pichler [2]

[1] Department of Biomedical Imaging and Image-guided Therapy, Division of Nuclear Medicine, Medical University of Vienna, Austria
[2] Division of Pharmaceutical Chemistry, Faculty of Life Sciences, University of Vienna, Austria
[3] CBmed GmbH - Center for Biomarker Research in Medicine, Graz, Austria

Disclosure statement: The authors declare no conflicts of interest.

Keywords: muscarinic acetylcholine receptors, molecular docking

Objective
Muscarinic acetylcholine receptors have been found to regulate many physiological processes and are involved in pathologies like Alzheimer's disease. Despite ongoing research efforts, clinicians' portfolios are characterized by a lack of truly subtype-selective mAChR ligands. Our group recently reported the discovery of highly M1 selective benzhydrol esters of arecaidine with Ki values in the single-digit nanomolar range.[1] However, nonspecific binding limits the usability of these ligands for molecular imaging purposes. Thus, we envisioned a structural modification of the 1,2,3,6-tetrahydropyridine moiety, which will be accompanied by replacement of the ester-linkage with a carbamate motif.

Methods and Materials
A set of commercially available diamines was computationally linked with 4,4'-difluorobenzhydrol via a carbamate bridge. These molecules were docked into the binding site of M1 (5CXV) using Vina.[2] A post-docking filtering work-flow resulted in readily accessible compounds for further experimental evaluation.

Results
A structurally diverse set of 13 carbamates was synthesized in moderate yields of up to 38% using CDI as coupling agent. The carbamates' HPLC-log$P_{ow}^{pH7.4}$ values were found to be in a narrow range of 2.2- 3.33, supporting the assumption of lower non-specific binding and BBB permeability. All substances act as antagonists toward CHO-M1 cells, exhibiting Ki-values in the low µM to nM range.

Conclusion
We present the design, synthesis, and preliminary biological evaluation of thirteen 4,4'-difluorobenzhydrol carbamates available for both, radiofluorination or -methylation. The compounds show promising binding features for the potential application as antagonistic imaging agents. Ongoing evaluation of their binding affinities towards all mAChR subtypes will reveal their subtype-selectivity.

References:
[1] M. Ozenil, K. Pacher, T. Balber, C. Vraka, A. Roller, W. Holzer, H. Spreitzer, M. Mitterhauser, W. Wadsak, M. Hacker, V. Pichler, Eur. J. Med. Chem. 2020, 204, 112623
[2] O. Trott, A.J. Olson, J. Comput. Chem. 2010, 31, 455-461

P4 Super-resolution MultiVane Technique for 3D-Visualization of Large Vessel Anomalies in fetal MRI

Florian Prayer [1], Ernst Schwartz[1], Gregor Kasprian[1]

[1] Department of Biomedical Imaging and Image-guided Therapy, Medical University of Vienna, Austria

Objective
To investigate the feasibility of super-resolution-based three-dimensional reconstruction of the heart and large vessels using MultiVane technique in fetal MRI.

Methods and Materials
Thirty fetuses consisting of 15 cases with anomalies of the large vessels, and 15 normal cases were included. The pathology group included: tetralogy of Fallot (n=4), aortic coarctation (3), right descending aorta (2), common arterial trunk (2), persistent left superior vena cava (1), unilateral pulmonary agenesis (1), hypoplastic left heart (1), and heterotaxy syndrome (1). Fetal MRI scans performed at a mean gestational age of 28+1 gestation weeks (GW) (pathology group) and 29+5 GW (normal group) were obtained using one 1.5T scanner. T2-weighted sequences in three orthogonal planes acquired using MultiVane technique were used to calculate super-resolution datasets. Manual segmentation was performed to obtain three-dimensional models. Imageswere reviewed in three orthogonal planes, axial super-resolution images, and three-dimensional models for anomalies of the large vessels.

Results
Super-resolution post-processing based on T2-weighted MultiVane sequences and three-dimensional reconstruction of the fetal heart and large vessels were feasible in all (30 of 30) cases. Review of T2-weighted MultiVane sequences in three orthogonal planes identified large vessel anomalies in 13 of 15 cases. If super-resolution images and three-dimensional models were available, all (15 of 15) pathologic cases were correctly classified. Vessel anomalies were found in none of the fetuses in the normal group.

Conclusion
Novel MultiVane fetal MRI technique in combination with super-resolution post- processing yields morphologic characterisation of fetal large vessels.

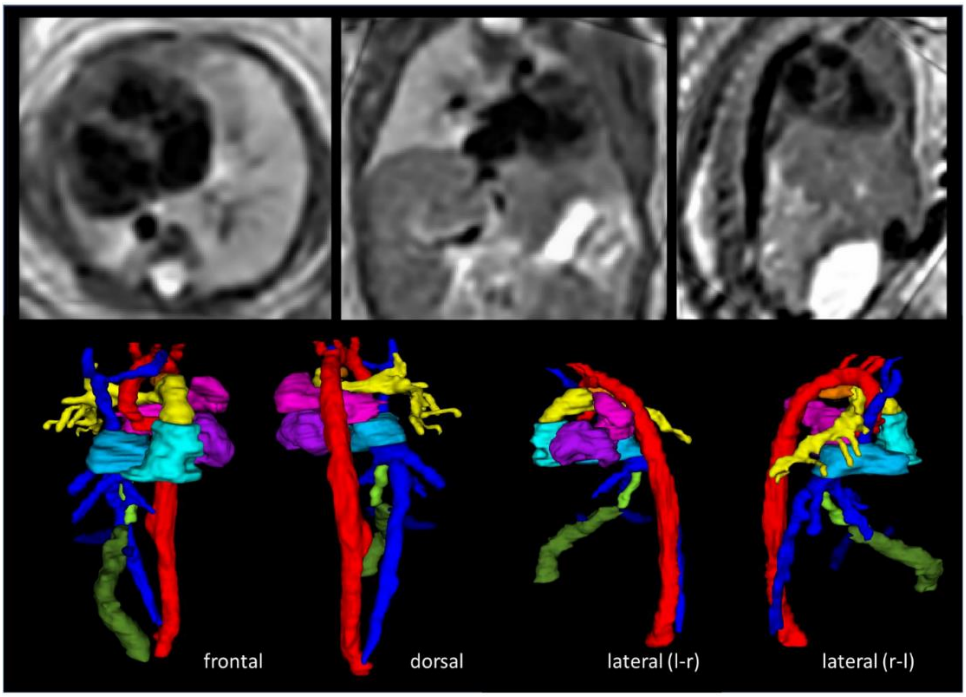

P5 4D iterative reconstruction of brain fMRI in the moving fetus

Athena Taymourtash, Hamza Kebiri, Sebastien Tourbier, Ernst Schwartz, Karl-Heinz Nenning, Roxane Licandro, Daniel Sobotka, Helene Lajous, Priscille de Dumast, Gregor Kasprian, Daniela Prayer, Meritxell Bach Cuadra, and Georg Langs*

Computational Imaging Research Lab, Department of Biomedical Imaging and Image-guided Therapy, Medical University of Vienna, Vienna, Austria.
Department of Radiology, Lausanne University Hospital (CHUV) and University of Lausanne (UNIL), Lausanne, Switzerland.

Objective
Resting-state functional Magnetic Resonance Imaging (fMRI) is a powerful imaging technique for studying functional development of the brain *in utero*. However, unpredictable and excessive fetal movements have limited its clinical application. Previous studies have focused on the accurate estimation of the motion parameters and used a 3D single step interpolation to separately reconstruct each 3D volume of the fMRI data from motion scattered slices. Here we propose a new method that, rather than treating each volume independently, takes both spatial- and the temporal domain into account and iteratively reconstruct 4D fetal fMRI time series through inverse problem framework.

Methods and Materials
Our algorithm involves iterative backprojection of the motion scattered slices onto a regular 4D grid using a 4D Gaussian point spread function, estimating the slice intensities given the current estimate of the 4D image using the slice acquisition model, and computing the residual error between these two. This error is backprojected and added to the regularization term which is computed using a first order Tikhonov function. Optimization terminates when the residual error between estimated and measured data converges. We quantitatively evaluated the proposed algorithm on clinical fetal fMRI scans of 14 subjects between 22 and 39 weeks of gestation using the sharpness of the resulting image and the standard deviation of BOLD signal fluctuations at each voxel over time.

Results
In 12 out of 14 subjects the proposed method yields higher sharpness than 3D interpolation, with an overall average sharpness 26% higher than 3D interpolation, in 11 it exhibits lower standard deviation, with an average standard deviation reduction of 41% compared to 3D interpolation. For several subjects with lower gestational age the highest sharpness and lowest standard deviation occured with un-corrected images. One possible cause is that the advanced gyrification at later gestational ages results in a pronounced sharpness advantage with correction, while for younger fetuses this is not the case and might reflect image noise rather than anatomical structure.

Conclusion
A robust reconstruction technique is extremely beneficial in case of large motions and missing data, and the results confirm the successful application of our new technique for the reconstruction of the fetal fMRI on clinically acquired data.

Funding Sources: This work has received funding from the European Union's Horizon 2020 research and innovation programme under the Marie Sk lodowska-Curie grant agreement No 765148, Swiss National Science Foundation (project 205321-182602), and partial funding from the Austrian Science Fund (FWF, P35189).

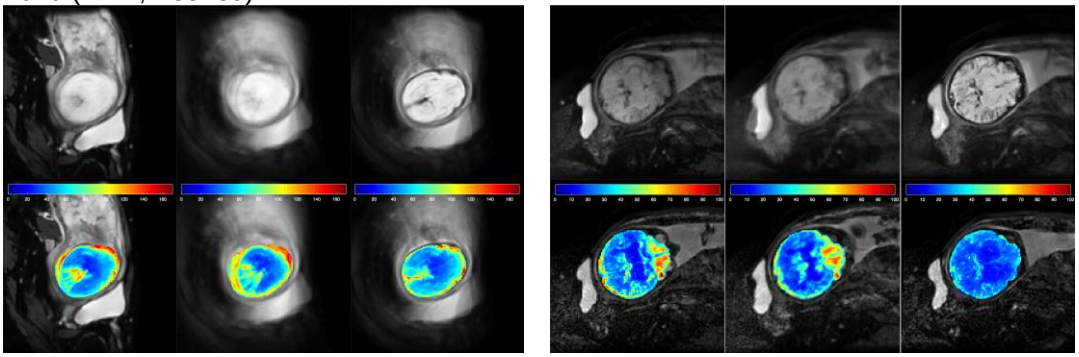

Figure 1: Examples in the average volume (top rows) and voxelwise standard deviation of the signal (bottom rows) for two fetal subjects of **S14** and **S8** whit strong rotational parameters. The columns correspond to the original data, single step 3D linear interpolation, and the proposed 4D iterative reconstruction.

P6 Retinal layer segmentation in OCT with a curvature prior and uncertainty estimation using deep learning

Botond Fazekas[1,2], Dmitrii Lachinov[1,2], Guilherme Aresta[1,2], Sophie Riedl[2], Julia Mai[1,2], Ursula Schmidt-Erfurth[2], Hrvoje Bogunovic[1,2]

[1] Christian Doppler Laboratory for Artificial Intelligence in Retina, Department of Ophthalmology and Optometry, Medical University of Vienna
[2] Laboratory for Ophthalmic Image Analysis, Department of Ophthalmology and Optometry, Medical University of Vienna

Disclosure statement: The authors declare no conflicts of interest.

Keywords: Deep Learning, Image segmentation, Retina.

Objective
Age-related Macular Degeneration (AMD) is a serious retinal condition, which is characterized by the presence of fluid or fibrous tissues between the retinal pigment epithelium (RPE) and the Bruch's membrane (BM) layers. Segmenting these two layers is important for monitoring AMD progression. In this work we propose a new deep learning method for a robust and trustworthy layer segmentation of BM in optical coherence tomography (OCT).

Methods and Materials
The backbone fully convolutional neural network is trained to produce a probability map corresponding to the likely position of BM for each OCT A-scan. The network takes prior anatomical considerations into account regarding the low curvature of the layer. As part of the prediction, the position uncertainty is quantified and the sections of BM considered uncertain are subsequently interpolated using Thin Plate Splines.

Results
Our work was evaluated on all three stages of AMD and on images from different device vendors. Results showed an 8% and 20% improvement in MAE and RMSE, respectively, compared to the baseline [1], while reducing the number of outliers. Additionally, on an external public dataset of images acquired with a different device vendor, it improved by 5% over the state-of-the-art [1]. The proposed position uncertainty measurement was found positively correlated with the error rate.

Conclusion
Incorporating anatomical priors in the training process are shown to improve the segmentation accuracy of BM, especially in difficult samples. The proposed uncertainty measurement proved to be a viable method for detecting and correcting wrong segmentations.

Funding Sources:
The financial support by the Austrian Federal Ministry for Digital and Economic Affairs, the National Foundation for Research, Technology and Development and the Christian Doppler Research Association is gratefully acknowledged.

References:
[1] J. A. Sousa, A. Paiva, A. Silva, J. D. Almeida, G. B. Junior, J. O. Diniz, W. K. Figueredo, and M. Gattass, ''Automatic segmentation of retinal layers in OCT images with intermediate age-related macular degeneration using U-Net and DexiNed,'' PLOS ONE, vol. 16, no. 5, p. e0251591, May 2021.

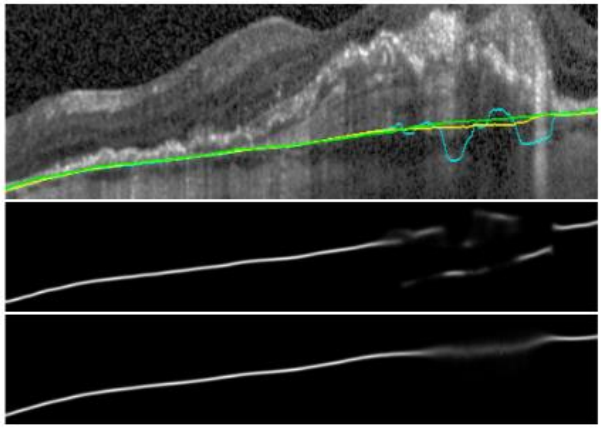

Figure 1: Top: sample segmentation without the curvature (blue), with the curvature (yellow) and the baseline (green). Middle: probabilistic output without the curvature term. Bottom: probabilistic output with the proposed curvature term.

P7 IDH mutation classification in glioma patients using 7T 3D-FID-MRSI.

Sukrit Sharma[*1], Cornelius Cadrien[*1,2], Philipp Lazen[2], Julia Furtner[3], Roxane Licandro[8], Alexandra Lipka[1,4], Eva Heckova[1], Lukas Hingerl[1], Stanislav Motyka[1], Stephan Gruber[1], Bernhard Strasser[1], Barbara Kiesel[2], Mario Mischkulnig[2], Matthias Preusser[5], Thomas Roetzer[6], Adelheid Wohrer[6], Michael Weber[7], Christian Dorfer[2], Karl Rossler[2], Siegfried Trattnig[1,4], Wolfgang Bogner[1], Georg Widhalm[2], Gilbert Hangel[1,2] * Shared first authors

[1] High Field MR Centre, Department of Biomedical Imaging and Image-guided Therapy, Medical University of Vienna, Vienna, Austria
[2] Department of Neurosurgery, Medical University of Vienna, Vienna, Austria
[3] Division of Neuroradiology and Musculoskeletal Radiology, Department of Biomedical Imaging and Image-guided Therapy, Medical University of Vienna, Vienna, Austria
[4] Christian Doppler Laboratory for Clinical Molecular MR Imaging, Vienna, Austria
[5] Division of Oncology, Department of Inner Medicine I, Medical University of Vienna, Vienna, Austria
[6] Division of Neuropathology and Neurochemistry, Department of Neurology, Medical University of Vienna, Vienna, Austria
[7] Division of Medical Imaging and Nuclear Medicine, Medical University of Vienna, Vienna, Austria
[8] Department of Biomedical Imaging and Image-guided Therapy, Computational Imaging Research Lab (CIR), Medical University of Vienna, Vienna, Austria

Disclosure statement: The authors declare no conflicts of interest.

Keywords: 7T-MRSI , Glioma , IDH

Objective
We intend to identify biomarkers to differentiate glioma grades and neoplastic mutations like isocitrate dehydrogenase. We recently demonstrated glutamine and glycine as potential biomarkers of interest in high-grade gliomas with the help of increased spatial and spectral resolution of 7T (7 Tesla) magnetic resonance spectroscopic imaging (MRSI). Our study might benefit therapeutic choices and definition of maximum safe resection in future.

Methods and Materials
37 Patients with Grade II-IV, 27 high grade gliomas (HGGs) and 10 low grade gliomas (LGGs), without contraindication for 7T MRI were recruited at Department of Neurosurgery. Grades were diagnosed histologically by the division of Neuropathology and Neurochemistry according to WHO 2021 classification.(Louis et al., 2021) 3D-MRSI with 64x64x39 matrix and 3.4 mm isotropic voxel size was acquired using Siemens Magnetom 7T with 32-channel coil (Nova MEdical) (Hangel et al., 2020). LCModel (Provencher, 2001) was used for spectral quantification. Manual tumor segmentation with contrast-enhancing (CE), non-contrast-enhancing (NCE) and necrosis (NEC) regions was provided by neurologist. CSV database was created out of all the original metabolite spectroscopy image and tumor region was labeled. The ratios of metabolites to total creatine (tCr) , n-acetyl-asparatate (NAA), total n-acetyl-asparatate (tNAA) and total Choline (tCh) was calculated and further used for boxplots and Mann-Whitney Wilcoxon test (MWW) to analyze statistical significant differences in IDH mutation status.

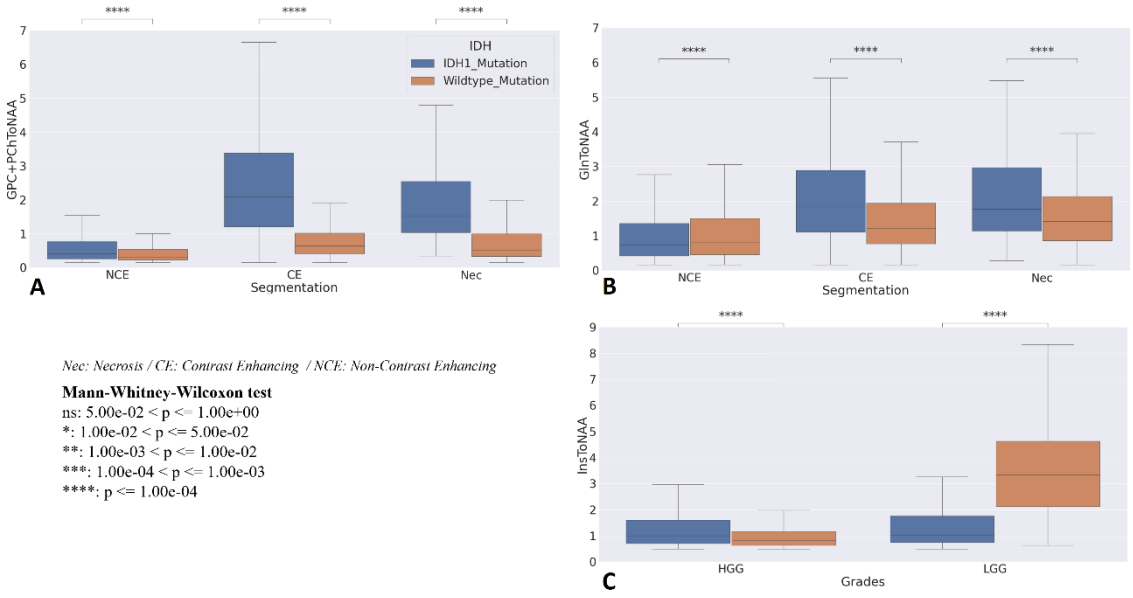

Figure 1: A: GPC+PCh to NAA differentiation for tumor regions B: Gln to NAA differentiation for tumor regions C:Gln to NAA differentation for LGGs and HGGs

Results

The differentiation of ratio metabolite in IDH-1 vs IDH Wildtype in different tumor regions yields significant differences for tCh to NAA and Gln to NAA (In figure 1 A and B). Also for LGGs and HGGs the significant difference was seen for Ins to NAA (In figure 1 C).

Conclusion

The significant difference for IDH mutation in different regions and grades of glioma provide good prospect for biomarker definition and IDH classification.

References:

[1] Hangel, G., Cadrien, C., Lazen, P., Furtner, J., Lipka, A., He˘ckov´a, E., Hingerl, L., Motyka, S., Gruber, S., Strasser, B., Kiesel, B., Mischkulnig, M., Preusser, M., Roetzer, T., W¨ohrer, A., Widhalm, G., R¨ossler, K., Trattnig, S., & Bogner, W. (2020). High-resolution metabolic imaging of high-grade gliomas using 7T-CRT-FID-MRSI. NeuroImage: Clinical, 28, 102433. https://doi.org/10.1016/j.nicl.2020.102433

[2] Louis, D. N., Perry, A., Wesseling, P., Brat, D. J., Cree, I. A., Figarella-Branger, D., Hawkins, C., Ng, H. K., Pfister, S. M., Reifenberger, G., Soffietti, R., von Deimling, A., & Ellison, D. W. (2021). The 2021 WHO Classification of Tumors of the Central Nervous System: A summary. Neuro-Oncology, 23 (8), 1231–1251. https://doi.org/10.1093/neuonc/noab106

[3] Provencher, S. W. (2001). Automatic quantitation of localized in vivo 1H spectra with LCModel [eprint: https://analyticalsciencejournals.onlinelibrary.wiley.com/doi/pdf/10.1002/nbm.698]. NMR in Biomedicine, 14 (4), 260–264. https://doi.org/10.1002/nbm.698

P8 An MRI sequence independent Convolutional Neural Network for synthetic head CT generation in proton therapy

Peter Kuess[1,2], Barbara Knäusl[1,2], Markus Stock[2], Carola Lütgendorf-Caucig[2], Dietmar Georg[1], Lukas Zimmermann[1,3]

[1] Department of Radiation Oncology, Medical University of Vienna, Austria
[2] MedAustron Ion Therapy Center, Austria
[3] Faculty of Engineering, University of Applied Sciences Wiener Neustadt, Austria

Disclosure statement: The authors declare no conflicts of interest.

Keywords: proton therapy, synthetic CT, transfer learning

Objective
An MRI sequence independent deep learning technique was developed and validated to generate synthetic CT (sCT) scans for MR guided proton therapy.

Methods and Materials
47 meningioma patients previously undergoing proton therapy based on pencil beam scanning were divided into training (33), validation (6), and test (8) cohorts. T1, T2, and contrast enhanced T1 (T1CM) MRI sequences were used in combination with the planning CT (pCT) data to train a 3D U-Net architecture with ResNet-Blocks. A hyperparameter search was performed including two loss functions, two group sizes of normalisation, and depth of the network. The performance was evaluated based on a metric and dosimetric analysis as well as spot difference maps. Furthermore, the influence of immobilisation masks was investigated.

Results
The final model was trained with fixed features per group for the group normalisation, six down-convolution steps, an input size of 128x192x192, and feature loss. For the test dataset for body/bone the mean absolute error (MAE) values were on average 79.8/216.3 HU when trained using T1 images, 71.1/186.1 HU for T2, and 82.9/236.4 HU for T1CM. The investigated dose parameters of the target structures agreed within 1% between original proton treatment plans and plans recalculated on sCTs (cf. Figure 1). The spot difference maps had peaks at +/-0.2 cm and for 98% of all spots the difference was less than 1 cm.

Conclusion
A novel MRI sequence independent sCT generator was developed, which suggests that the training phase of neural networks can be disengaged from specific MRI acquisition protocols.

Funding Sources:
The research was funded by the Austrian Science Fund (FWF) (project number: P30065-B27) and the Austrian Research Promotion Agency (FFG, project number 867619), and the European Union (EUROSTARS-2 CoD9: 12326 ILLUMINUS).

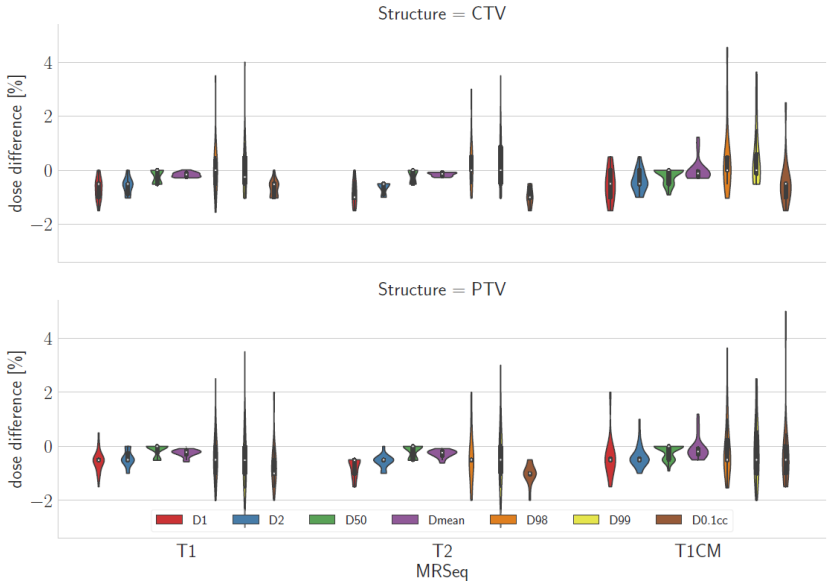

Figure 1: Difference of dose volume parameters for CTV (upper figure) and PTV (lower figure) comparing the sCTs (based on three different MRI sequences) with the pCT.

P9 Characterization of the androgen receptor in androgen-sensitive and castration-resistant human prostate cancer cell lines

Julia Raitanen[1,2,3], Katarína Benčurová[1,2], Patrik Schwarzl[1], Gerda Egger[1,4], Marcus Hacker[2], Thomas L. Mindt[1,3], Markus Mitterhauser[1,2], Theresa Balber[1,2]

[1] Ludwig Boltzmann Institute Applied Diagnostics, Vienna, Austria
[2] Department of Biomedical Imaging and Image-guided Therapy, Division of Nuclear Medicine, Medical University of Vienna, Vienna, Austria
[3] Institute of Inorganic Chemistry, Faculty of Chemistry, University of Vienna, Vienna, Austria
[4] Department of Pathology, Medical University of Vienna, Vienna

Disclosure statement: The authors declare no conflicts of interest.

Keywords: androgen receptor, [^{18}F]FDHT, prostate cancer

Objective
The androgen receptor (AR) and its signalling axis in the progression of prostate cancer is the key to our understanding of castration resistance. This *in vitro* study was designed to investigate AR expression, localization and functionality in androgen-sensitive and castration-resistant human prostate cancer cell lines.

Methods and Materials
Cellular uptake of 16β-[^{18}F]fluoro-5α-dihydrotestosterone ([^{18}F]FDHT), a radiotracer for positron emission tomography targeting the AR [1], was investigated in LNCaP [2] and PC-3 [3] cell lines by collecting membrane-bound, internalized and nuclear fractions. Western blot (WB) analyses and immunofluorescence (IF) microscopy were employed to determine target expression and receptor localization in support of obtained data.

Results
Significantly higher specific [^{18}F]FDHT membrane binding and nuclear uptake was found in LNCaP cells compared to PC-3 cells. WB analyses and IF confirmed the presence of ARs of different isoforms in both investigated cell lines: LNCaP cells demonstrated cytoplasmic and pronounced nuclear AR expression, while in PC-3 cells only the AR variant was detected.

Conclusion
[^{18}F]FDHT uptake in all fractions was significantly higher in androgen-sensitive LNCaP than in androgen-independent PC-3 cells suggesting androgen-dependence as the driving force for higher expression of androgen-binding membrane proteins. This data further suggests that androgen-sensitive cells quickly translocate the tracer-receptor complex to the nucleus to initiate gene transcription and consequent tumor growth. However, the AR isoform expressed by castration-resistant PC-3 cells is not capable of binding relevant amounts of [^{18}F]FDHT, pointing at impaired AR functionality. This *in vitro* data contributes to a deeper understanding of [^{18}F]FDHT PET in a clinical context.

Funding Source: FFG Talente: FEMtech (no.:880332)

References:
[1] A. Liu, K. E. Carlson, J. A. Katzenellenbogen, “Synthesis of High Affinity Fluorine-Substituted Ligands for the Androgen Receptor. Potential Agents for Imaging Prostatic Cancer by Positron Emission Tomography” J. Med. Chem., vol. 35, no. 11, pp. 2113–2129, 1992
[2] T. M. Chu, G. P. Murphy, E. Kawinski, and E. A. Mirand, “Lncap model of human prostatic carcinoma” Cancer Res., vol. 43, no. 4, pp. 1809–1818, 1983
[3] M. E. Kaighn, K. S. Narayan, Y. Ohnuki, J. F. Lechner, and L. W. Jones, “Establishment and characterization of a human prostatic carcinoma cell line (PC-3)” Invest Urol., vol. 17, no. 1, pp. 16–23, 1979

P10 Evaluation of a novel Cone Beam CT conversion method for dose calculation

Wolfgang Lechner[1], Sarah Haupt[1], David Kanalas[2], Lukas Zimmermann[2], Dietmar Georg[1]

[1] Department of Radiation Oncology, Medical University of Vienna, Austria
[2] Faculty of Engineering, University of Applied Sciences, Wiener Neustadt, Austria

Disclosure statement: The authors declare no conflicts of interest.

Keywords: CBCT, dose calculation, adaptive radiotherapy

Objective
To evaluate a novel implementation of a CBCT conversion algorithm for dose calculation implemented in RayStation (Development Version 10B-DTK, RaySearch, Stockholm, Sweden). The algorithm is able to estimate artifacts and creates a CBCT correction map.

Methods and Materials
CBCTs acquired for ten head and neck (HN) and ten gynecological (GY) patients were collected and converted using the new algorithm (CBCTc). A bulk density overriding technique implemented in the same version of RayStation was used for comparison (CBCTb). Clinical treatment plans, which were optimized on the pCT, were recalculated on both the CBCTc and the CBCTb. The resulting dose distributions were analyzed using local gamma analysis with 1% dose difference and 1 mm distance to agreement criteria. Four different dose threshold level were used for the analysis: 10%, 30%, 50 % and 90%. A paired student's t-test was applied to test the differences in gamma pass rates (GPRs) between the CBCTc and CBCTb method. A p-value smaller than 0.05 considered statistically significant.

Results
Figure 1 shows box-plots of the GPRs grouped by conversion method and threshold for the HN and GY cases, respectively. The GPRs for the CBCTb method were systematically lower compared to the CBCTc method. These differences were also statistically significant for all test cases and thresholds.

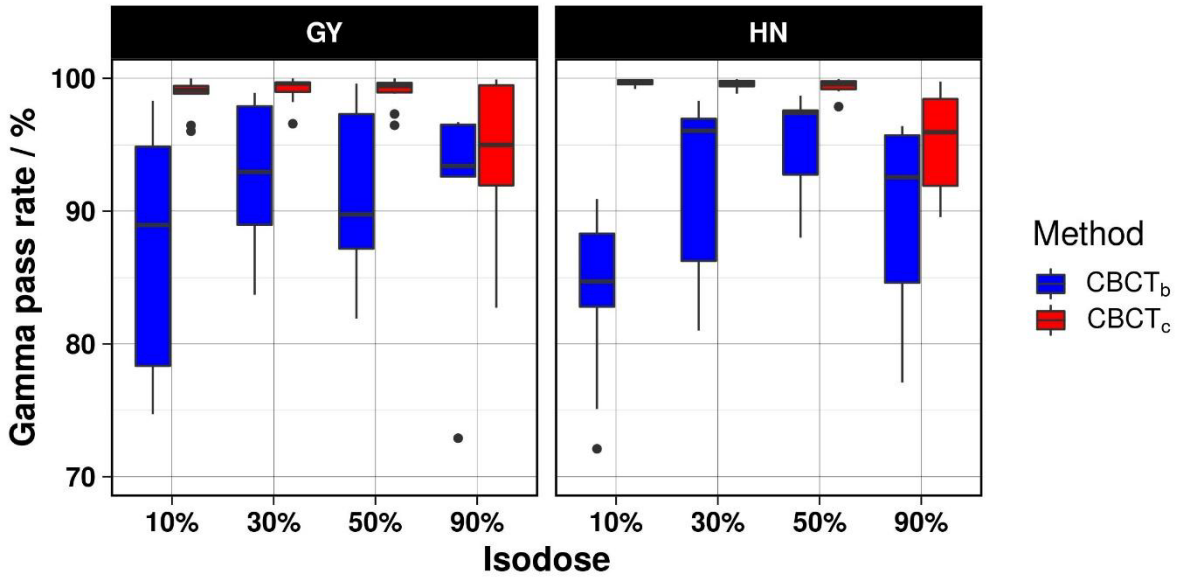

Figure 1: Boxplot of the results of the gamma analysis for GY and HN cancer patients for four different dose thresholds.

Conclusion
The dose distribution calculated using the new CBCTc method showed excellent agreement with the pCT based dose calculation, with superior accuracy compared to the CBCTb method. The clinical introduction of the novel CBCTc method will improve the accuracy of the dose estimation in adaptive radiotherapy workflows.

P11 Are we ready to use sCTs in an adaptive carbon-ion treatment workflow?

Barbara Knäusl[1,2], Peter Kuess[1,2], Markus Stock[2], Dietmar Georg[1], Piero Fossati[2], Petra Georg[2], Lukas Zimmermann[1,3]

[1] Department of Radiation Oncology, Medical University of Vienna, Austria
[2] MedAustron Ion Therapy Center, Austria
[3] Faculty of Engineering, University of Applied Sciences Wiener Neustadt, Austria

Disclosure statement: The authors declare no conflicts of interest.

Keywords: carbon-ion therapy, synthetic CT

Objective
Anatomical surveillance during treatment is the basis for an excellent dose calculation and delivery accuracy in ion-beam therapy. Synthetic CT (sCT) based on MRI information proved as a valuable replacement for the planning CT (pCT) in photon radiation oncology and improved the workflow efficiency. The transfer to the particle world, especially carbon ions, is highly challenging; patient-specific immobilisation, complex non-standard treatment plans for rare indications, limited training data, and a reduced benefit by omitting an imaging modality are only a few problems in this domain (Figure 1).

Methods and Materials
30 carbon-ion treatment plans consisting of 60 beams were analysed. Dose and spot differences between sCT and pCT were reported and evaluated on a patient individual basis.

Results
The spot maps showed a systematic displacement by 0.22 cm, most likely caused by the immobilization mask invisible on the MRI. 64.5% of all spot displacements were located within 1 cm. The mean PTV dose D50% agreed within (-0.1+/-0.6)%, while D0.01cc differed up to (7.6+/-7.8)%. For the OARs the deviation between sCT and pCT depended strongly on the position and the dose gradient. For one patient D2% of the chiasm differed by almost 30%.

Conclusion
The usage of sCTs in carbon-ion therapy opens several new questions, and at the same time provides a limited benefit in the existing workflow. Omitting the pCT seems unfavourable, but sCTs could be included in the carbon-ion therapy workflow for monitoring, re-planning, and adaption of the initial dose distribution.

Funding Sources:
The research was funded by the Austrian Science Fund (FWF) (project number: P30065-B27) and the Austrian Research Promotion Agency (FFG, project number 867619), and the European Union (EUROSTARS-2 CoD9: 12326 ILLUMINUS).

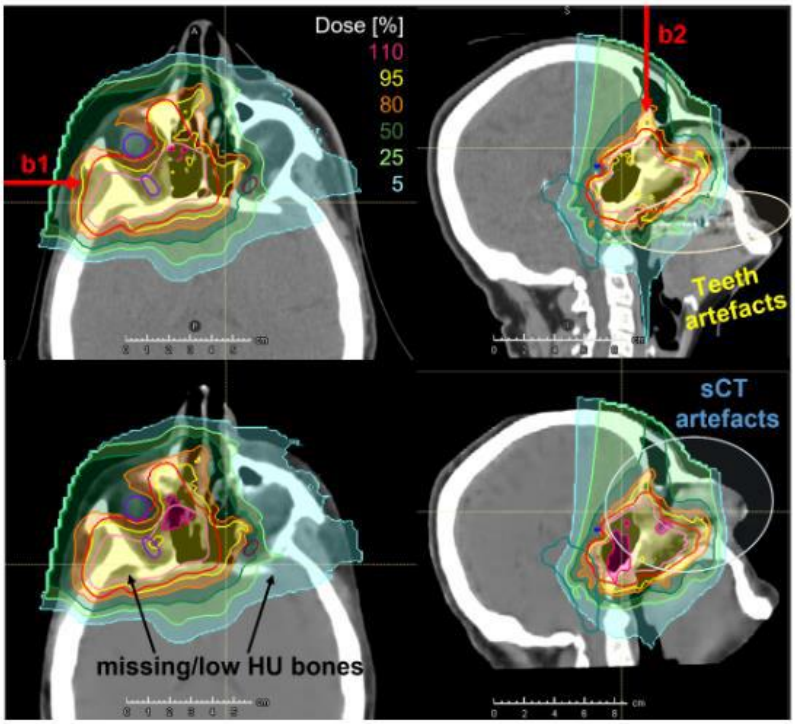

Figure 1: Representative patient for a hyperextended head position with a tumour located close to the surface. The patient was treated with a horizontal beam (b1) and a vertex beam (b2). The top line shows the dose distribution on the pCT and the bottom line the dose distribution on the sCT. Highlighted areas show teeth artefacts on the pCT that are non-existing on the sCT and wrongly assigned densities on the sCT caused by the conversion method.

P12 Phenotype analysis of Zfp516 -/- and Zfp516 -/+ mouse embryos based on High resolution episcopic microscopy

Stefan H. Geyer[1], Joanna Przewrocka[2], Eva Grönroos[2], Fabrice Prin[3], Tim Mohun[4], Charles Swanton[2], Wolfgang J. Weninger[1]

[1] Division for Anatomy, Centre for Anatomy and Cell Biology, Medical University of Vienna, Austria
[2] Cancer Evolution and Genome Instability Lab, The Francis Crick Institute, UK
[3] Advanced Light Microscopy, The Francis Crick Institute, UK
[4] Heart Development Lab, The Francis Crick Institute, UK

Disclosure statement: The authors declare no conflicts of interest.

Keywords: HREM, phenotyping, Zfp516

Objective
In mice *Zfp516* is known to regulate brown fat tissue formation and stemness in embryonic stem cells. Loss of its function leads to embryonic lethality. Yet, information whether morphogenesis and fetal anatomy is abnormal in homozygous and heterozygous mice is scarce and contradicting. The function of the gene is therefore still not fully characterised and it is not yet clear whether it fits as model for studying the function of the human orthologue *ZNF516*. Our study aims at providing comprehensive and high detail information on the morphological phenotype of homozygous and heterozygous harvested at embryonic day (E) 14.5.

Methods and Materials
High resolution episcopic microscopy (HREM) was used to create digital volume data with voxel sizes of 3x3x3 µm^3 from 4 *Zfp516-/-* and 10 *Zfp516-/+* E14.5 mouse embryos. A standardised protocol, involving scrolling through the images of all three body planes, virtual slicing, volume and surface rendering was followed to perform systematic phenotype analysis.

Results
Both, *Zfp-/-* and *Zfp-/+* E14.5 embryos showed a wide range of structural abnormalities, in particular of the cardiovascular and nervous systems. Four homozygous and two heterozygous embryos showed perimembraneous or muscular ventricular septal defects. Four homozygous and two heterozygous embryos showed brain defects or cranial nerve abnormalities.

Conclusion
Our analysis demonstrate that *Zfp516* plays an essential role in cardiovascular formation and the development of the nervous system.

P13 Morphologic indicators for severe central nervous system defects in genetically engineered mouse embryos

Lukas F. Reissig[1], Atieh Seyedian Moghaddam[1], Fabrice Prin[2], Robert Wilson[2],Antonella Galli[3], Catherine Tudor[3], Jaqueline K. White[3], Stefan H. Geyer[1],Timothy J. Mohun[2] and Wolfgang J. Weninger[1]

[1] 1Division of Anatomy, MIC, Center for Anatomy and Cell Biology, Medical University of Vienna, Vienna, Austria
[2] TheFrancis Crick Institute, London, United Kingdom
[3] Wellcome Trust Sanger Institute, Wellcome Genome Campus, Cambridge,United Kingdom

Disclosure statement: The authors declare no conflicts of interest.

Keywords: phenotyping, mouse embryo, HREM

Objective
In researching human central nervous system (CNS) disorders the identification of appropriate knockout (KO) mouse models is essential. As many KO-lines produce pre- or perinatally lethal homozygous offspring, their analysis rests upon phenotyping accessible embryonic stages. This is complicated by the fact that many mouse lines show highly variable penetrance of phenotypes, wherefore severe phenotypes, causing early lethality are easily missed and large numbers of embryos have to be bred and harvested. To facilitate reduction of numbers and to ensure that early lethal malformations are not missed, we aimed at identifying mild morphologic abnormalities that have the potential to serve as indicators for low penetrant CNS defects in genetically modified mouse lines.

Methods and Materials:
Approximately 500 homozygous null mutant embryos of 81 single gene KO-lines were harvested at embryonic day 14.5 and digital volume data were created using High-resolution episcopic microscopy (HREM). Employing the data stacks and volume rendered computer models the phenotypes of the embryos were systematically analysed following a standardized protocol.

Results:
First analysis identified two promising indicator candidates. Hypoglossal nerve (HGN) abnormalities (absent, thin, and abnormal topology) and abnormal morphology and topology of head arteries. Both are frequently associated with the full spectrum of morphological CNS defects. Statistical analysis however confirmed only for HGN abnormalities a significant correlation with CNS defects.

Conclusion:
These results demonstrate that KO-lines showing HGN abnormalities are also likely to produce CNS defects. Therefore the HGN can be used as indicator to identify KO-lines featuring low penetrant CNS malformations.

Funding Information:
This work was supported by the Wellcome Trust (100160) andthe Francis Crick Institute, which receives its corefunding from Cancer Research UK (FC001117), the UKMedical Research Council (FC001117), and the WellcomeTrust (FC001117).

P14 Monitoring of Cutaneous Wound Healing in Diabetic and Non- Diabetic Mice using Optical Coherence Tomography Angiography

Martin Pfister[1,2], Kornelia Schützenberger[1], Nathalie Fuhrmann[1], Bhavapriya Jasmin Schäfer[1], Stefan Puchner[1], Hannes Stegmann[1], Christine Hohenadl[3], Michael Mildner[4], Gerhard Garhöfer[5], Leopold Schmetterer[1,5,6], René M. Werkmeister[1]

[1] Center for Medical Physics and Biomedical Engineering, Medical University of Vienna, Austria
[2] Institute of Applied Physics, Vienna University of Technology, Austria
[3] Croma Pharma GmbH, Austria
[4] Department of Dermatology, Medical University of Vienna, Austria
[5] Department of Clinical Pharmacology, Medical University of Vienna, Austria
[6] Singapore Eye Research Institute, Singapore

Disclosure statement: The authors declare no conflicts of interest.

Keywords: preclinical imaging, optical coherence tomography angiography, wound healing

Objective
To evaluate vascular remodelling in an excisional wound model in the pinnae of healthy and type 2 diabetic mice receiving proangiogenic treatment using optical coherence tomography angiography (OCTA).

Methods and Materials
OCTA is a non-invasive imaging modality that allows in vivo investigation of the superficial vasculature in skin. We used a custom-built swept source OCT system operating in the 1300 nm wavelength range to acquire OCT angiograms immediately before and after setting an excisional wound in the pinnae of C57BL/6 and db/db mice and at six additional time points up to 18 days after wounding.
The four quantitative OCTA parameters vessel density, vessel length, number of bifurcations, and vessel tortuosity were determined from the high-resolution angiograms and compared between different treatment groups.

Results
Analysis of the angiograms showed changes of the microvasculature and allowed identification of the overlapping wound healing phases hemostasis, inflammation, proliferation, and remodelling. In the proliferative phase, the OCTA parameters vessel density, normalized vessel length, number of bifurcations, and vessel tortuosity reached peak values 28-47 %, 39-52 %, 33-48 %, and 3-8 % above baseline, respectively, on study days four to seven. Subsequently, observed values decreased slowly but remained elevated on the last study day 18 days after wounding, which suggests that the remodelling phase is still ongoing.

Conclusion
OCTA can be used for in vivo monitoring of the dynamic changes in the vascular network during wound healing and may serve as a valuable tool in preclinical research studying impaired vascular remodelling and potential treatment strategies.

Funding Sources:
This research was funded by Christian Doppler Research Association, the Austrian Federal Ministry of Digital and Economic Affairs, and the National Foundation of Research, Technology and Development with grant number CD10260502.

References:
Pfister, M.; Schützenberger, K.; Schäfer, B.J.; Puchner, S.; Stegmann, H.; Hohenadl, C.; Mildner, M.; Garhöfer, G.; Schmetterer, L.; Werkmeister, R.M. Optical Coherence Tomography Angiography Monitors Cutaneous Wound Healing under Angiogenesis-Promoting Treatment in Diabetic and Non- Diabetic Mice. Appl. Sci. 2021, 11, 2447. https://doi.org/10.3390/app11052447

P15 Assessing metabolic differences in rodents on high fat diet using Deuterium Metabolic Imaging

Ehret V. [1], Ustsinau U.[2], Friske J.[3], Scherer, T.[1], Fürnsinn, C.[1], Helbich, T.[3], Philippe, C.[2], Kršśák, M.[1]

[1] Division of Endocrinology and Metabolism, Department of Medicine III, Medical University of Vienna, Vienna, Austria
[2] Division of Nuclear Medicine, Department of Biomedical Imaging and Image-Guided Therapy, Medical University of Vienna, Vienna, Austria
[3] Division of Molecular and Structural Preclinical Imaging, Department of Biomedical Imaging and Image-Guided Therapy, Medical University of Vienna, Vienna, Austria

Disclosure statement: The authors declare no conflicts of interest.

Keywords: MR Spectroscopy**,** metabolism

Objective
Deuterium Metabolic Imaging (DMI) is an innovative approach for evaluating metabolism using ^{2}H MR Spectroscopy (MRS) after an injection of deuterated substrates. It provides metabolic maps for visualizing glucose transport and downstream metabolism [1-3]. In the present pilot study, we use DMI to show metabolic differences in rats on high fat (HFD) and standard diet (SD).

Methods and Materials
Following the intravenous injection of [6,6'^{2}H2]glucose(1.95g/kg bodyweight), a 2-dimensional chemical shift imaging (CSI) sequence (TR=350ms, Avg=128, FA=61.6°, matrix 12x12mm, FOV=50x36mm) is applied. DMI measurements are performed on Biospec 94/30 (Bruker Biospin, Germany) MR system with 2H/1H surface RF coil adjusted for abdominal region. Groups of Sprague Dawley rats following a high fat (n=3, m=530-550g, age=11 weeks) or standard diet (n=3, m=340-390g, age=11 weeks) were examined. The acquired MRS data are analyzed using the Matlab based tool DMIWizard provided by Yale university and adapted for the use of this project. Spectra are quantified with linear least-squares fitting and the amplitudes translated to concentration according to the ^{2}H natural abundance water peak.

Results
The first results of the pilot study show much lower post-infusion glucose levels in rodent livers following a HDF than with SD, giving evidence of an impaired and slower liver metabolism in fatty animals.

Conclusion
DMI is a promising method for assessing differences in metabolically healthy and impaired rodents, holding potential for the study of a wide variety of metabolic diseases, such as fatty liver disease.

Funding Source:
This study was funded by the Vienna Science and Technology Fund (WWTF #LS19-046).

References:
1. De Feyter, H. M., et al. (2018). Deuterium metabolic imaging (DMI) for MRI-based 3D mapping of metabolism in vivo. *Science Advances 4*(8):eaat7314.
2. De Graaf, R. A., et al. (2020). On the magnetic field dependence of deuterium metabolic imaging. *NMR in Biomedicine 33:*e4235.
3. Riis-Vestergaard, et al. (2020). Glucose metabolism in brown adipose tissue determined by deuterium metabolic imaging in rats. *International Journal of Obesity 44*: 1417-1427.

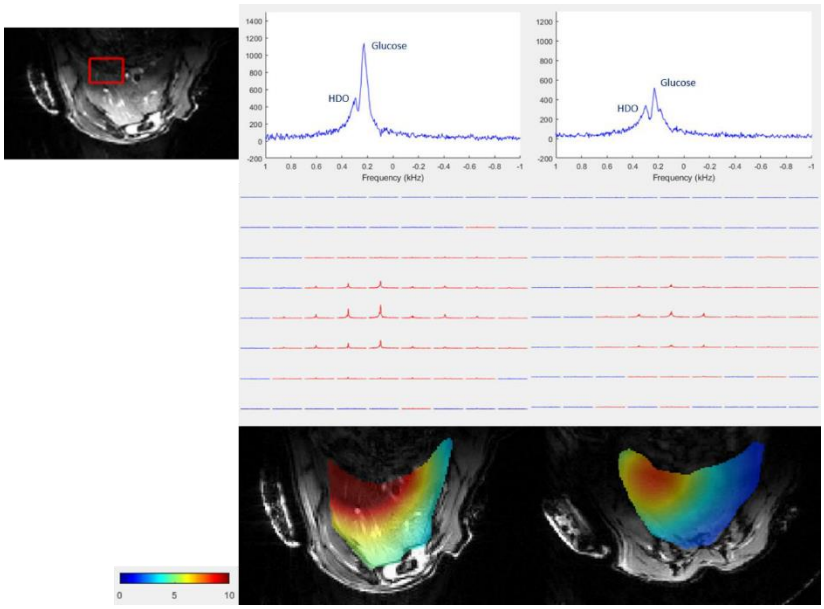

Figure 1: Spectra in rodent liver voxel (red box) and color maps of whole liver with standard (left) and high fat diet.

P16 The *in ovo* model as a potential alternative to rodents for CRC research

Benčurová K[1,2], Coban M[1,2,3], Leipold M[1,2,3], Mayrhofer M[4], Zacher A[2], Ponti S[2], Friske J[5], Helbich T[5], Egger G[1,6], Hacker M[2], Haug A[2], Mitterhauser M[1,2,7], Balber T[1,2]

[1] Ludwig Boltzmann Institute Applied Diagnostics, Vienna, Austria
[2] Division of Nuclear Medicine, Department of Biomedical Imaging and Image-guided Therapy, Medical University of Vienna, Vienna, Austria
[3] FH Wiener Neustadt, Wiener Neustadt, Austria
[4] FH Oberösterreich, Linz, Austria
[5] Division of General Radiology, Department of Biomedical Imaging and Image-guided Therapy, Medical University of Vienna, Vienna, Austria
[6] Department of Pathology, Medical University of Vienna, Vienna, Austria
[7] Department for Inorganic Chemistry, Faculty of Chemistry, University of Vienna, Vienna, Austria

Disclosure statement: The authors declare no conflicts of interest.

Keywords: *in ovo*, imaging, 3R principle

Objective
Development of novel radiotracers for cancer research involves costly and time-demanding animal testing. In accordance with the 3R principle[1], rodents can be replaced by immature forms of non-mammalian vertebrates, such as chick embryos (*in ovo*). We aimed at establishing this model for colorectal cancer (CRC) with the focus on C-X-C chemokine receptor type 4 (CXCR4) expression, as this receptor is of prognostic significance for CRC[2,3].

Methods and Materials
Fertilized chicken eggs were incubated at 37°C and 60% humidity. Human CRC cancer cells expressing CXCR4[4] (HT29 and HCT116) were inoculated onto the CAM. Multimodal imaging was performed. Xenografts were preserved.

Results
A workflow for incubation, tumour cell inoculation, intravascular injection and anaesthesia was established. µMRI showed superior soft tissue contrast compared to µCT. Immunohistochemical (IHC) analysis using an antibody against desmin proved vascularization of the grafts. Staining of cells of epithelial origin (cytokeratin 19 IHC) differentiated between the inoculated cancer cells and the CAM. Tumor accumulation of the radiolabeled glucose-analogue, [^{18}F]FDG, indicated glucose turnover and viability of the grafts. The latter was proven with IHC (ki67, cleaved caspase 3). Preliminary results showed accumulation of [^{68}Ga]Ga-Pentixafor, PET-tracer targeting CXCR4, in xenografts derived from HT29 and HCT116 cells. Specificity was shown by co-injection of an excess of CXCR4 Antagonist I (blocking). Target expression was confirmed immunohistochemically.

Conclusion
These results show the potential of the *in ovo* model for investigating radiotracer accumulation in xenografts derived from CRC cell lines. The model may lead to reduction of animal experiments in the future.

Funding Sources:
FFG funding for industrial PhD, project number: 879117

References:
[1] Russell WMS, Burch RL. The principles of humane experimental technique. [Reissued: 1992, Universities Federation for Animal Welfare, Potters Bar, Herts., UK] Special ed. London: Methuen; 1959
[2] Kim J, Takeuchi H, Lam ST, *et al.* Chemokine receptor CXCR4 expression in colorectal cancer patients increases the risk for recurrence and for poor survival. *J Clin Oncol.* 2005;23(12):2744-2753. doi: 10.1200/JCO.2005.07.078
[3] Xu C, Zheng L, Li D, *et al.* CXCR4 overexpression is correlated with poor prognosis in colorectal cancer. *Life Sci.* 2018;208:333-340. doi: 10.1016/j.lfs.2018.04.050
[4] Murakami T, Kawada K, Iwamoto M, *et al.* The role of CXCR3 and CXCR4 in colorectal cancer metastasis. *Int J Cancer.* 2013;132(2):276-287. doi: 10.1002/ijc.27670

P17 Simultaneous PET-MRI using 18F-Fluoroethylcholine can provide accurate diagnosis and characterization of breast cancer

Paola Clauser, Sazan Rasul, Panagiotis Kapetas, Barbara Fueger, Ruxandra-Iulia Milos, Theresa Balber, Marcus Hacker, Thomas H. Helbich, Pascal A.T. Baltzer

Department of Biomedical Imaging and Image-guided Therapy, Medical University of Vienna, Austria

Disclosure statement: The authors declare no conflicts of interest.

Keywords: breast cancer, PET-MRI, Imaging biomarker

Objective
This prospective, monocentric study was approved by the ethic committee and patients gave their written informed consent. Patients with lesions classified as suspicious on mammography, tomosynthesis and/or ultrasound and no contraindications to contrast-enhanced MRI and PET were included. PET-MRI of the breast were performed simultaneously in a prone position with a dedicated 16-channel MRI breast coil. A board-certified nuclear medicine physician and an experienced breast radiologist evaluated the images and measured the maximum standardized uptake vale (SUVmax) of the MRI suspicious findings. Pathology was considered as reference standard. Immunohistochemical (IHC) analysis was available for malignant lesions. Differences in SUVmax between benign and malignant lesions and between malignant lesion IHC were evaluated with the Mann-Whitney-U-test. The area under the curve (AUC) was calculated.

Results
101 patients (mean age 52.3 years, standard deviation 12.0) with 117 lesions were included (30 benign, 7 ductal carcinomas in situ (DCIS), 80 invasive carcinomas (IC)). FEC-SUVmax was higher in malignant compared to benign lesions ($p<0.001$), with an AUC of 0.846. FEC-SUVmax was higher in IC compared to DCIS ($p<0.001$). FEC-uptake was higher for lesions with a higher proliferation rate ($p=0.011$) and Her2 positive ($p=0.041$).

Conclusion
The lesion uptake of FEC was significantly higher in malignant than in benign breast lesions. FEC SUVmax is a promising new imaging biomarker and seems to allow cancer subtyping.

Funding Sources:
This study has received funding by the Austrian National Bank Jubiläumsfonds project number 17186.

P18 Implementation of a spatially-variant and tissue-dependent position range correction for PET/CT imaging

Hunor Kertész[1], Thomas Beyer[1], Vladimir Panin[2], Walter Jentzen[3], Jacobo Cal-Gonzalez[1,4], Alexander Berger[1], Laszlo Papp[1], Peter Kench[5], Deepak Bharkhada[2], Jorge Cabello[2], Maurizio Conti[2] and Ivo Rausch[1]

[1] QIMP Team, Center for Medical Physics and Biomedical Engineering, Medical University of Vienna, Vienna, Austria
[2] Siemens Medical Solutions USA, Inc., Knoxville, TN, United States of America
[3] Clinic for Nuclear Medicine, University Hospital Essen, Essen, Germany
[4] Ion Beam Applications, Protontherapy Center Quironsalud, Madrid, Spain
[5] Discipline of Medical Imaging Science and Brain and Mind Centre, Faculty of Medicine and Health, The University of Sydney, Sydney NSW, Australia

Disclosure statement: Dr. Vladimir Panin, Dr. Deepak Bharkada, Dr. Jorge Cabello and Dr. Maurizio Conti are employees of Siemens Medical Solutions USA, Inc., (Knoxville, TN, USA) and report no conflict of interest with this study.

Keywords: positron range correction, image reconstruction, PET quantification

Objective
Positron range (PR) represents the path travelled by the positron from the emission to the annihilation position. For high energy positron emitter radionuclides this effect is leading to increased image noise and reduced image contrast in the reconstructed images.
The aim was to develop an approach for spatially-variant (SV) and tissue-dependent positron range correction (PRC) for correction during the iterative PET image reconstruction.

Materials and methods
The PR distributions of ^{18}F, ^{68}Ga, and ^{124}I were simulated using GATE framework in lung, water, and bone medium. Uniform PR kernels were created by mapping the simulated 3D PR point cloud to a 3D matrix. The SV kernels were composed from the uniform PR kernels by analysing the underlying material. The PRC was included into the iterative image reconstruction as an additional correction method. The PRC method was evaluated using the NEMA image quality (IQ) phantom; two unique PR phantoms by means of contrast recovery, contrast-to-noise ratio, image noise and spatial-resolution which was evaluated in terms of full-width at half- maximum (FWHM).

Results
The effect of PRC on ^{18}F-imaging was negligible. In contrast, PRC improved image contrast for the 10-mm sphere of the NEMA-IQ phantom filled with ^{68}Ga and ^{124}I by 33% and 24%, respectively. While PRC was less noticeable for the larger spheres, contrast recovery still improved by 5%. The spatial resolution was improved by 26% for ^{124}I (FWHM of 4.7 vs. 3.6 mm).

Conclusion
For high energy positron emitting radionuclides, the proposed PRC method helped recover image contrast with reduced noise levels and with improved spatial resolution.

Funding
The financial support of Siemens Medical Solutions USA, Inc. (Knoxville, TN, USA) is gratefully acknowledged.

P19 Quantification of intrinsic optical signals in the outer human retina using optical coherence tomography

Rene Werkmeister[1], Alina Messner[1] , Hannes Stegmann[1], Leopold Schmetterer[2], Doreen Schmidl[1], Rainer A. Leitgeb[3], Valentin Aranha dos Santos[1]

[1] Medical University of Vienna
[2] Singapore Eye Research Institute
[3] Center for Medical Physics and Biomedical Engineering, Medical University of Vienna, Waehringer Guertel 18-20, 4L, 1090 Vienna

Objective
Intrinsic optical signals (IOS) constitute a non-invasive biomarker promising the objective assessment of retinal photoreceptor function. We aimed to employ a commercial optical coherence tomography (OCT) system and a OCT signal model for evaluation of optical path length (OPL) changes in the outer retina during light adaptation.

Methods
The temporal retina of five healthy subjects was measured. Volumetric OCT data was acquired at 30 timepoints in ambient light and during long duration stimulation with white light and analyzed, employing a signal model based on the sum of seven Gaussian curves corresponding to all relevant anatomical structures of the outer retina.

Results
During light stimulation, the mean OPL between rod outer segment tips (ROST) and retinal pigment epithelium (RPE) decreased by 20.9 ± 9.7 %. Further, the OPL between external limiting membrane (ELM) and RPE decreased by 5.2 ± 0.9 % versus baseline while the OPL between ELM and ROST showed an initial decrease (2.1 ± 1.6 % vs. baseline) and, thereafter, increased by 2.8 ± 2.1 % vs. baseline.

Conclusion
Our approach allowed to measure OPL changes in the outer retina in response to light stimulation and provided distinction between outer retinal structures of close spatial relation. The subretinal space underwent a distinct change in the context of light adaptation that could be measured using a standard OCT platform and a dedicated signal model. The present study indicates that a commercial OCT can be used to obtain an insight into photoreceptor function in vivo.

P20 Real-time detection and quantification of retinal fluid in neovascular age-related macular degeneration on optical coherence tomography using artificial intelligence

Gregor S. Reiter, Philipp Fuchs, Leonard Coulibaly, Veronika Röggla, Stefan Sacu, Hrvoje Bogunovic, Ursula Schmidt-Erfurth

Medical University of Vienna, Department of Ophthalmology

Objective
To evaluate the implementation of artificial intelligence (AI)-supported, real-time detection and quantification of retinal fluid on optical coherence tomography (OCT) for neovascular age-related macular degeneration (nAMD).

Methods and Materials
Consecutive patients with active nAMD were included and OCT imaging (6x6 mm, Spectralis HRA+OCT, Heidelberg Engineering, Heidelberg, Germany) was performed in a real-world outpatient care setting. A validated deep learning based algorithm was used on the baseline OCT volumes (=active fluid present) to detect and quantify retinal fluid. Cohen's Kappa of fluid detection of AI in comparison with a human grader was assessed and possible reasons for discrepancies explored.

Results
Fifty-two eyes with nAMD were included and both assesses by the AI and the human grader. There was excellent agreement in the detection of retinal fluid between the AI and the human grader (Cohen's Kappa: 0.94, 0.92, 0.81 and 0.76 for SRF 1mm, IRF 1mm, SRF 6mm and IRF 6mm, respectively). Fluid volumes in the central 1mm for cases with discrepancies were clinically insignificant (all SRF and IRF <0.12nl). There was no difference in the detection of macular fluid between previously treated and treatment-naïve eyes.

Conclusion
AI-based detection and quantification of retinal fluid is a precise and reliable tool to assess macular OCT volumes on an individual level. In addition to detection, the quantification of fluid volumes is only feasible with AI support. An AI output for clinical consultations will support treatment management and ensure reading center precision for each patient in the real world.

P21 Real time remote symptom monitoring during chemotherapy for cancer: European multicentre randomised controlled trial (eSMART)

Alexander Gaiger, Simone Lubowitzki and Christian Singer on behalf of the ESMART Consortium

Eileen Furlong [# 1], Andrew Darley [1], Patricia Fox [1], Alison Buick [1], Grigorios Kotronoulas [2], Morven Miller [2], Adrian Flowerday [3], Christine Miaskowski [4], Elisabeth Patiraki [5], Stylianos Katsaragakis [5], Emma Ream [6], Jo Armes [6], Alexander Gaiger [7], Geir Berg [8 9], Paul McCrone [10], Peter Donnan [11], Lisa McCann [2], Roma Maguire [2]

[1] School of Nursing, Midwifery and Health Systems, University College Dublin, Dublin, Ireland.
[2] School of Psychological Sciences and Health, University of Strathclyde, Glasgow, United Kingdom.
[3] Docobo Ltd, Surrey, United Kingdom.
[4] Institute for Global Health Sciences, University of California San Francisco, San Francisco, CA, United States.
[5] National and Kapodistrian University of Athens, Athens, Greece.
[6] School of Health Sciences, University of Surrey, Surrey, United Kingdom.
[7] Division of Hematology and Hemaostaseology, Medical University of Vienna, Vienna, Austria.
[8] Faculty of Medicine and Health Sciences, Norwegian University of Science and Technology, Gjøvik, Norway.
[9] Innlandet Hospital Trust Division Lillehammer, Lillehammer, Norway.
[10] Institute of Psychiatry, Psychology & Neuroscience, King's College London, London, United Kingdom.
[11] Dundee Epidemiology and Biostatistics Unit, University of Dundee, Dundee, United Kingdom.

Keywords: Telemedicine, patient reported outcome measurements (e-PROs), advanced symptom management (ASyMS)

Objective
To evaluate effects of remote monitoring of adjuvant chemotherapy related side effects via the Advanced Symptom Management System (ASyMS) on symptom burden, quality of life, supportive care needs, anxiety, self-efficacy, and work limitations.

Methods and Materials
Design: Multicentre, repeated measures, parallel group, evaluator masked, stratified randomised controlled trial.829 patients with non-metastatic breast cancer, colorectal cancer, Hodgkin's disease, or non-Hodgkin's lymphoma receiving first line adjuvant chemotherapy or chemotherapy for the first time in five years were randomised to ASyMS (intervention; n=415) or standard care (control; n=414) over six cycles of chemotherapy.

Results
For the intervention group, symptom burden remained at pre-chemotherapy treatment levels, whereas controls reported an increase from cycle 1 onwards. Analysis of MSAS sub-domains indicated significant reductions in favour of ASyMS for global distress index (P<0.001), psychological symptoms (P<0.001), and physical symptoms (P<0.001). FACT-G scores were higher in the intervention group across all cycles (P<0.001), whereas mean scores for STAI-R trait (P=0.003) and STAI-R state anxiety (P=0.02) were lower. CASE-Cancer scores were higher in the intervention group (P=0.01), and most SCNS-SF34 domains were lower, including sexuality needs (P<0.05), patient care and support needs (P=0.03), and physical and daily living needs (P=0.01). Safety of ASyMS was satisfactory.

Conclusion
Significant reduction in symptom burden supports the use of ASyMS for remote symptom monitoring in cancer care. Remote monitoring systems will be vital for future services, particularly with blended models of care delivery arising from the covid-19 pandemic.

Trial registration: Clinicaltrials.gov NCT02356081

Funding Source:
This project has received funding from the European Union's Seventh Framework Programme for research, technological development and demonstration under grant agreement no 602289

References:
1. R. Maguire R, et.al.. BMJ. 2021 Jul 21;374:n1647. doi: 10.1136/bmj.n1647.
2. Furlong E, et.al. JMIR Cancer. 2019 Mar 14;5(1):e10813. doi: 10.2196/10813.
3. Maguire R, et.al.. BMJ Open. 2017 Jun 6;7(5)

e-Posters

eP1 Design, synthesis, and biological evaluation of orthosteric ligands for the muscarinic acetylcholine receptors

Marlon Millard,[1⊥] Jonas Kilian,[2⊥] Marius Ozenil,[2] Mariella Mogeritsch, Verena Maisetschläger, Wolfgang Holzer,[1] Helmut Spreitzer,[1] Marcus Hacker,[2] Thierry Langer,[1] Verena Pichler[1]

[1] Department of Pharmaceutical Sciences, Division of Pharmaceutical Chemistry, University of Vienna, Austria
[2] Department of Biomedical Imaging and Image-guided Therapy, Division of Nuclear Medicine, Medical University of Vienna, Austria
⊥ both authors contributed equally

Disclosure statement: The authors declare no conflicts of interest.

Keywords: Muscarinic acetylcholine receptors, orthosteric ligands

Objective
This interdisciplinary project aimed to develop and evaluate potent and selective orthosteric ligands targeting muscarinic acetylcholine receptor (mAChR) subtypes for potential diagnostic or therapeutic purposes. The starting point of the design and synthesis was a deazapurine scaffold, which has shown promising affinities towards mAChRs.

Methods and Materials
Initially, computational chemistry methods were used to design novel mAChRs ligands, such as docking and pharmacophore modelling. The most promising *in silico* designed compounds were synthesized and fully characterized by NMR, HRMS and HPLC. Physico-chemical characterization comprised stability, logP, clogP and tPSA. The ligands were further tested by a competitive radioligand binding, calcium-efflux and MTT assay.

Results
Overall, 16 compounds were successfully synthesized in high purity and were fully characterized. logP measurements revealed a lipophilicity ranging from 1.58 to 3.05. The structural modifications of the initial deazapurine scaffold increased affinity towards the mAChRs significantly, from low µM to a low double-digit nM range. The most promising hits advantageously showed high selectivity towards specific receptor subtypes – including the M5 subtype. Antiproliferative effect for all tested compounds were greater than 10 µM and therefore toxicity was not interfering with further cell-based assays. The calcium-efflux assay indicates antagonistic activity for all hits.

Conclusion
We successfully developed selective and potent mAChRs ligands, which were assessed with a comprehensive scope of chemical and biological assays. The most promising candidates will be subject for further investigations and optimizations.

eP2 Assessment of tumour cell plasticity in feline and equine papillomavirus-positive versus negative oronasal SCC

Carina Strohmayer[1], Andrea Klang[2], Ingrid Walter[3], Stefan Kummer[3], Christoph Jindra[4], Torben Redmer[5], Sibylle Kneissl[1], Sabine Brandt[4]

[1] Diagnostic Imaging, University of Veterinary Medicine, Vienna, Austria
[2] Department of Pathobiology, Institute of Pathology, University of Veterinary Medicine, Vienna, Austria
[3] VetCore Facility for Research, University of Veterinary Medicine, Vienna, Austria
Institute of Pathology, Department for Pathobiology, University of Veterinary Medicine, Vienna, Austria
[4] Research Group Oncology (RGO), Clinical Unit of Equine Surgery, University Clinic for Horses, University of Veterinary Medicine, Vienna, Austria
[5] Department of Biomedical Sciences, Institute of Medical Biochemistry, University of Veterinary Medicine, Vienna, Austria

Disclosure statement: The authors declare no conflicts of interest.

Keywords: Squamous cell carcinoma, horse, cat

Objective
Squamous cell carcinoma of the head and neck (HNSCC) is a common malignant tumour in humans and animals.[1-5] The ability of tumour cells to switch from epithelial to mesenchymal, endothelial or therapy-resistant stem cell-like phenotypes promotes disease progression and metastasis.[6] In animals, phenotype-switching is poorly understood. We screened papillomavirus (PV)-positive versus –negative equine and feline oronasal SCCs for expression of selected endothelial, mesenchymal and stem cell markers by immunohistochemistry (IHC) to address tumour cell plasticity.

Materials and Methods
DNA extracted from formalin fixed paraffin embedded (FFPE)-treated, native feline and equine oronasal SCC was PCR-screened for presence of carcinogenic PVs. FFPE-sections of PV-positive versus PV-negative tumours were analysed by IHC for the expression of cytokeratin, vimentin, COX2, β-catenin, CD271, and CD44.

Results
PV-PCR scored positive for 5/85 feline and 11/49 equine tumours. IHC from 15 PV- and one PV+ feline, and 11 PV- and 11 PV+ equine SCC revealed epithelial-to-mesenchymal transition events, with vimentin-positive cells ranging between <10 and >50%. The vast majority of tumours stained positive for CD44 and CD271, indicating the presence of stem cell-like cell phenotypes within lesions and infiltrative tumour cell fronts. These findings were in accordance with tumour stages.

Conclusion
Currently, reliable imaging markers for oronasal SCC prognosis and response to treatment in cats and horses are lacking. Our findings are suggestive for CD44 and CD271 representing interesting prognostic marker candidates for sensitive gadolinium-enhanced MR imaging of these tumours. In this context, we are looking for research cooperation to develop and test such a system.

Funding Sources: PhD Project Vetmeduni Vienna

References
1. Paver EC, Currie AM, Gupta R, Dahlstrom JE. Human papilloma virus related squamous cell carcinomas of the head and neck: diagnosis, clinical implications and detection of HPV. Pathology. (2020) 52(2):179–191. doi: 10.1016/j.pathol.2019.10.008.
2. Dixon PM, Head K. Equine nasal and paranasal sinus tumours: part 2: a contribution of 28 case reports. Vet J. (1999) 157:279–294. doi: 10.1053/tvjl.1999.0371.
3. Head KW, Dixon PM. Equine nasal and paranasal sinus tumours. Part 1: review of the literature and tumour classification. Vet J. (1999) 157:261–278. doi: 10.1053/tvjl.1998.0370.
4. Stebbins KE, Morse CC, Goldschmid MH. Feline oral neoplasia: a ten-year survey. Vet Pathol. (1989) 26: 121–128. doi: 10.1177/ 030098588902600204.
5. Bilgic O, Duda L, Sánchez MD, Lewis JR. Feline oral squamous cell carcinoma: clinical manifestations and literature review. J Vet Dent. (2015) 32:30–40. doi: 10.1177/089875641503200104.
6. Jayanthi P, Varun BR, Selvaraj J. Epithelial-mesenchymal transition in oral squamous cell carcinoma: An insight into molecular mechanisms and clinical implications. J Oral Maxillofac Pathol. (2020) 24(1):189. doi: 10.4103/jomfp.JOMFP_334_19.

eP3 Investigating the Impact of the Bit Depth of Fluorescence- Stained Images on the Performance of Deep Learning-Based Nuclei Instance Segmentation

Amirreza Mahbod [1], Gerald Schaefer [2], Christine Löw [1], Georg Dorffner [3], Rupert Ecker [4], Isabella Ellinger [1]

[1] Institute for Pathophysiology and Allergy Research, Medical University of Vienna, Vienna, Austria
[2] Department of Computer Science, Loughborough University, Loughborough, UK
[3] Section for Artificial Intelligence and Decision Support, Medical University of Vienna, Vienna, Austria
[4] Department of Research and Development, TissueGnostics GmbH, Vienna, Austria

Disclosure statement: The authors declare no conflicts of interest.

Keywords: bit depth, nuclei segmentation, deep learning

Objective
Nuclei instance segmentation can be considered as a key point in the computer-mediated analysis of histological fluorescence-stained (FS) images. Many computer-assisted approaches have been proposed for this task, and among them, supervised deep learning (DL) methods deliver the best performances. An important criterion that can affect the DL-based nuclei instance segmentation performance of FS images is the utilised image bit depth, but to our knowledge, no study has been conducted so far to investigate this impact.

Methods and Materials
We released a fully annotated FS histological image dataset of nuclei at different image magnifications and from five different mouse organs. Moreover, by different pre-processing techniques and using one of the state-of-the-art DL-based methods, we investigated the impact of image bit depth (i.e., eight bits vs. sixteen bits) on the nuclei instance segmentation performance.

Results
The results obtained from our dataset and another publicly available dataset showed very competitive nuclei instance segmentation performances for the models trained with 8-bit and 16-bit images. This suggested that processing 8-bit images is sufficient for nuclei instance segmentation of FS images in most cases.

Conclusion
In this study, we investigated the impact of image bit depth on the performance of DL-based nuclei instance segmentation using different datasets. Exploring the impact of image bit depth on other whole slide image analysis tasks can be addressed in future studies. Our created dataset including the raw image patches, as well as the corresponding segmentation masks is publicly available in the published GitHub repository: https://github.com/masih4/BitDepth_NucSeg

Funding Sources:
This research was funded by the Austrian Research Promotion Agency (FFG), No.872636.

Reference:
https://doi.org/10.3390/diagnostics11060967

eP4 Visual Outcomes after Anterior Temporal Lobectomy and transsylvian Selective Amygdohippocampectomy – A Quantitative Comparison of Clinical and Diffusion Data

P. Pruckner[1], M. S. Yildirim[1], E. Pataraia[1], C. Baumgartner[2], A. Reitner[1], K. Rössler[1], C. Dorfer[1], K-H. Nenning[1], G. Kasprian[1], S. Bonelli[1]

[1] Medical University of Vienna, Vienna, Austria
[2] Klinik Hietzing, Vienna, Austria

Objective
Anterior temporal lobectomy (ATL) and selective amygdalohippocampectomy (SAHE) are effective treatment strategies for intractable temporal lobe epilepsy [1] but may result in a contralateral superior visual field deficit (VFD). VFDs following epilepsy surgery are caused by intraoperative damage to portions of the optic radiation (OR). [2] This imaging study aimed to predict visual outcomes using DTI based connectomes.

Methods
Inclusion criteria were: existing perimetry data, artifact free DTI (b-value=800s/mm²,32 gradient encoding directions) and T13D datasets. Whole Brain Connectomes were calculated using MRTrix3 and tracts were extracted from standardized atlas regions. Results were then warped onto postoperative T1 images. OR damage was determined by measuring the volume overlap with the resection zone.

Results
34 patients (ATL:SAHE,50:50) were included. Altogether, 59% (20/34) showed postoperative VFDs (65% after ATL,53% after SAHE,p=0,235). There was a statistical tendency of ATL patients to show more severe VFDs (MD -3,36 vs. -1,18,p=0,09; OR damage 47ml vs. 8ml,p=0,082). Volumes of the damaged OR predicted postoperative VFDs with a sensitivity of 95% and a specificity of 50%. OR damage correlated with vision decline and could explain 55% of variance (r=-0,73,R^2=0,55, p=0,0001). When excluding three patients (ATL:SAHE = 1:2) with VFDs before surgery, quantified OR damage was able to explain 19% of variance (r=-0,44,R^2=0,19, p=0,02).

Conclusion
Using the presented DTI based method allows to predict VFDs in epilepsy-surgery patients. It is robust against interobserver variability since tracts are extracted from standardized atlas regions. VFD incidence and severity did not differ between SAHE and ATL.

Limitations
The retrospective design and use of single shell DTI data are limitations to this study. More patients are required to clarify potential VFD group differences.

References
1. Dorfer, C., T. Czech, and K. Rössler, *Chirurgie der Temporallappenepilepsie.* Zeitschrift für Epileptologie, 2020. **33**(1): p. 37-41.
2. Piper, R.J., et al., *Application of diffusion tensor imaging and tractography of the optic radiation in anterior temporal lobe resection for epilepsy: a systematic review.* Clin Neurol Neurosurg, 2014. **124**: p. 59-65.

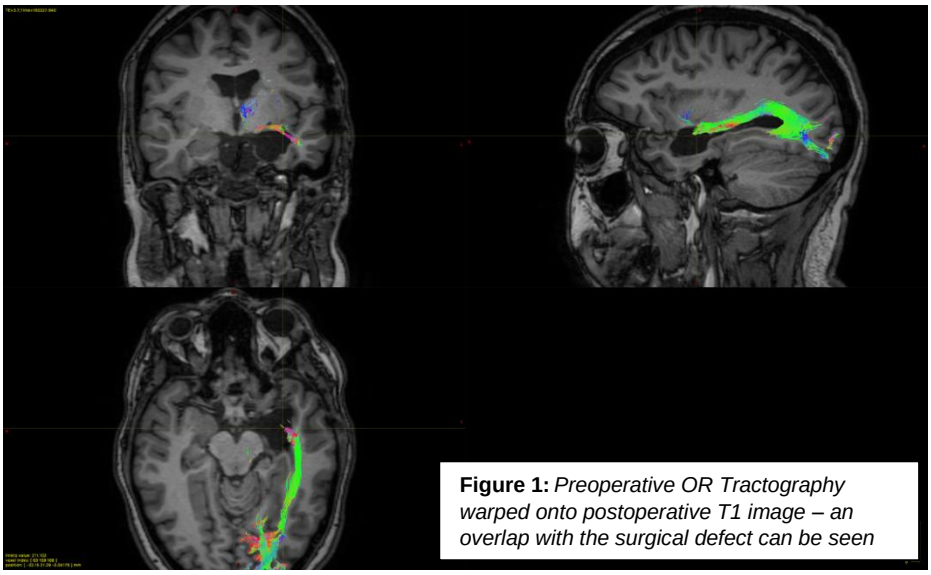

Figure 1: *Preoperative OR Tractography warped onto postoperative T1 image – an overlap with the surgical defect can be seen*

eP5 Imaging the functional and structural language network – lessons learned from preoperative fMRI

Mehmet Salih Yildirim[1], Victor Schmidbauer[1], Karl-Heinz Nenning[1], Philip Pruckner[1], Ekaterina Pataraia[1], Doris Moser[1], Christian Dorfer[1], Daniela Prayer[1], Christoph Baumgartner[2], Karl Rössler[1], Silvia Bonelli[1], Gregor Kasprian[1]

[1] Medical University of Vienna, Waehringer Guertel 18-20, 1090 Vienna, Austria
[2] Hospital Hietzing with Neurological Center Rosenhuegel, Riedelgasse 5, 1130 Vienna, Austria

Disclosure statement: The authors declare no conflicts of interest.

Keywords: fMRI, Epilepsy, Tractography

Objective
Structural and functional neuronal networks underlying atypical language lateralisation (ALL) in patients are poorly unknown. This study aimed to identify functional and structural connectivity differences in temporal lobe epilepsy (TLE) patients with ALL or left- hemispherical language lateralisation (LLL).

Methods:
22 TLE patients with ALL (rTLE: n=9, 4 lesional; lTLE: n=13, 4 lesional) and 29 with LLL (rTLE: n=13, 6 lesional; lTLE: n=16, 7 lesional) were included in this study. Activation pattern (AP) analysis was performed using SPM12. The CONN-toolbox was used for the functional connectome (FC) analysis. The structural connectome (SC) was studied with MRtrix3, based on single-shell DTI sequences.

Results
rTLE patients with ALL showed a sparse AP and weak functional language network. In contrast there were strong but more variable individual activations in the same group that may explain sparse activations by reduction in AP overlap. SC analysis showed a lateralisation of the structural connectivity of the inferior frontal gyrus to right hemisphere (mean laterality index:-0.04) in patients with ALL and to left hemisphere (mean laterality index:0.03) in patients with LLL. There is a significant difference between these two groups (two-tailed test:p-value:<0.001).

Conclusion
Language networks share a range of commonalities amongst right and left TLE patients. Atypical language connectome shows larger variability in TLE - especially in patients with rTLE. LLL and ALL language networks are supported by specific and asymmetric structural connectivity networks of the right and left hemisphere. Improved imaging based understanding of structural and functional language networks opens new diagnostic possibilities in modern neuroradiology.

eP6 Synthetic MRI-based Fast Gray Matter Acquisition T1 Inversion Recovery (FGATIR) Contrasts identify Neonatal Brainstem Pathways *in Vivo*

Schmidbauer Victor[1], Yildirim Mehmet Salih[1], Stuempflen Marlene[1], Dovjak Gregor[1], Goeral Katharina[2], Prayer Daniela[1], Berger Angelika[2], Kasprian Gregor[1]

[1] Department of Biomedical Imaging and Image-guided Therapy, Medical University of Vienna, Waehringer Guertel 18-20, 1090 Vienna, Austria
[2] Comprehensive Center for Pediatrics, Department of Pediatrics and Adolescent Medicine, Division of Neonatology, Pediatric Intensive Care and Neuropediatrics, Medical University of Vienna, Waehringer Guertel 18-20, 1090 Vienna, Austria

Disclosure statement: The authors declare no conflicts of interest.

Keywords: Neuroradiology, MRI, Neonatal imaging

Objective
SyMRI® allows to reconstruct different MRI contrasts using a single multi-dynamic multi-echo (MDME) sequence acquisition[1]. This study aimed to investigate the feasibility of synthetic MRI-based fast gray matter acquisition T1 inversion recovery (FGATIR) contrasts[2] for the qualitative identification of early myelinating neonatal brainstem pathways *in vivo*.

Methods and Materials:
Thirty-one cases of neonatal MRI (median gestational age at birth: 27+0; range, 23+4–41+6) were collected, which included MDME sequences and conventional T1- weighted/T2-weighted sequence acquisitions (standard-of-reference). MDME-based FGATIR contrasts (TR/TE/TI: 3000/5/410 ms) were generated using the MR data post-processing software SyMRI®. The identification of seven brainstem pathways was assessed on synthetic FGATIR contrasts and conventionally acquired T1- weighted/T2-weighted imaging data: decussation of superior cerebellar peduncle (DSCP); left/right medial lemniscus (ML); left/right central tegmental tract (CTT); and left/right longitudinal medial fascicle (LMF)[2].

Results:
SyMRI® provided FGATIR contrasts of diagnostic quality in 31/31 cases (100%). Based on MDME-based FGATIR contrasts, the DSCP [31/31 (100%)]; left/right ML [31/31 (100%)]; left/right CTT [20/31 (65%)]; and left/right LMF [31/31 (100%)] were reliably identified. Based on conventional T1-weighted contrasts, the DSCP [14/31 (45%)]; left/right ML [25/31 (81%)/23/31 (74%)]; left/right CTT [3/31 (10%)/7/31 (23%)]; and left/right LMF [15/31 (48%)] were reliably identified. Based on conventional T2-weighted contrasts, the DSCP [30/31 (97%)]; left/right ML [30/31 (97%)/29/31 (94%)]; left/right CTT [26/31 (84%)/25/31 (81%)]; and left/right LMF [30/31 (97%)] were reliably identified.

Conclusion:
Synthetic generation of FGATIR contrasts enables radiological identification of neonatal brainstem pathway anatomy *in vivo*. The investigated MR approach depicts early myelinating tracts more reliable than standard-of-reference contrasts.

References:
1. Schmidbauer V, Geisl G, Diogo M, Weber M, Goeral K, Klebermass-Schrehof K, et al. SyMRI detects delayed myelination in preterm neonates. *Eur Radiol*. 2019;29:7063–7072.
2. Shepherd TM, Ades-Aron B, Bruno M, Schambra HM, Hoch MJ. Direct in vivo MRI discrimination of brain stem nuclei and pathways. *AJNR Am J Neuroradiol*. 2020;41(5):777–84.

eP7 Continual Active Learning for Efficient Image Labelling while Image Characteristics Change

Matthias Perkonigg[1], Johannes Hofmanninger[1], Christian Herold [1], Helmut Prosch[1], Georg Langs[1]

[1] Department of Biomedical Imaging and Image-guided Therapy, Medical University of Vienna, Austria

Disclosure statement: The authors declare no conflicts of interest.

Keywords: Machine Learning, Scanner Adaptation, Segmentation

Objective
To develop a machine learning method for effectively choosing examples for ground truth labelling to adapt models to new scanners and image characteristics in a continuous stream of medical imaging data.

Methods and Materials
The proposed approach continuously trains models on a stream of imaging data by recognizing shifts in image acquisition characteristics and selecting optimal examples for labelling. Those examples are stored in a rehearsal memory to keep a machine learning model up-to-date, while at the same time not forgetting previous knowledge. A style embedding is extracted from each image to assign it to a pseudo-domain. Those pseudo-domains are used to balance the rehearsal memory and training procedure.
The benefits of the method were evaluated for cardiac MR image segmentation in 2D, on a data set of 7230 2D MR slices of the Multi-Centre, Multi-Vendor & Multi-Disease Cardiac Image Segmentation Challenge (M&Ms) challenge including four different scanners.

Results
Results showed that the method is capable of learning on a continuous stream, while keeping the number of required manual annotations low. The mean dice scores for the four scanners were 0.81, 0.73, 0.80 and 0.68 respectively, compared to continual training on the stream without the proposed method (0.82, 0.71, 0.76, 0.56) or a static model (0.81, 0.69, 0.72, 0.34).

Conclusion
The proposed method was capable of training models on a continuous stream of imaging data, with a limited labelling budget and outperformed baseline methods.

Funding Sources:
Austrian Science Fund (FWF): P 35189, Vienna Science and Technology Fund (WWTF): LS20-065, Novartis Pharmaceuticals Corporation.

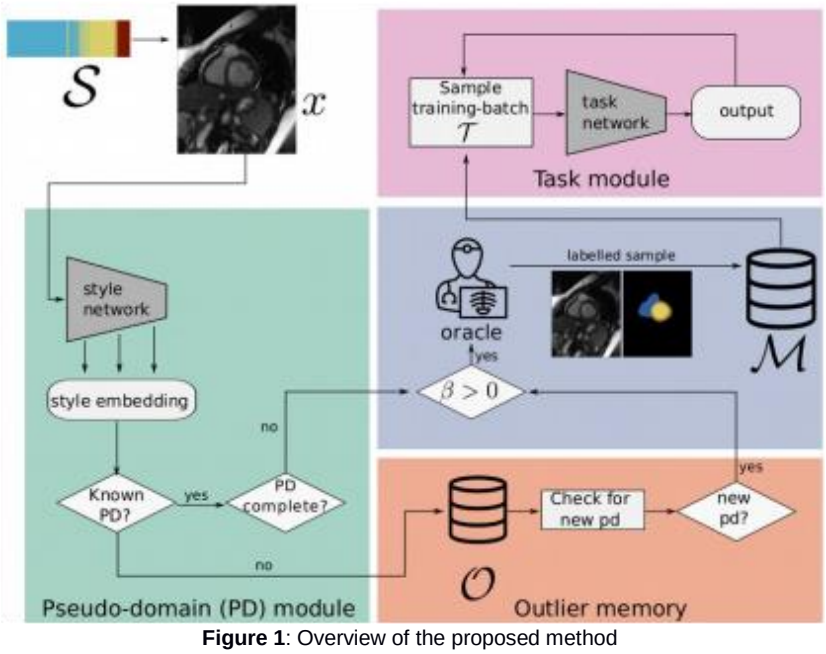

Figure 1: Overview of the proposed method

eP8 Stimulus-specific biases in population receptive field mapping

Michael Woletz[1], David Linhardt[1], Martin Tik[1], Allan Hummer[1], Christian Windischberger[1]

[1] Zentrum für Medizinische Physik und Biomedizinische Technik, Medizinische Universität Wien, Austria

Disclosure statement: The authors declare no conflicts of interest.

Keywords: fMRI, retinotopy, bias

Objective

Mapping the population receptive fields (pRFs) in the human visual system[3] has enabled insights into the visual systems and its disorders. This mapping technique is used to evaluate the retinotopic organisation of the human visual cortex, using BOLD-fMRI during a visual stimulation task[1]. Here we present a novel method of comparing the results of different stimuli on a group level based on voxelwise correspondences on the single-subject level.

Methods and Materials

All 181 subjects, published in the HCP 7T Retinotopy Dataset[2] were re-analysed for pRF estimates using analyzePRF[4] separated according to stimulus type, i.e. seperated into a combined wedge and ring, and a moving bar stimulus. Single-subject results were then sampled on a circular grid and group results were obtained by averaging the single-subject results at those points. Vector fields of the differences and the contrast between the stimuli were then plotted.

Results

The estimates obtained using the bar stimulus are shifted towards the centre of the visual field and show a slight difference in polar angle for areas outside a 3° radius, while they are relatively similar inside this radius compared to the wedge/ring stimulus. Also, pRF size estimates based on the bar stimulus tend to be higher compared to the combined wedge/ring stimulus.

Conclusion

We have presented a new method for generating group results using pRF estimates and used it to compare stimuli in a publicly available dataset. The consistent differences across visual areas indicate the stimulus dependence of the pRF mapping results.

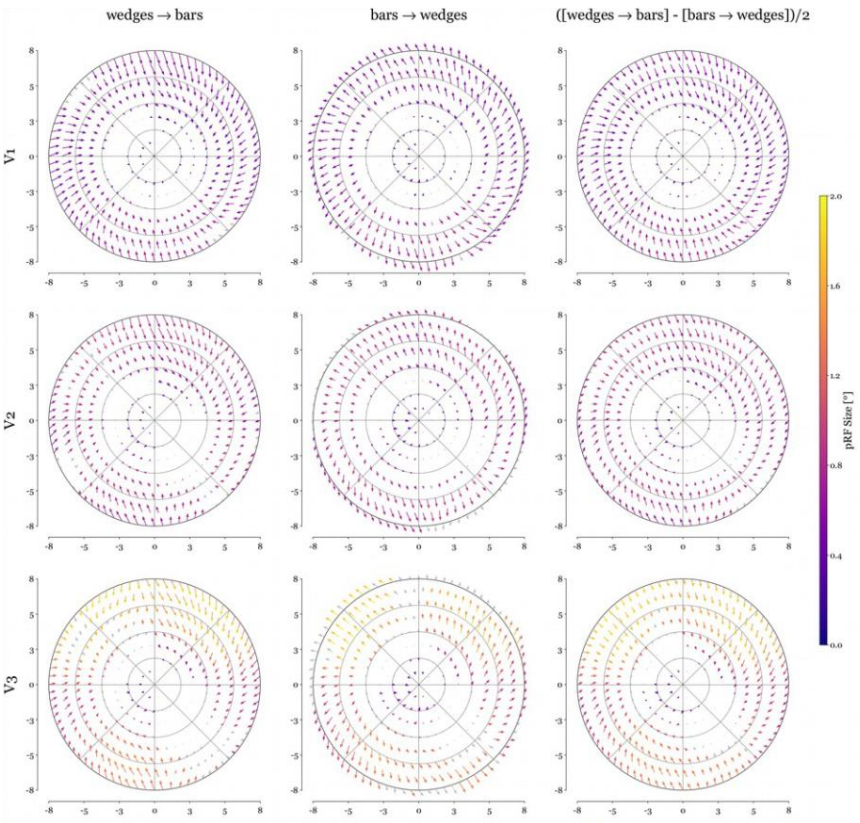

Figure 1 Shifts in the population receptive fields (pRFs) in terms of position and size from the wedge stimulus to the bar stimlus and vice versa for V1, V2 and V3, averaged across subjects as well as the contrast between both vector maps. The shaft of each arrow is at a position determined using one stimlus, while the tip points to the position estimated using the other stimulus. The colour at the shaft represents the size, that is the standard deviation of a 2D Gaussian, of the pRF in one stimulus, while the colour at the tip represents the size of the other stimulus. Arrows that failed a Bonferroni corrected significance test ($p < 0.05$) using a Hotelling's t-squared test are shown in grey. All positions are in degree of the visual field.

References:

1. Alverez, I. (2015), 'Comparing different stimulus configurations for population receptive field mapping in human fMRI', Frontiers in Human Neuroscience.
2. Benson, N.C. (2018), 'The Human Connectome Project 7 Tesla retinotopy dataset: Description and population receptive field analysis', Journal of Vision.
3. Dumoulin, S.O. (2008), 'Population receptive field estimates in human visual cortex', Neuroimage, vol. 39 no. 2, pp. 647-660.
4. Kay, K.N. (2013), 'Compressive spatial summation in human visual cortex', Journal of Neurophysiology.

eP9 The influence of EPI parameter choice on reliability of sgACC- DLPFC functional connectivity

M Vasileiadi[1], M. Tik[1], M. Woletz[1], D. Linhardt[1], C. Windischberger[1]

[1] MR Center of Excellence, Center for Medical Physics and Biomedical Engineering, Medical University of Vienna, Austria

Disclosure statement: The authors declare no conflicts of interest.

Keywords: resting-state fMRI, TMS, DLPFC

Objective
Clinical treatment efficacy of TMS targets on left DLPFC has been related to functional connectivity to the sgACC[1,2,3]. Resting-state fMRI (rs-fMRI) is increasingly used to derive these functional TMS targets in clinical settings[4] Therefore, the reliability of the acquired functional targets must be quantified and assessed. Here we examined the influence of echo time (TE) parameter choice on the reliability of the sgACC-DLPFC target network.

Methods and Materials
Three runs of rs-fMRI with short TE (30ms) and three with long TE (38ms) were acquired at 3 Tesla in five healthy subjects. Functional connectivity maps were calculated for each run and seed voxel correlations were computed with a seed in the sgACC. Intraclass Correlation Coefficients (ICC) were calculated for each TE. ICC values below 0.5, between 0.5 and 0.75, 0.75 and 0.90, and greater than 0.90 are considered to indicate poor, moderate, good and excellent reliability[5].

Results
Overall, similar functional connectivity networks were derived for both TE's. However, connectivity maps acquired with TE = 38ms showed higher ICC values within the DLPFC region. Specifically, the peak within the left DLPFC had a reliability value of 0.95 for TE = 38ms compared to 0.54 for TE = 30ms.

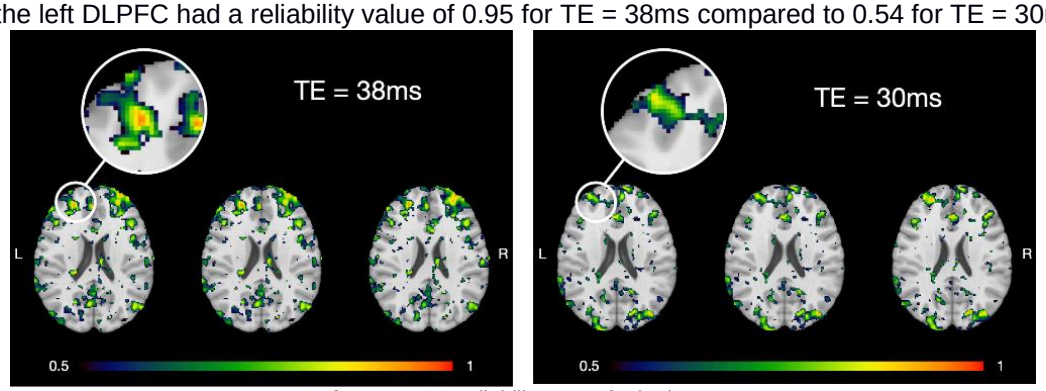

Figure 1. *ICC reliability maps for both TEs.*

Conclusion
Resting-state acquisition echo time affects the reliability of the resulting functional connectivity maps. This has an effect on TMS targeting approaches that base their DLPFC target on its functional connectivity to the sgACC. Our results clearly indicate that optimized acquisition parameters are beneficial for ensuring high-reliability resting-state acquisition protocols to be used for TMS targeting.

Funding Sources:
Austrian Science fund FWF P33180 Focus grant: ÖAW DOC Stipend

References:
1. Fox, M. D., Buckner, et al. (2012). Efficacy of transcranial magnetic stimulation targets for depression is related to intrinsic functional connectivity with the subgenual cingulate. *Biol psychiatry*, *72*(7), 595-603.
2. Salomons, T. V., Dunlop, et al. (2014). Resting-state cortico-thalamic-striatal connectivity predicts response to dorsomedial prefrontal rTMS in major depressive disorder. *Neuropsychopharmacology*, *39*(2), 488-498.
3. Cash, R. F., Weigand, A., et al. (2020). Using brain imaging to improve spatial targeting of transcranial magnetic stimulation for depression. *Biol psychiatry*.
4. Weigand, A., Horn, et al. (2018). Prospective validation that subgenual connectivity predicts antidepressant efficacy of transcranial magnetic stimulation sites. Biol psychiatry, 84(1), 28-37
5. Koo, T. K., & Li, M. Y. (2016). A guideline of selecting and reporting intraclass correlation coefficients for reliability research. *Journal of chiropractic medicine*, *15*(2), 155-163.

eP10 Towards objective scotomata assessment using fMRI-based retinotopic mapping: a connectomic approach

David Linhardt[1], Maximilian Pawloff[2], Michael Woletz[1], Martin Tik[1], Markus Ritter[2], Maria Vasileiadi[1], Ursula Schmidt-Erfurth[2], Christian Windischberger[1]

[1] Highfield MR Center, Center for Medical Physics and Biomedical Engineering, Medical University of Vienna, Austria
[2] Department of Ophthalmology and Optometry, Medical University of Vienna, Austria

Disclosure statement: The authors declare no conflicts of interest.

Keywords: fMRI, pRF mapping, visual field

Objective
fMRI combined with population receptive field (pRF) mapping allows for the assessment of visual field functionality (Ritter et al., 2018). The critical point in pRF-based scotomata assessment lies in setting the threshold between activated and non-activated voxels. Here we present a new method based on reference data (HCP) that enables automatic scotomata assessment independent of threshold levels.

Methods and Materials
Functional classification is based on the comparison of individual results to group reference data. For this, the HCP retinotopy dataset (Benson, 2018) including 181 healthy subjects was used. We quantified the relative number of pRF centres on a defined grid in the visual field. Following, we defined three levels in the classification: fully functional, dysfunctional, partly functional.
We tested our implementation on data of 20 healthy subjects with simulated scotomata acquired on our 7T scanner. For each subject, data consisted of a single 5min fMRI measurement including an artificial central scotoma of 2° radius.

Results
Figure 1 shows the results of one subject for different explained variance thresholds. The right column displays the standard coverage map, while results of the new scotomata assessment method are shown on the left. While coverage maps change considerably across threshold levels the new method shows perfect classification results for all thresholds.

Conclusion
When interpreting pRF mapping results on patients with retinal dysfunctions, the choice of the threshold has a tremendous influence on scotomata detection making objective staging on pRF results impossible. The suggested procedure yields the possibility for an unbiased investigation of scotomata, independent of the chosen threshold.

Funding Sources:
This work was supported by the Austrian Science Fund (FWF; grant numbers: KLI 670, P33180).

References:
Benson, N.C., Jamison, K.W., Arcaro, M.J., Vu, A.T., Glasser, M.F., Coalson, T.S., Van Essen, D.C., Yacoub, E., Ugurbil, K., Winawer, J., Kay, K., 2018. The Human Connectome Project 7 Tesla retinotopy dataset: Description and population receptive field analysis. Journal of vision 18, 23-23.
Ritter, M., Hummer, A., Ledolter, A.A., Holder, G.E., Windischberger, C., Schmidt-Erfurth, U.M., 2018. Correspondence between retinotopic cortical mapping and conventional functional and morphological assessment of retinal disease. British Journal of Ophthalmology.

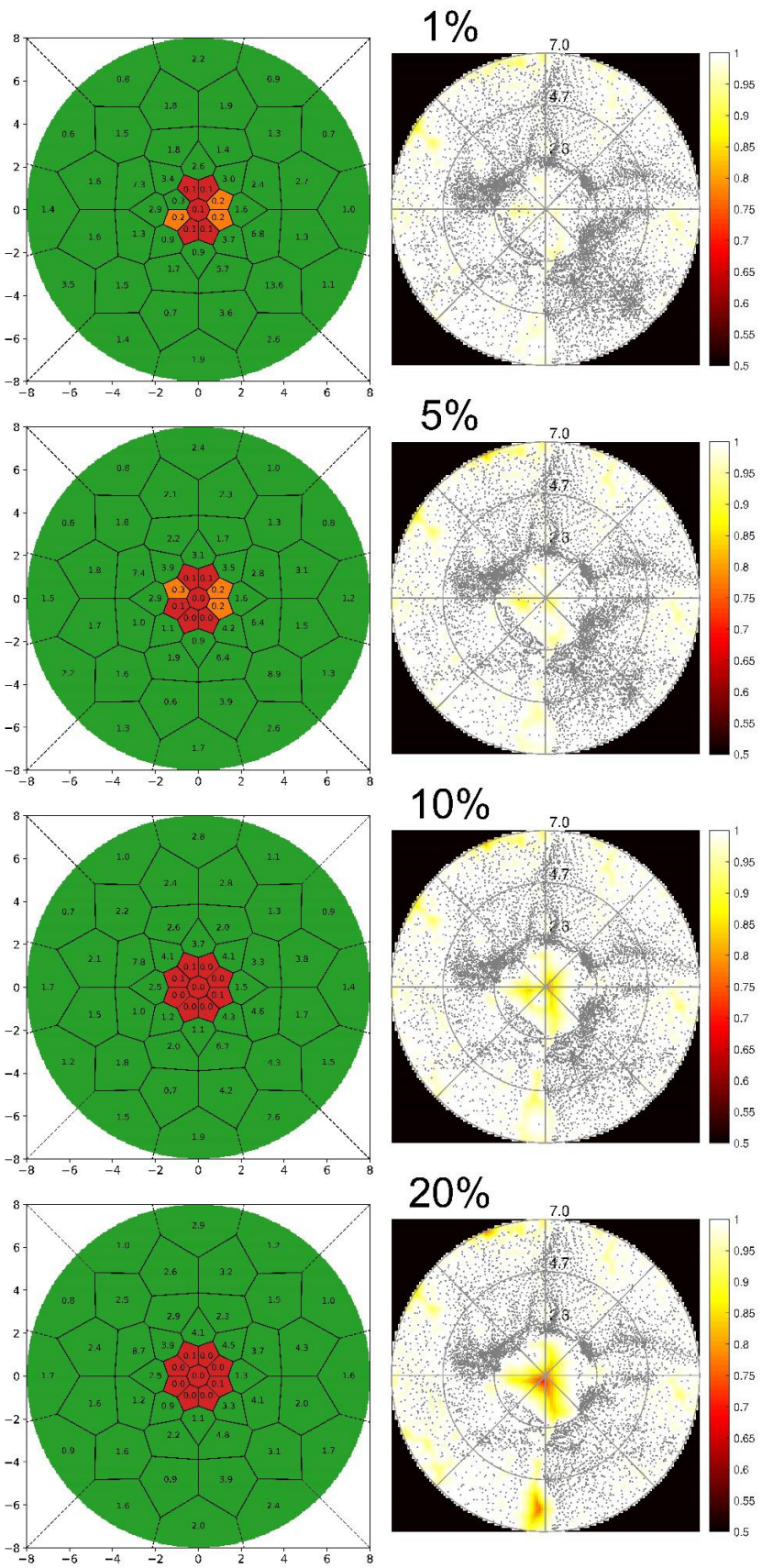

Figure 1: This figure shows pRF mapping results of an exemplary healthy subject's single run. These measurements were performed using a sweeping bar aperture with a simulated scotoma of 2° radius. Different rows indicate different variance explained thresholds. On the right-hand side, the classical coverage map as obtained from mrVista is shown. This map is flipped along the y-axis to rather be in the space of an ophthalmologic fundus image, than in visual field space. The detected scotoma varies a lot between different threshold coverage maps. The left column shows the novel plotting method based on a circular grid. Here, irrespective of the chosen variance explained threshold, the artificial scotoma is detected consistently.

eP11 Neuropsychological outcome prediction in epilepsy patients after surgery

Bianca Burger[1], Silvia Bonelli-Nauer[2], Karl-Heinz Nenning[1], Gregor Kasprian[1], Olivia Fösleitner[3], Victor Schmidbauer[1], Michelle Schwarz[2], Ekaterina Pataraia[2], Christoph Baumgartner[4], Karl Rössler[5], Doris Moser[6], Gudrun Mayr-Geisl[5], Christian Dorfer[5], Daniela Prayer[1], Georg Langs[1]

[1] Dep. of Biomedical Imaging and Image-guided Therapy, Medical University of Vienna, Austria
[2] Dep. of Neurology, Medical University of Vienna, Austria
[3] Dep. of Neurology, University of Heidelberg, Germany
[4] Dep. of Neurology, Hietzing Hospital, Austria
[5] Dep. of Neurosurgery, Medical University of Vienna, Austria
[6] Dep. of Oral and Maxillofacial Surgery

Disclosure statement: The authors declare no conflicts of interest.

Keywords: epilepsy, neuropsychological outcome prediction, AI

Objective

Epilepsy is a disabling disease[1]. If medication fails, surgical resection of seizure foci is an option to render patients seizure free, however, it may be accompanied by neuropsychological impairment such as language related difficulties. Predicting individual neuropsychological outcome is therefore important for doctors advising patients and deciding for surgical options.

Methods and Materials

We propose a graph variational auto-encoder[2] (GVAE) as feature extractor in a transfer learning setting due to the small but typical sample size of epilepsy patients. Input are the subject-specific unweighted connectivity matrix of the brain parcellated in 100 areas and corresponding mean fMRI time series. Output is only the connectivity matrix.
The GVAE was trained on a large cohort of resting-state fMRI data from healthy subjects and applied to the task-regressed fMRI data of epilepsy patients after completed training. Features for the epilepsy patients were extracted from the bottleneck layer and feature selection was performed using a random forest. Then selected features were used by a support vector machine to predict postoperative neuropsychological outcome, which was represented by 3 language-related tests whose outcome was either “bellow average” or “average and above”.

Results

Experiments show that our approach can predict results of 2 out of 3 tests with higher accuracy than using only chosen surgery type and/ or presurgical neuropsychological outcome for prediction. Prediction accuracy was calculated for 5 different seeds based on which a mean and 95% confidence intervals were calculated (Figure).

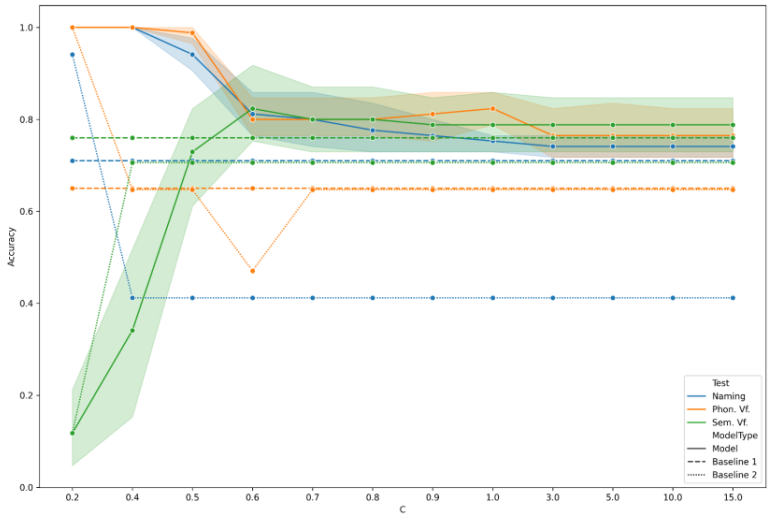

Conclusion

The features extracted can be used as complementary predictors of neuropsychological outcome.

Funding Sources:
Medical University of Vienna

References:

1. Devinsky, O., et al.: Epilepsy. Nat Rev Dis Primers 4, 18024 (2018).
2. Grover, A., *et al.*: Graphite: Iterative generative modeling of graphs. In: Chaudhuri,K.; Salakhutdinov, R. (ed.) Proceedings of the 36th International Conference onMachine Learning. Proceedings of Machine Learning Research, vol. 97, pp. 2434–2444. PMLR (09–15 Jun 2019), http://proceedings.mlr.press/v97/grover19a.html,code: https://github.com/ermongroup/graphite

eP12 Evaluation of the protective layer formation of Ophthalmic Viscosurgical Devices in ex vivo porcine eyes using intraoperative Optical Coherence Tomography

Philipp Matten[1], Melanie Wüst[1,2], Anja Britten[1], Wolfgang Drexler[1], Rainer A. Leitgeb[1], and Tilman Schmoll[1,3]

[1] Center for Medical Physics and Biomedical Engineering, Medical University of Vienna, Austria
[2] Dep. of Appl. Sciences and Mechatronics, Muenchen University of Applied Sciences, Germany
[3] Carl Zeiss Meditec Inc., Dublin (CA), United States of America

Disclosure statement: The authors declare no conflicts of interest.

Keywords: optical coherence tomography, ophthalmic viscosurgical devices, medical image segmentation

Objective
In patients undergoing cataract surgery, the most frequently performed ophthalmic surgery [1], fragments of the lens swirl around and can cause damage to the corneal endothelium – for the prevention of which a viscose liquid is injected, a so called Ophthalmic Viscosurgical Device (OVD). These protective layers have previously been evaluated [2,3], however, never utilizing Optical Coherence Tomography (OCT) over a large field of view (FOV), which is the aim of this work.

Methods and Materials
We performed mock cataract surgeries on 100 ex-vivo porcine eyes, divided into groups of ten eyes each, where every group was injected with a different OVD. We performed irrigation and aspiration (I/A), followed by phacoemulsification (phaco). After each step a OCT-volume was acquired. Each volume scan covered a FOV of 2.9x6x6 mm^3 (see Fig. 1 (2)). We also developed a data processing pipeline, including a deep CNN, which was capable of segmenting the data semi-automatically as well as determining the thickness of the residual layers (see Fig. 1 ((1) A-C)).

Results
We found that, after semi-automatic segmentation of the data, there are significant differences (see Fig. 1 (3)) in the residual layer thickness between the different steps during cataract surgery. We also found that the topology of the layers is very undulating over the large FOV (see Fig. 1 (4)).

Conclusion
We reported for the first time that there are significant differences in the residual layer thickness between the different types of OVDs. This has not been shown before over such large FOVs, utilizing OCT [4].

Funding Sources:
Advanced Development project of Carl Zeiss Meditec AG, Oberkochen, Germany

References:
[1] M. Wenzel et al., OPHTHALMO-CHIRURGIE 31: 347–357 (2019).
[2] Yoshino M, et al. (2009). Jpn J Ophthalmol 53(1):62–64. doi:10.1007/s10384-008-0601-3
[3] Mori H, et al. (2018). Heliyon 4(9):e00822. doi:10.1016/j.heliyon.2018.e00822
[4] P. Matten et al., ARVO Annual Meeting 2021, Abstract#3543230

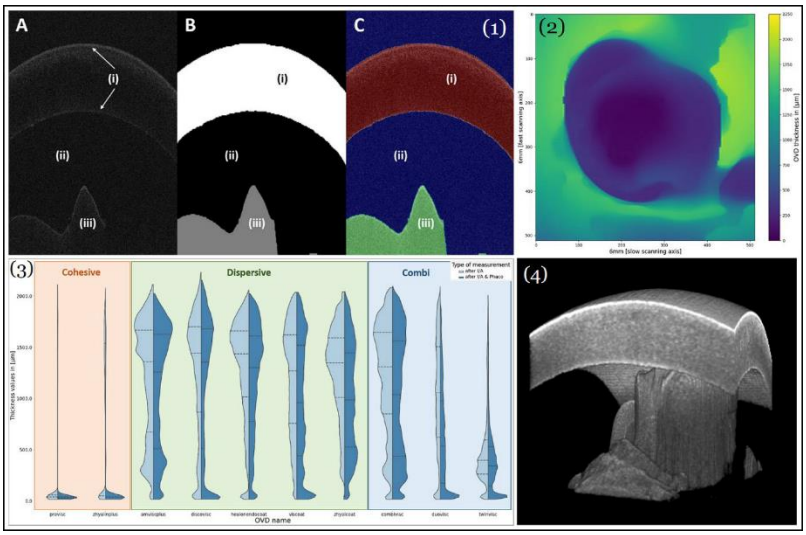

Figure 1: (1) Segmented B-scans. (i) Cornea of ex vivo porcine eye, (ii) OVD layer (signal void), (iii) milk-BSS-solution. Images after different parts of segmentation; A: original B- scan, B: segmented B-scan in greyscale; C: false-color overlay of segmented masks, where (ii) indicates the residual OVD layer; (2) Heat map of the OVD thickness layer over a FOV of 6x6mm^2; (3) Violin plots of the combined thickness value distributions (light blue after I/A and dark blue after I/A and phaco) for all OVDs. The three different groups of OVDs (cohesive, dispersive and combi-systems) are highlighted and grouped together; (4) 3D- rendering of the segmented cornea (hyperbolic top layer) and milk-BSS-solution (mountainous structure on the bottom).

eP13 Detection of Amplitude Modulated Glottal Area Waveforms: Application to Detecting Disorders of the Vocal Folds

Vinod Devaraj[1,2], Philipp Aichinger[1]

[1] Dept. of Otorhinolaryngology, Division of Phoniatrics-Logopedics, Medical University of Vienna, Austria
[2] Signal Processing and Speech Communication Lab, Graz University of Technology, Austria

Disclosure statement: The authors declare no conflicts of interest.

Keywords: High-speed videos, glottal area waveforms, voice quality

Objective
Characterization of voice qualities is important for the clinical care of disordered voices. Vocal fry is a voice qualiity that is characterized by individually audible glottal pulses, which may be a sign of a voice disorder [1, 2, 3]. The aim is to detect amplitude modulated glottal area waveform (GAW) segments frequently found in vocal fry.

Methods and Materials
Three hundred and ninty eight high-speed videos of vocal fold vibration and audio files were recorded simultaneously for sustained phonation of vowels. GAWs are extracted from the high-speed videos using deep neural networks [4]. The GAWs are annotated with regard to the presence or absence of amplitude modulation. The corresponding audio files are annotated with regard to the presence or absence of vocal fry. The intersection set is the positive group.
The extracted GAWs are modelled using an analysis-by-synthesis approach [5]. Modelling errors are used as features for distinguishing modulated and unmodulated segments using a support vector machine (SVM) followed by a hidden Markov model (HMM).

Results
For amplitude modulated GAW segments, the model resulted in a better modelling error than for the unmodulated segments. The difference is exploited for explainable detection of amplitude modulated vocal fry GAW segments which resulted in a sensitivity and specificity of 0.79 and 0.92 respectively.

Conclusion
The results indicate the possibility of detecting amplitude modulated vocal fry GAW segments. Prediction accuracy could possibly be improved by analysing the regularity and symmetry of vocal fold vibration. Preliminarily, spatial bimodality of the vocal fold vibration frequency is used to distinguish vocal fry from other voice qualities.

Funding Sources:
This work was supported by the Austrian Science Fund (FWF), KLI 722-B30 and the University Hospital Erlangen kindly provided the segmentation tool.

References:
[1] J.Kane, T.Drugman, and C.Gobl. “Improved automatic detection of creak“. *Computer Speech & Language 2013*, *27*(4), 1028-1047.
[2]. C.T. Ishi, K. I. Sakakibara, H. Ishiguro, and N. Hagita. “A method for automatic detection of vocal fry“. *IEEE transactions on audio, speech, and language processing 2008*, *16*(1), 47-56.
[3] R.Ylitalo, and B.Hammarberg. “Voice characteristics, effects of voice therapy, and long-term follow- up of contact granuloma patients“. *Journal of Voice 2000*, *14*(4), 557-566.
[4] Glottis Analysis Tools (GAT-2018), Computer Program: Version 5; Department of Phoniatrics and Pediatric Audiology, University Hospital Erlangen: Erlangen, Germany
[5] V.Devaraj, P. Aichinger. “Modelling of Amplitude Modulated Vocal Fry Glottal Area Waveforms Using an Analysis-by-Synthesis Approach”. *Applied Sciences 2021*, *11*(5), 1990.

eP14 Prediction of Neoadjuvant Chemotherapy Response of Breast Cancer using Deep Learning based on Ultrasound Images

Christoph Fürböck[1], Georg Langs[1], Pascal A. T. Baltzer[1], Paola Clauser[1], Thomas H. Helbich[1], Panagiotis Kapetas[1]

[1] Department of Biomedical Imaging and Image-guided Therapy, Medical University of Vienna, Vienna, Austria

Disclosure statement: Georg Langs: Shareholder and Co-Founder contextflow GmbH.

Keywords: deep learning, breast cancer, ultrasound

Objective
Use pre-therapeutic, B-mode ultrasound (US) images to predict non-responders after neoadjuvant chemotherapy (NAC) with a deep learning algorithm.

Methods and Materials
The dataset for this study includes 203 patients with histologically confirmed invasive breast cancer. Each patient underwent NAC and postoperative histology is used as the reference standard. Pathological complete response (pCR) is defined as the lack of invasive tumor in the breast or metastases in the axillary lymph-nodes. 120 patients have not achieved pCR after NAC (59.1% of all patients).
For each tumor a representative B-mode US image has been selected from the baseline examination. A resnet18 based neural network is trained on these images to predict the treatment outcomes complete response (CR) vs. non-complete response (non-CR). 10-fold cross-validation is used for training and validation. The performance of the algorithm is evaluated by descriptive statistics.

Results
The overall accuracy of the model is 76%. Concerning the prediction of non-responders in the validation set the model demonstrates a sensitivity of 88% with a specificity of 59% and has a positive and negative predictive value of 76% and 78%.

Conclusion
This deep learning model based on baseline, pre-treatment breast ultrasound images has the potential to aid in the prediction of breast cancer patients, who do not respond to NAC.

eP15 Cell-graphs for quantifying architectural changes in kidney histomorphometry

Christopher Kaltenecker[1], Maximilian Köller[1], Maximilian Gletthofer[1], Renate Kain[1]

[1] Department of Pathology, Medical University of Vienna, Austria

Disclosure statement: The authors declare no conflicts of interest.

Keywords: kidney pathology, neural network, artifical intelligence

Objective

Tissue sections represented by digital whole slide images (WSIs) contain morphological evidence of diseases, but integrating all this information – especially on serial sections with multiple stains – is tedious and often not done objectively, i.e. by statistical means. Here we extract patch-wise image features (embedded into graph nodes) and generate graph networks on varying abstraction levels – cellular to superstructures – to quantify histomorphological alterations in diseased vs. healthy kidney tissue.

Methods and Materials

A slide scanner produced WSIs of routinely stained human kidney sections. The python package “histocartography” was used to detect cell nuclei and generate cell graphs. Graph size was limited by cell distance (k-nearest neighbors) or based on annotations corresponding to kidney structures (tubular, glomerular).

Results

Cell-graphs could be generated from different stains (hematoxylin eosin, acid fuchsin orange G, periodic acid-schiff). Since this is work-in-progress, results from graph neural network analysis will be presented at the conference.

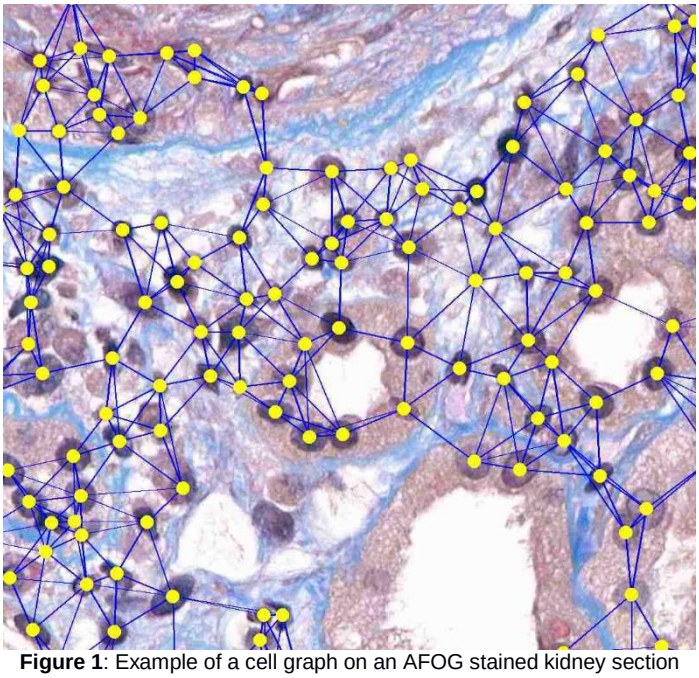

Figure 1: Example of a cell graph on an AFOG stained kidney section

Conclusion

Graph representations of complex kidney architecture can be used to programmatically access and compute on large scale histopathological image databases.

References:

https://github.com/histocartography/histocartography

eP16 A Graph Neural Network for the Reconstruction of Undersampled Concentric ring k-space data

Paul Weiser[1], Stanislav Motyka[2], Wolfgang Bogner[2], Georg Langs[1]

[1] Computational Imaging Research Lab, Department of Biomedical Imaging and Image-guided Therapy, Medical University of Vienna, Austria
[2] High Field MR Center, Department of Biomedical Imaging and Image-Guided Therapy, Medical University of Vienna, Austria

Keywords: Magnetic Resonance Spectroscopy Imaging, Deep Learning, k-space Reconstruction

Objective
To accelerate the acquisition time of Magnetic Resonance Spectroscopic Imaging (MRSI) with a deep learning approach, a novel graph neural network (GNN) is proposed for the reconstruction of undersampled k-space data.

Methods and Materials
Non-water suppressed MRSI data was collected from 7 volunteers in 10 random positions. In each MRSI scan concentric ring trajectories in k-space (16 rings, 388 points per ring) were acquired. Based on a acquisition a graph was defined. Each k-space point defines a node and an edges connects point pairs with a distance less than 1.5 times Nyquist criterion. During training the inner 6 rings were not changed, and every second outer ring was undersampled, resulting in an acceleration factor of R=1,45. The GNN consists of 4 gaussian mixture model (GMM) convolutional layers with a tanh activation function between each two layers. As comparison a naive GRAPPA approach was implemented. The trajectories were spilt up in segments with a width of 24 nodes and a length of all 16 rings. The GRAPPA weights were optimized on the inner 6 fully sampled rings and used to re- construct the missing outer rings of its segment.

Results
Our model was trained on data of 6 volunteers and evaluated on 4 positions of the 7th volunteer. We could achieve a mean squared error of 137.0, 55.7, 42.5, 126.9 compared to naive GRAPPA with 5908.9, 6713.1, 2610.4, 7548.6.

Conclusion
It could be shown that Graph Neural Networks are an excellent choice for the reconstruction undersampled k-space MRSI data.

Funding Sources
Austrian Science Fund (FWF): P 35189 & P 34198-N, Vienna Science and Technology Fund (WWTF): LS20-065

eP18 Parameter vs logfile based 4D proton dose tracking for small movers

F. Lebbink[1,2], S. Stocchiero[1], E. Engwall[3], M. Stock[2], D. Georg[1], B. Knäusl[1,2]

[1] Medical University of Vienna, Department of Radiation Oncology, Vienna, Austria
[2] MedAustron Ion Therapy Centre, Medical Physics, Wiener Neustadt, Austria
[3] RaySearch Laboratories AB, Stockholm, Sweden

Objective

The prerequisite for improving treatment concepts for moving targets in particle therapy is the quantification of the interplay effect. While retrospective logfile based analysis gives insight into the patient's breathing and beam-delivery dynamic, prospective 4D dose-tracking (4DDT) allows patient-specific adaptations.

Methods

Dose distributions of 6 cancer patients (3 pancreas and 3 liver) with motion amplitudes <4mm treated with scanned pulsed proton beams were analysed. 4DDT was performed: (1) file-based (f-4DDT) considering accelerator and breathing time-structure; (2) parameter-based (p-4DDT) (input parameters: dose rate, scanning speed and breathing cycle length). Both methods tracked the static dose on 8 4DCT phases followed by the accumulation on the planning CT using deformable image registration. Evaluation tools were DVH parameters and γ-pass rates (2%/2mm).

Results

D50% for target structures was accurate within 1% considering the interplay effect. Static D98% was disturbed up to 7% for the PTV and up to 2% for the CTV for 5/6 patients. The two 4DDT methods agreed within 2% for D98% and D2% for PTV and CTV for 5/6 patients but increased up to 7% for one liver patient (Fig1). For liver patients D33%_liver deviated up to 14% comparing the two tools, while for pancreas patients D1%_stomach varied up to 6.5%. The γ-pass rate > 91% confirmed the usability of p- 4DDT for dose prediction (Fig1).

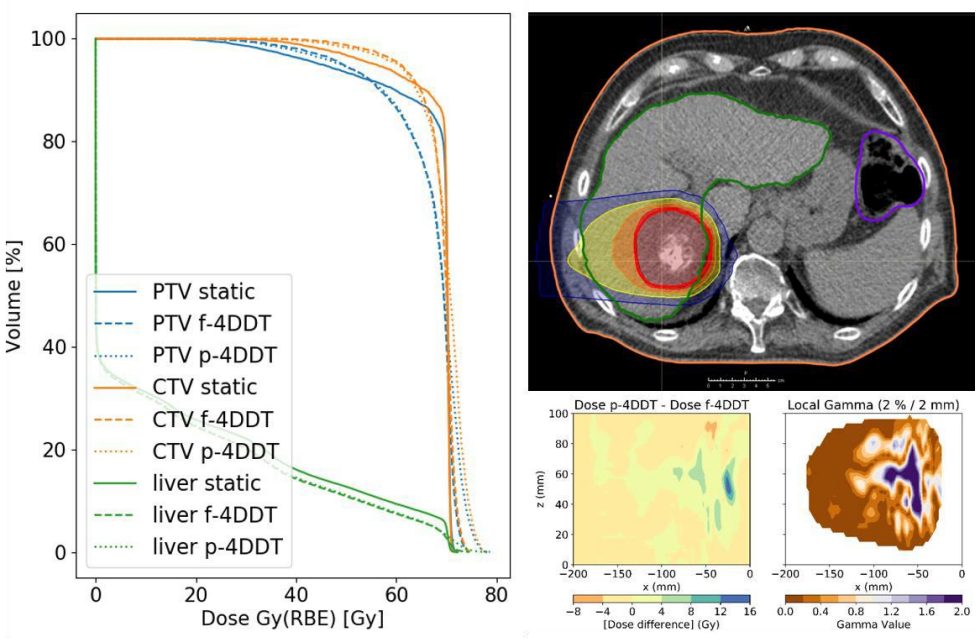

Figure 1 DVH curves, planned dose, dose difference and gamma analysis of liver patient #1

Conclusion

P-4DDT could be used prospectively to determine the impact of beam and organ motion in proton therapy. The systematic uncertainties covered by PTV margins compensated for the motion effects preserving the CTV coverage.

eP19 Deep learning automatic applicator-based MRI registration in image guided adaptive brachytherapy

Stefan Ecker[1], Lukas Zimmermann[1], Christian Kirisits[1], Nicole Nesvacil[1]

[1] Department of Radiation Oncology, Medical University of Vienna, Austria

Keywords: Image-guided Brachytherapy, Deep Learning, Image Registration

Objective

MRI based image-guided adaptive brachytherapy (IGABT) is considered state of the art for treatment of cervical cancer. Currently, applicator-based rigid registration of two MRIs from subsequent fractions is time-consuming, but important to monitor organ motion.
We compare different image registration algorithms for MR-IGABT and train a neural network (NN) to predict the applicator structure to automate the registration process.

Methods and Materials

A cohort of 56 patients was available for this study. MR-images had in-plane resolution of 256x256 (1.17 mm), and 5 mm slice thickness.
The contours of the applicator, which are usually not available were generated with an Elekta Applicator Slicer research plugin and treated as ground-truth masks.
Automatic registration of the image pairs was performed with five different registration algorithms written in Python.
As ground-truth masks would not be available in clinical routine, a NN (UNET, implemented in PyTorch) was trained to predict the applicator. The best performing registration algorithm was re-run with the output of the NN.
Registration results were evaluated, using the root mean squared error of the applicator dwell positions (RMSE). Performance of the NN was measured using the DICE-coefficient.

Results

The best algorithm achieved an RMSE with ground-truth and predicted mask of 0.7 ± 0.5 mm and 2.7 ± 1.4 mm, respectively. Mean DICE of the predicted applicator masks is 0.7 ± 0.07.

Conclusion

This study shows that automatic applicator-based image registration for MR-IGABT could be achieved by combining classical image registration algorithms with modern deep learning methods.

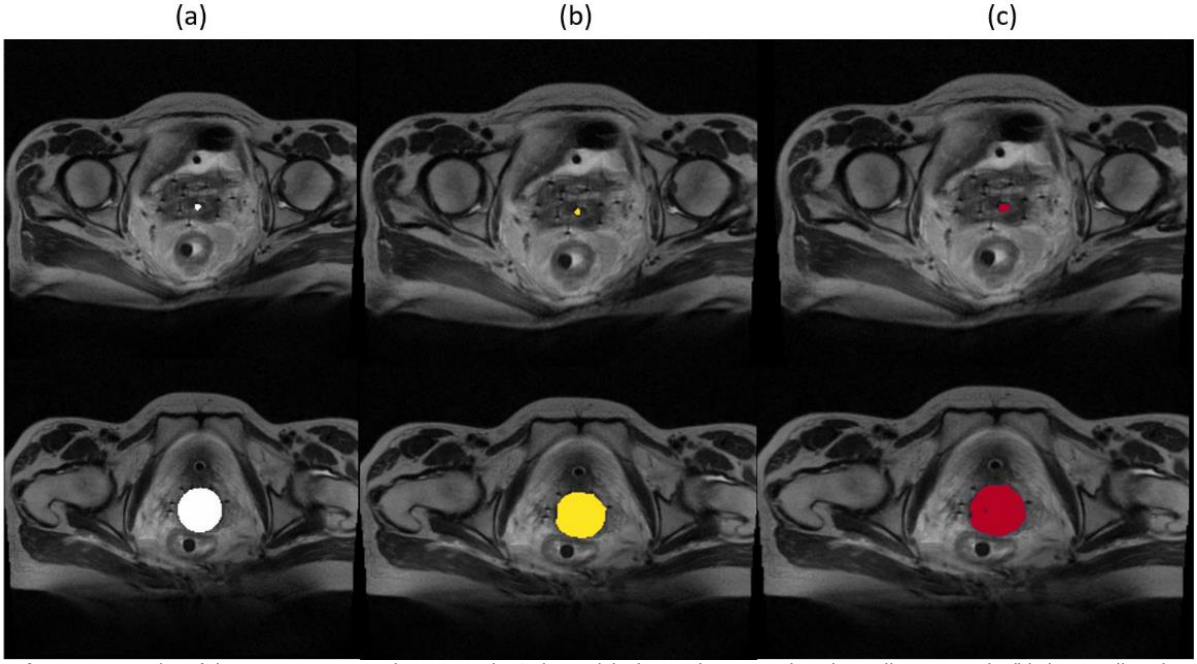

Figure 1: Results of the auto-segmentation network. Column (a) shows the ground truth applicator mask, (b) the predicted mask, and (c) the transformed mask from the moving fraction

eP20 Imidazole-osmium reduces elution of lipids from cryofixed rat hepatic tissue for ultrastructural analysis

Sabine Dürr[1], Siegfried Reipert[2], Martin Kršsák[1], Cécile Philippe[3], Viktoria Ehret[1], Matthias Luft[4,5,6], Arno Schintlmeister[7], Thomas Scherer[1], Clemens Fürnsinn[1]

[1] Department of Medicine III, Medical University of Vienna, Vienna, Austria
[2] Core Facility Cell Imaging and Ultrastructural Research, University of Vienna, Vienna, Austria
[3] Division of Nuclear Medicine, Department of Biomedical Imaging and Image-Guided Therapy, Medical University of Vienna, Vienna, Austria
[4] Clinical Laboratory for Bionic Extremity Reconstruction, Department of Plastic, Reconstructive and Aesthetic Surgery, Medical University of Vienna, Vienna, Austria
[5] Center for Biomedical Research, Medical University of Vienna, Vienna, Austria
[6] Karl Landsteiner University of Health Sciences, Department of Plastic, Aesthetic and Reconstructive Surgery, University Hospital St. Poelten, St. Poelten, Austria
[7] Department of Microbiology and Ecosystem Science/Large-Instrument Facility for Environmental and Isotope Mass Spectrometry, University of Vienna, Vienna, Austria

Disclosure statement: The authors declare no conflicts of interest.

Keywords: androgen receptor, [^{18}F]FDHT, prostate cancer

Objective
Transmission electron microscopy (TEM) is the main tool for studying the ultrastructural properties of metabolically diseased tissue. For impactful micrographs as well as for interpretation of TEM specimens, the integrity of cellular components is crucial. Elution of substances is a major problem in TEM preparation with no universal solution found so far. Investigating fatty liver disease in a rat model, an important factor is the depiction of undamaged lipid droplets. Imidazole, a highly polar heterocyclic compound, is hypothesized to enhance the binding ability of osmium tetroxide. This study aimed to investigate the effect of imidazole-osmium application before cryopreparation to prevent elution from lipid droplets.

Methods
Perfusion-fixed (4.5 % phosphate buffered formaldehyde, pH 7) hepatic tissue from male Sprague-Dawley rats (n=6; 8 weeks old) on high fat diet (60% of calories as fat; fed for 4 weeks) was processed for TEM. Prior to the procedure of high pressure freezing and freeze substitution, samples (n=3) were pre-exposed to 1% OsO4 in 0.1M imidazole for 30 min. For comparison, a control group was not subject to such pre-exposure (n=3). Specimens were embedded in Agar 100 resin, and the ultrastructure was analyzed in ultrathin sections (70 nm, Leica EM UC7; ZEISS Libra 120 TEM).

Results
Screening a multitude of ultrathin sections from steatotic rat livers from three separate animals revealed expletive electron dense material within the membrane of lipid droplets in imidazole-osmium pre-treated tissue. At variance to this, the conventional approach without imidazole pre-treatment displayed translucent areas with minimal granular content.

Conclusion
The chemical bond between osmium tetroxide and imidazole obviously reduced the elution of contrastable lipid molecules from lipid droplets prior to preparation and high pressure freezing with freeze substitution. This procedure promises a major advantage in the ultrastructural study of fat accumulation in hepatic tissue. Further investigations including NanoSIMS (Nanoscale secondary ion Mass Spectrometry) will be conducted to confirm this hypothesis.

Funding Source: WWTF LS19-046

eP22 pathoDISCO-HE: Ultramicroscopy and fluorescent labelling of glioblastoma multiforme for 3D virtual H&E imaging and improved pathohistological evaluation

James Oakes[1,2], Sabina Kirnbauer[1], Saiedeh Saghafi[2], Klaus Becker[2], Adelheid Wöhrer[3], Georg Widhalm[4], Hans-Ulrich Dodt[1,2]

[1] Section for Bioelectronics, Centre for Brain Research, Medical University of Vienna, Austria
[2] Department of Bioelectronics, Institute for Solid State Electronics, TU Vienna, Austria
[3] Institute of Neurology, Medical University of Vienna, Austria
[4] Department of Neurosurgery, Medical University of Vienna, Austria

Disclosure statement: The authors declare no conflicts of interest.

Keywords: glioblastoma, tissue clearing, ultramicroscopy

Objective
Traditional evaluation of glioblastoma relies on haematoxylin and eosin (HE) staining of sectioned tissue. Whilst this technique allows excellent visualisation of nuclei and cytoplasm alike, there are a number of limitations. For example, only a small number of sections from each case can be analysed meaning that key diagnostic features may be missed. To circumvent this problem we aimed to develop a novel technique for 3D-imaging of large glioblastoma specimens with HE-like labelling.

Methods
We identified cresyl violet as a suitable fluorescent haematoxylin analogue for nuclei labelling in glioblastoma. This was followed by rapid tissue clearing using a pathoDISCO approach. Subsequently, samples were imaged with high resolution by ultramicroscopy; two stacks were recorded – one exhibiting nuclear labelling by cresyl violet, the other recording autofluorescence to serve as an eosin analogue. Subsequently, stacks were processed using a false-colouring algorithm to produce virtual HE images, which were then volumetrically rendered.

Results
This approach allowed us to visualise glioblastoma samples in 3D with HE-like labelling in a comparable timeframe to standard HE preparations. Various hallmark histological findings of glioblastoma were identified in our virtual HE images, indicating accurate recapitulation of staining patterns seen in standard HE preparations. In addition, we were able to visualise glioblastoma vasculature with a high level of detail.

Conclusion
This study represents an exciting and novel approach to 3D histopathology of tumour specimens. 3D virtual histopathology has the potential to revolutionise and improve the way cancers are diagnosed, possibly leading to better informed treatment regimens and patient outcomes.

Funding sources:
WWTF (CS 18-019), FWF (P 31263)

eP23 Structural and functional assessment of muscle regeneration utilizing multimodal imaging and deep learning volumetry following peripheral nerve injury in rats

Supper P[1], Leitner S[2], Vraka C[3], Shiyamsundar L[4], Techt LM[2], Semmler L[1], Millesi F[1], Wiesner P[1], Hacker T[3], Helbich M[3], Zeilinger M[2], Radtke C[1]

[1] Medical University of Vienna, Department of Plastic, Reconstructive and Aesthetic Surgery, Austria
[2] University of Applied Sciences Wiener Neustadt, MedTech, Austria
[3] Medical University of Vienna, Department of Radiology and Nuclear Medicine, Austria
[4] Medical University of Vienna, Center for Medical Physics and Biomedical Engineering, Austria

Disclosure statement: The authors declare no conflicts of interest.

Keywords: multimodal imaging, peripheral nerve regeneration, deep learning

Objective
Neuromuscular injury results in dramatic changes of muscle structure and function. The following muscle atrophy is marked by decreased volume and metabolic disbalance. Current clinical assessment using physical examination and electromyography is limited in differentiating atrophy and incipient regeneration.

Methods and Materials
Computed tomography (CT) and positron emission tomography (PET) using fluorodeoxyglucose protocols were established in healthy Sprague-Dawley rats. Threshold-based segmentations of 20 hind limbs enabled manual volumetry for training of a deep-learning algorithm for semi-automated volumetry. Following peroneal nerve injury, 12 rats were examined weekly by PET-CT and gait analysis. After four weeks, animals with contusion injury and after 8 weeks, animals with transection injury underwent final imaging, biodistribution, ex-vivo volumetry and histology.

Results
While healthy muscle is primarily active during force production, de- or reinnervated muscle also show increased metabolism at rest. In addition, glucose metabolism changes due to the transformation from slow to fast fibre types. Muscle denervation initially showed denervation oedema, followed by muscle atrophy. Eventual reinnervation leads to increased protein synthesis and regeneration of volume.

Conclusion
The volumetric measurement and the semi-automatic algorithm could be directly transferred into clinical practice. Determination of the muscle's regeneration status could improve diagnostic accuracy. Further, early detection of irreversible atrophy or signs of muscle regeneration before first clinical signs, could facilitate early reconstructive surgery.

Funding Sources:
Medizinisch wissenschaftlicher Fond des Bürgermeisters

References:
Pak K, Shin MJ, Hwang SJ, Shin JH, Shin HK, Kim SJ, Kim IJ: Longitudinal Changes in Glucose Metabolism of Denervated Muscle after Complete Peripheral Nerve Injury. Mol Imaging Biol; 18:741– 7, 2016.

eP24 Non-invasive assessment of fatty acid metabolism via PET/MRI

Ustsinau U.[1], Ehret V. [2], Friske J. [3], Fürnsinn, C. [2], Scherer, T. [2], Helbich, T. [3], Hacker, M. [1], Krššák, M. [2], Philippe, C. [1]

[1] Division of Nuclear Medicine, Department of Biomedical Imaging and Image-Guided Therapy, Medical University of Vienna, Vienna, Austria
[2] Division of Endocrinology and Metabolism, Department of Medicine III, Medical University of Vienna, Vienna, Austria
[3] Division of Molecular and Structural Preclinical Imaging, Department of Biomedical Imaging and Image-Guided Therapy, Medical University of Vienna, Vienna, Austria

Keywords: fatty acid, metabolism, PET/MR

Objective
Non-invasive techniques are at the forefront to analyse metabolism. Free fatty acid (FFA) metabolism and its alterations are implicated in pathogenesis of fatty liver disease and diabetes. In the present progress of simultaneous Positron Emission Tomography (PET) / Magnetic Resonance Imaging (MRI) systems, we can measure FFA metabolism with a detailed MRI protocol and a suitable PET tracer as 4(R,S)-[^{18}F]Fluoro-6-thia-heptadecanoic acid (FTHA).

Methods and Materials
Production of [^{18}F]FTHA is set up at the Division of Nuclear Medicine. The process consists of azeotropic drying of fluorine-18, followed by nucleophilic substitution of the commercial tosyl precursor (100ºC, 10 mins + 85ºC, 5 mins) with a final step of C-18 Sep-Pak purification. The radiochemical yield is 6-11% at EOS, pH=7 and osmolality 320-370 mosm/kg. Bruker BioSpec 94/30 MRT with microPET insert has been used for imaging. The measurements were performed on healthy Sprague Dawley rats, which are well-characterized models of liver metabolism.

Results
PET images were recorded dynamically with parser 6x10;1x85;1x195;14x225 to allocate the time of FFA metabolism. Coronal T1-w FLASH MR images (TE=2.354ms, TR=600ms, matrix=256x192, slice=1mm, res=0.195x0.391mm) were registered to PET data. Thus, we can define liver, heart, kidneys and bladder. Ex vivo bio-distribution confirmed the PET/MRI scans.

Conclusion
[^{18}F]FTHA accumulates in the liver and shows metabolic properties. The generated images can be considered as a starting point for evaluation and comparison with pathological conditions such as fatty liver disease or diabetes.

Funding Sources:
This study was conducted with support of the Medical Imaging Cluster (MIC) and was funded by the Vienna Science and Technology Fund (WWTF #LS19-046).

References:
1. Savisto, N. et al. Automated production of [18F]FTHA according to GMP. J Labelled Comp Radiopharm 61:84-93 (2018).
2. Iozzo, P. et al. Liver uptake of free fatty acids in vivo in humans as determined with 14(R,S)-[18F]fluoro-6-thia-heptadecanoic acid and PET. Eur J Nucl Med Mol Imaging 30:1160–1164 (2003).

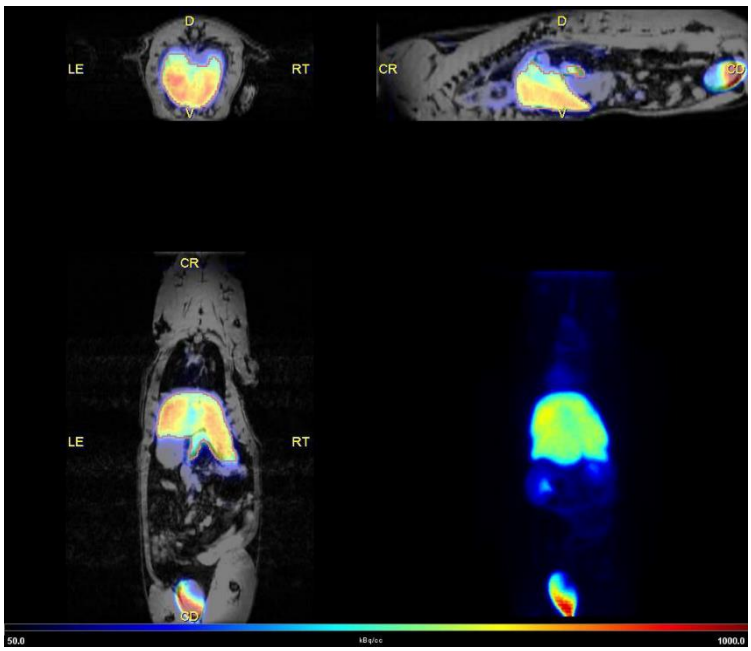

Figure 1: Co-registered PET and MR (FLASH) image of healthy female rat: distribution of [^{18}F]FTHA tracer in 1 h period

eP25 Multiparametric MRI for non-invasive, non-contrast-enhanced deciphering of breast cancer heterogeneity and molecular subtyping

Bartsch S.J.[1], Ehret V.[2], Friske J.[1], Fröhlich V.[3], Gombocz S.J.[1], Laimer-Gruber D.[1], Helbich T.H.[1], Pinker K.[4]

[1] Department of Biomedical Imaging an Image-Guided Therapy, Medical University of Vienna, Vienna, Austria
[2] Department of Internal Medicine III, Division of Endocrinology and Metabolism, Medical University of Vienna, Vienna, Austria
[3] University of Applied Sciences, Fachhochschule Wiener Neustadt GmbH, Wiener Neustadt, Austria
[4] Department of Radiology, Breast Imaging Service, Memorial Sloan Kettering Cancer Center, New York, USA

Disclosure statement: The authors declare no conflicts of interest.

Keywords: Intravoxel incoherent motion (IVIM) imaging, BOLD/TOLD imaging, molecular breast cancer subtyping

Objective
BC is a heterogeneous disease, and its development is driven by genomic instability and alternating selective pressures from the hypoxic tumor microenvironment. Non-invasive, multiparametric MRI using novel functional sequences can decipher BC heterogeneity and thus guide the treatment. Novel MRI sequences that provide imaging biomarkers for tissue oxygenation and tumor neovascularity include blood/tissue oxygen level dependent (BOLD/TOLD) MRI, depending on oxygen saturation in the blood and tumor tissue, and intravoxel incoherent motion (IVIM) imaging, depending on intracellular and intravascular diffusion.
A combination of BOLD/TOLD and IVIM imaging may identify differently aggressive molecular subtypes of BC non-invasively and without i.v. application of gadolinium-based contrast agents.

Methods and Materials
Twenty-six nude mice were inoculated into the flank with low, intermediate, and highly aggressive BC cells and imaged using the 9.4T Bruker BioSpin 94/30USR scanner. For BOLD imaging, anaesthesia was supplemented with four different levels of oxygen to trace the accumulation of erythrocyte-bound oxygen. TOLD measurements were performed at 21% and 100% oxygen supply. IVIM measurements included 16 b-values and data analysis was based on 2D segmentations of solid tumor regions.

Results
Among several IVIM-DWI parameters, fIVIM, capturing the amount of microvessels, allows the most accurate differentiation of low and intermediate from highly aggressive BCs ($p=0.007$). Significant differences in oxygen delivery were found between low and high aggressive BC xenografts via BOLD imaging ($p=0.03$). TOLD measurements did not yield significant differences.

Conclusion
Our data indicate that multiparametric MRI provides non-invasive imaging biomarkers to decipher breast cancer heterogeneity and enables molecular subtyping without i.v. application of contrast agents.

Funding Sources:
This work was funded by the WWTF project number LS19-018.

eP26 In utero effects of prenatal alcohol exposure on the human fetal brain - an atlas-based MRI study

Stümpflen Marlene,[1] Schwartz Ernst,[1] Diogo Mariana Cardoso,[2] Glatter Sarah,[3] Pfeiler Birgit,[1] Schmidbauer Victor,[1] Bartha-Doering Lisa,[3] Krampl-Bettelheim Elisabeth,[4] Seidl Rainer,[3] Prayer Daniela,[1] Kasprian Gregor[1]

[1] Department of Biomedical Imaging and Image Guided Therapy, Division of Neuroradiology and Muskuloskeletal Radiology, Medical University of Vienna, Austria
[2] Department of Neuroradiology, Hospital Garcia de Orta, 2805-267 Almada, Portugal
[3] Department of Pediatrics and Adolescent Medicine, Medical University of Vienna, Austria
[4] Department of Obstetrics and Feto-maternal Medicine, Medical University of Vienna, Austria

Disclosure statement: The authors declare no conflicts of interest.

Keywords: fetal imaging, neuroradiology, fetal MRI

Objective
Numerous postnatal imaging studies have shown structural brain anomalies in patients suffering from Fetal Alcohol Spectrum Disorders, potentially resulting in long-lasting behavioral changes.[1–3] This atlas-based fetal MRI study aimed to identify regional effects of prenatal alcohol exposure (PAE) on human fetal brain development.

Methods and Materials
This IRB approved, prospective single-center study identified pregnant women referred for fetal MRI with variable amounts of alcohol intake during gestation using two standardized, anonymized questionnaires (TACE[4] and PRAMS[5]). Postprocessing generated super-resolution imaging and semiautomated atlas-based segmentations. After visual inspection, assessment of data quality and manual correction, an atlas-based analysis of twelve fetal brain structures was performed (Fig.1). Linear models were applied with an additional factor to account for varying gestational ages and corrected for multiple comparisons using the Benjamini-Hochberg procedure.

Results
After excluding 476 subjects with structural brain anomalies and/or poor super-resolution image quality, a total of 24 patients (26 observations) with and 52 age- and gender-matched controls without PAE (gestational age 21-37 weeks, mean 27.4 GW) were included and analyzed. In fetuses with PAE the corpus callosum ($p < 0.001$) showed significantly larger volumes, whereas the periventricular/germinal zone ($p = 0.001$) showed smaller volumes compared to controls.

Conclusion
This study systematically documented the selective effects of PAE on regional brain volumes at prenatal stages: Besides the reduction of the periventricular zone, an increased regional growth of the corpus callosum was found indicating a change in the developmental dynamics of the normal trajectory of interhemispheric connectivity - even with minor prenatal alcohol exposure (1-3 standardized drinks/week).

Funding Sources:
Austrian Research Fund grant I 3925-B27 in collaboration with French National Research Agency (ANR)

References:
1. Caputo C, et al. doi:10.1002/bdrc.21129
2. Gupta KK, et al. doi:10.1111/acer.13135
3. Norman AL, et al. doi:10.1002/ddrr.72
4. Sokol RJ, et al. doi:10.1016/0002- 9378(89)90302-5
5. Shulman HB, et al. doi:10.2105/AJPH.2018.304563

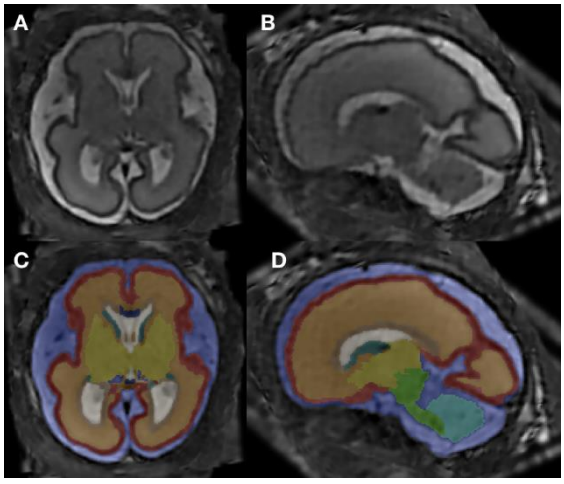

Figure 1: A, B: Postprocessed MRI super-resolution reconstructions in axial and sagittal planes of a fetus at 26+6 gestational weeks. E, F: Respective manually corrected atlas-based tissue segmentation. Color coding: blue - external CSF-spaces, red - cortex, orange - subcortical parenchyma, brown - periventricular zone, dark green - ganglionic eminence, white - ventricular system, dark blue - corpus callosum, yellow – deep gray nuclei, light green - brainstem, light blue - cerebellum, turquoise - left hippocampus, gray - right hippocampus.

eP27 Quantitative MRI of the human fetal ganglionic eminence – neuroradiological insights into a transient brain structure

Stümpflen Marlene,[1] Christian Mitter,[1] Schwartz Ernst,[1] Diogo Mariana Cardoso,[2] Glatter Sarah,[3] Pfeiler Birgit,[1] Schmidbauer Victor,[1] Haberler Christine,[4] Krampl-Bettelheim Elisabeth,[5] Prayer Daniela,[1] Kasprian Gregor[1]

[1] Department of Biomedical Imaging and Image Guided Therapy, Division of Neuroradiology and Muskuloskeletal Radiology, Medical University of Vienna, Austria
[2] Department of Neuroradiology, Hospital Garcia de Orta, 2805-267 Almada, Portugal
[3] Department of Pediatrics and Adolescent Medicine, Medical University of Vienna, Austria
[4] Division of Neuropathology and Neurochemistry, Department of Neurology, Medical University of Vienna
[5] Department of Obstetrics and Feto-maternal Medicine, Medical University of Vienna, Austria

Disclosure statement: The authors declare no conflicts of interest.

Keywords: fetal imaging, neuroradiology, fetal MRI

Objective
Failure of fetal interneuron migration arising from the ganglionic eminence (GE) may lead to neuropsychiatric and neurodevelopmental disorders.[1,2] Early detection of alterations of this transient brain structure at prenatal stages, may improve the MRI phenotyping of neurodevelopmental diseases. This atlas-based fetal MRI study aimed to quantitatively assess longitudinal development of the GE.

Methods and Materials
In this retrospective IRB-approved single-center study, postprocessing was conducted based on semiautomated segmentation of super-resolution fetal brain 1.5T and 3T MR datasets. After assessment of data quality, a longitudinal, quantitative atlas-based analysis of the ganglionic eminence was conducted by several raters.

Results
A total of 112 patients (gestational age 19-39 weeks, mean 27.5 GW) without structural brain anomalies, cardiac defects, fetal growth restriction, and/or poor super-resolution image quality were included and analyzed. In the observed time interval, the volume of the ganglionic eminence ranged from 1,100.25mm^3 to 53.25mm^3 (mean 572.31mm^3, SD 232.01) with average volumes continuously decreasing from 19 to 39 GW. For each gestational day, a volumetric reduction of 3.59mm^3 (95% CI 2.45 – 4.73) within the GE was detected.

Conclusion
Super-resolution based quantitative MR volumetry allowed to analyze the continuous decline in size of the GE from 19GW onwards - initially documenting a physiological degenerative process in the developing human brain. The first set of reference values of this structure was provided, enabling radiologists to objectively quantify GE development using fetal MRI.

References:
1. Yokota Y, Gashghaei HT, Han C, Watson H, Campbell KJ, Anton ES. Radial glial dependent and independent dynamics of interneuronal migration in the developing cerebral cortex. *PLoS One*. 2007;2(8):e794. doi:10.1371/journal.pone.0000794
2. Righini A, Frassoni C, Inverardi F, et al. Bilateral cavitations of ganglionic eminence: a fetal MR imaging sign of halted brain development. *AJNR Am J Neuroradiol*. 2013;34(9):1841-1845. doi:10.3174/ajnr.A3508

eP28 Positron range distributions estimations using Monte Carlo simulations and U-Nets for PET imaging

Daria Ferrara[1], Hunor Kertész [1], David Iommi [1], Ivo Rausch [1]

[1] QIMP Team, Center for Medical Physics and Biomedical Engineering, Medical University of Vienna, Vienna, Austria

Keywords: positron range, U-Net, PET imaging

Objective
Training and validation of a U-Net for the estimation of positron range kernels in different materials with high-energy positron emitters.

Methods and Materials
PR distributions of ^{124}I were simulated using monte carlo simulations in different material compositions: uniform, complex or spatially-variant CT derived combinations of bone, water and lung. PR kernels were created by mapping the simulated annihilation points clouds to 3D matrixes, with sizes defined by the maximum PR in lung (~30 mm) and the PET voxel size (~2 mm). Material maps derived from the attenuation CT scan and the corresponding kernels with voxel sources were used as input pairs for the training of a U-Net. The resulting distributions were compared to GATE results, which were regarded as ground-truth, using a percentage matrix difference. The comparison was also repeated with a simple voxel-specific, material-dependent PR distribution method which was based on a material dependent combination of the respective homogeneous kernels.

Results
The U-Net underestimated PR distributions in bone introducing image artefacts. However, PR distributions in water and lung as well as combination thereof were correctly estimated. The network required just a fraction of the computational power needed for MC simulations.

Conclusion
U-Net seems a promising method for the estimation of PR distribution, with an accuracy similar to MC simulations and a much lower computational cost. With improvements in the implementation, the method could be used in image reconstruction for PR corrections.

eP29 Metabolite Concentration Estimations in the Brain Using 7 T MRSI

Philipp Lazen[1], Gilbert Hangel[1,2], Benjamin Spurny-Dworak[3], Cornelius Cadrien[1,2], Sukrit Sharma[1], Lukas Hingerl[1], Eva Heckova[1], Bernhard Strasser[1], Stanislav Motyka[1], Alexandra Lipka[1,4], Stephan Gruber[1], Christoph Brandner[5], Rupert Lanzenberger[3], Karl Rössler[2], Siegfried Trattnig[1,4], Wolfgang Bogner[1]

[1] High-field MR Center, Department of Biomedical Imaging and Image-guided Therapy, Medical University of Vienna, Austria.
[2] Department of Neurosurgery, Medical University of Vienna, Austria.
[3] Division of General Psychiatry, Department of Psychiatry and Psychotherapy, Medical University of Vienna, Austria.
[4] Institute for Clinical Molecular MRI, Karl Landsteiner Society, Austria.
[5] High-field MR Center, Center for Medical Physics and Biomedical Engineering, Medical University of Vienna, Austria.

Disclosure statement: The authors declare no conflicts of interest.

Keywords: MRSI, 7 T, quantitative metabolic imaging

Objective
Magnetic resonance spectroscopic imaging (MRSI) is capable of non-invasively quantifying different metabolites and mapping their distributions. One of its drawbacks is the lack of standardized units; generally, only relative signal intensities are used. The goal of this study was to estimate the concentration of various metabolites and to compare them to literature values.

Methods and Materials
A whole-brain 3D-CRT-FID-MRSI was acquired at 7 T (matrix size 64x64x39, 3.4 mm isotropic resolution, 15 minutes acquisition duration) in 24 healthy volunteers. The measurement protocol further entailed an unsuppressed MRSI acquisition in order to measure a water signal which could be used to estimate the concentrations of 15 metabolites. For analysis, 55 different brain regions were defined based on the segmentation of T1w-MRI, and different metabolite concentrations were estimated in each region. The estimations' reliability was assessed based on CRLB values. The reproducibility of the acquired data was evaluated by calculating coefficients of variations between volunteers.

Results
The calculated metabolite concentrations of choline, creatine, glutamate, myo-inositol and N-acetylaspartate were shown to be of good or acceptable quality in 44 of the 55 defined brain regions. The average CVs for those metabolites were relatively low at around 9% to 11%. Furthermore, concentration estimates of almost all metabolites were in good agreement with literature values.

Conclusion
This study successfully created a baseline for future research by providing a large amount of data. Further work shall include the implementation of metabolite-specific B1 corrections as well as the evaluation of intra-subject data stability.

Funding Sources:
P 34198 (FWF), P 30701 (FWF), KLI-646 (FWF)

References:
- G. Hangel, B. Spurny-Dworak, P. Lazen, C. Cadrien, S. Sharma et al. Inter-subject stability and regional concentration estimates of 3D-FID-MRSI in the human brain at 7 T. NMR Biomed. 2021. doi: 10.1002/nbm.4596
- G. Hangel, C. Cadrien, P. Lazen, J. Furtner, A. Lipka et al. High-resolution metabolic imaging of high-grade gliomas using 7T-CRT-FID-MRSI. Neuroimage Clin. 2020. doi: 10.1016/j.nicl.2020.102433

eP30 Volumetric DCE-MRI Analysis for Breast Cancer Detection

Bennani-Baiti Barbara [1], Helbich Thomas [1], Baltzer Pascal [1]

[1] Department of Biomedical Imaging and Image-guided Therapy, Medical University of Vienna, Vienna, Austria

Disclosure statement: The authors declare no conflicts of interest.

Keywords: breast MRI, DCE-MRI

Objective
While computer aided detection is already routinely employed in conventional mammography imaging, few data are available on automated cancer detection at MRI[1,2]. Given its excellent diagnostic performance (sensitivities >95%), breast MRI is being increasingly used in routine imaging. An automated approach pre-assessing the risk of malignancy would be most helpful in assisting inexperienced readers [3-5]. We therefore aimed to assess whether volumetric DCE-MRI analysis could detect the presence of malignancy.

Methods and Materials
This retrospective IRB-approved study, included 50 consecutive patients, that underwent two subsequent breast MRI exams for suspicious findings at conventional imaging with 0.075 mmol/kg gadobenic and 0.15 mmol/kg gadoteric acid. Two independent readers, blinded to the histopathological outcome, assessed unenhanced and early post-contrast images using semiautomated software (Brevis, Siemens Healthcare)[6]. Diagnostic performance was measured by applying ROC-analysis using the percentage of ipsilateral voxel volume enhancement as predictor and histological outcome (benign/malignant) as reference variable.

Results
50 cases (36 malignant, 14 benign) were assessed. Ipsilateral enhancing voxel volume versus histological outcome indicated an AUC of 0.669 ± 0.09 (95%-CI:0.521–0.795) and 0.671 ± 0.087 (95%-CI:0.523–0.797) for gadobenic acid, reader 1 and 2, respectively and an AUC of 0.758±0.079 (95%-CI: 0.616–0.868) and 0.758 ± 0.073 (95%-CI: 0.616–0.868) for gadoteric acid, reader 1 and 2, respectively, with excellent inter-reader agreement.

Conclusion
The findings from this pilot study suggest, that quantitatively assessed enhancing breast tissue as a percentage of the entire breast may serve as an indicator for breast cancer. However, differences in contrast media should be considered, before further developing this method.

Funding Source:
Study data were acquired within the context of a prospective randomized diagnostic study sponsored by BRACCO (Milan, Italy).

References:
1. Song SE, et al. Cancer Imaging. 2015;15:1.
2. Renz DM, et al. J Magn Reson Imaging. 2012;35(5):1077–1088.
3. Bennani-Baiti B, et al. PLoS ONE. 2016;11(8):e0160346.
4. Houssami N, et al. J Clin Oncol. 2008;26(19):3248–3258.
5. Warner E, et al. Ann Intern Med. 2008;148(9):671– 679.
6. Baltzer PAT, et al. Acad Radiol. 2009;16(4):435–442.

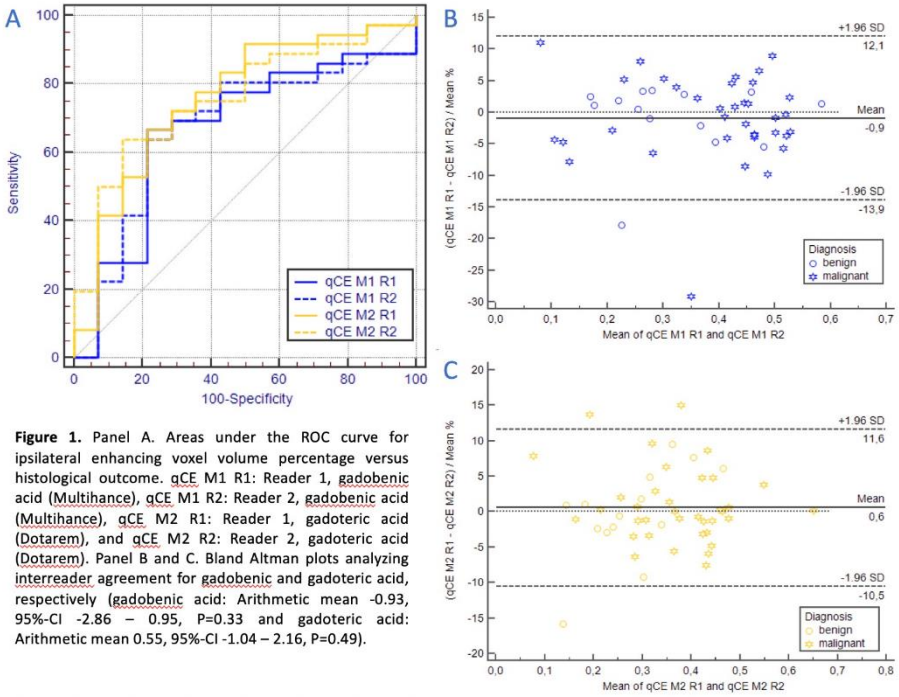

Figure 1. Panel A. Areas under the ROC curve for ipsilateral enhancing voxel volume percentage versus histological outcome. qCE M1 R1: Reader 1, gadobenic acid (Multihance), qCE M1 R2: Reader 2, gadobenic acid (Multihance), qCE M2 R1: Reader 1, gadoteric acid (Dotarem), and qCE M2 R2: Reader 2, gadoteric acid (Dotarem). Panel B and C. Bland Altman plots analyzing interreader agreement for gadobenic and gadoteric acid, respectively (gadobenic acid: Arithmetic mean -0.93, 95%-CI -2.86 – 0.95, P=0.33 and gadoteric acid: Arithmetic mean 0.55, 95%-CI -1.04 – 2.16, P=0.49).

eP31 GMI might overestimate quality of glycemic control in diabetes patients

Fellinger Paul[1], Rodewald Karin[1], Ferch Moritz[1], Kautzky-Willer Alexandra[1], Winhofer Yvonne[1]

[1] Division of Endocrinology and Metabolism, Department of Medicine III, Medical University of Vienna, Austria

Disclosure statement: The authors declare no conflicts of interest.

Keywords: CGM, GMI, glycemic control

Objective
The introduction of continuous glucose monitoring (CGM) in the last years improved management of diabetes and new parameters were established to define glycemic control. To estimate HbA1c, the parameter glucose management index (GMI), based on average glucose measurements, was introduced. This study aims to investigate the reliability of GMI for glycemic control as many patients rely on it, especially when using telemedicine.

Methods and Materials
A retrospective data analysis of 170 patients was performed. GMI of two different time spans, namely 14 days (GMI1) and 30 days (GMI2) prior to the HbA1c measurement were compared. To detect deviations of GMI from HbA1c, we plotted GMI versus HbA1c. We defined a clinically relevant deviation from HbA1c as more than 0.4% points in either direction.

Results
Of the 170 patients, 77 were female, 113 patients had T1DM/LADA, 41 were T2DM, with 16 patients having an unspecified type of diabetes. Mean HbA1c was 7.53±1.25% and correlations between HbA1c and GMI1 (R^2=.82;p<0.001) as well as GMI2 (R^2=.845;p<0.001) were statistically significant. When plotting the two measurements against each other, GMI-values are on average more than 0.4% lower than HbA1c at a HbA1c above 8%.

Conclusion
Within the last years CGM had a big impact in diabetes management. As expected, GMI and HbA1c correlate statistically significant with each other, with a slightly higher R^2 for GMI2 compared to GMI1. However, relying on GMI as a parameter for glycemic control could lead to inadequate treatment, especially in patients with poor glycemic control.

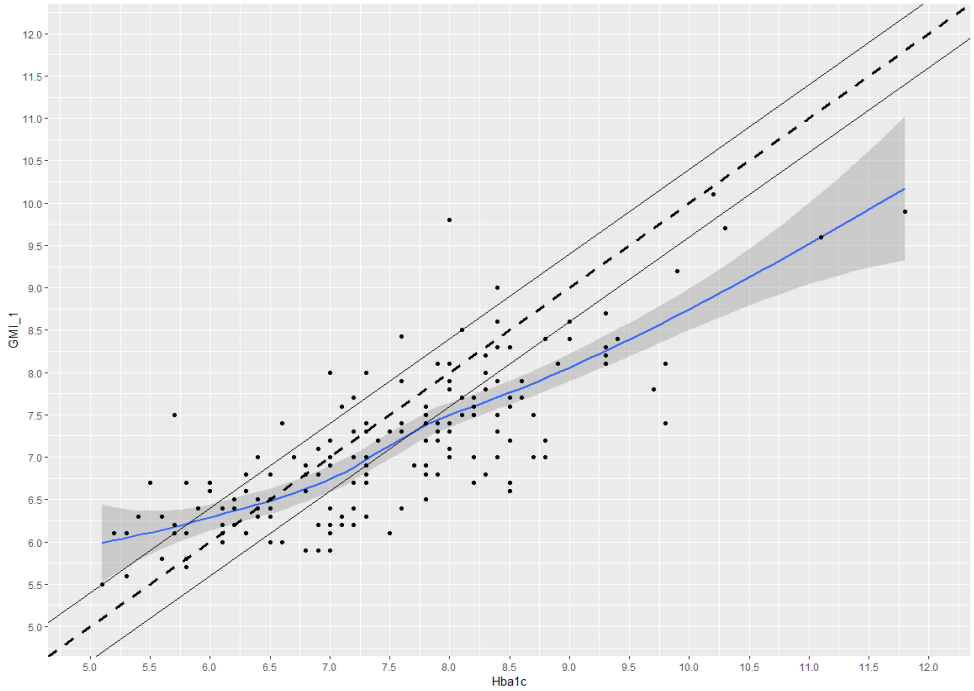

Figure 1: HbA1c vs GMI1 (2 weeks prior HbA1c measurement): blue line: loess curve with +/- 95%CI (grey); dotted line HbA1c=GMI with +/- 0.4% interval (continuous lines)

eP32 Adaptation and Implementation of a Mobile Phone- Based Remote Symptom Monitoring System for People With Cancer in Europe

Eileen Furlong [# 1], Andrew Darley [1], Patricia Fox [1], Alison Buick [1], Grigorios Kotronoulas [2], Morven Miller [2], Adrian Flowerday [3], Christine Miaskowski [4], Elisabeth Patiraki [5], Stylianos Katsaragakis [5], Emma Ream [6], Jo Armes [6], Alexander Gaiger [7], Geir Berg [8,9], Paul McCrone [10], Peter Donnan [11], Lisa McCann [2], Roma Maguire [2]

[1] School of Nursing, Midwifery and Health Systems, University College Dublin, Dublin, Ireland.
[2] School of Psychological Sciences and Health, University of Strathclyde, Glasgow, United Kingdom.
[3] Docobo Ltd, Surrey, United Kingdom.
[4] Institute for Global Health Sciences, University of California San Francisco, San Francisco, CA, United States.
[5] National and Kapodistrian University of Athens, Athens, Greece.
[6] School of Health Sciences, University of Surrey, Surrey, United Kingdom.
[7] Division of Hematology and Hemaostaseology, Medical University of Vienna, Vienna, Austria.
[8] Faculty of Medicine and Health Sciences, Norwegian University of Science and Technology, Gjøvik, Norway.
[9] Innlandet Hospital Trust Division Lillehammer, Lillehammer, Norway.
[10] Institute of Psychiatry, Psychology & Neuroscience, King's College London, London, United Kingdom.
[11] Dundee Epidemiology and Biostatistics Unit, University of Dundee, Dundee, United Kingdom.

Keywords: Telemedicine, patient reported outcome measurements (e-PROs), advanced symptom management (ASyMS)

Objective
This study aimed to describe the steps undertaken in the preparation of a multinational, multicenter randomized controlled trial (RCT) to test a mobile phone- based remote symptom monitoring system, that is, Advanced Symptom Management System (ASyMS), designed to enhance management of chemotherapy toxicities among people with cancer receiving adjuvant chemotherapy versus standard cancer center care.

Methods and Materials
There were 13 cancer centers across 5 European countries (Austria, Greece, Ireland, Norway, and the United Kingdom). Multiple steps were undertaken, including a scoping review of empirical literature and clinical guidelines, translation and linguistic validation of study materials, development of standardized international care procedures, and the integration and evaluation of the technology within each cancer center.

Results
The ASyMS was successfully implemented and deployed in clinical practices across 5 European countries. The rigorous and simultaneous steps undertaken by the research team highlighted the strengths of the system in clinical practice, as well as the clinical and technical changes required to meet the diverse needs of its intended users within each country, before the commencement of the RCT.

Conclusion
Adapting and implementing this multinational, multicenter system required close attention to diverse considerations and unique challenges primarily related to communication and clinical and technical issues. Success was dependent on collaborative and transparent communication among academics, the technology industry, translation partners, patients, and clinicians as well as a simultaneous and rigorous methodological approach within the 5 relevant countries.

Funding Sources:
This project has received funding from the European Union's Seventh Framework Programme for research, technological development and demonstration under grant agreement no 602289

References:
1. Maguire R, et al. Real Time Remote Symptom Monitoring Reduces Patient Reported Symptom Burden During Chemotherapy Treatment: Results from A European Multicentre Randomised Controlled Trial (eSMART - electronic Symptom management using the Advanced Symptom Management System (ASyMS) remote technology for patients with cancer). BMJ. 2021 Jul 21;374:n1647. doi: 10.1136/bmj.n1647.
2. Furlong E, et al. Adaption and Implementation of a Mobile Phone-Based Remote Symptom Monitoring System for People With Cancer in Europe. JMIR Cancer. 2019 Mar 14;5(1):e10813. doi: 10.2196/10813.
3. Maguire R, et al. The eSMART study protocol: a randomised controlled trial to evaluate electronic symptom management using the advanced symptom management system (ASyMS) remote technology for patients with cancer. BMJ Open. 2017 Jun 6;7(5)

Late-Breaking Abstracts

eLB1 How did you get in here? A closer look at the interaction between adipose stem cell derived extracellular vesicles and Schwann cells

Maximilian Haertinger [1,2], Anton Borger [1,2], Paul Supper [1], Sarah Stadlmayr [1], Zlata Kiseleva [1], Flavia Millesi [1], Anda Corinna Mann [1], Aida Naghilou [1], Tamara Weiss [1,2], Christine Radtke [1,2]

[1] Department of Plastic, Reconstructive and Aesthetic Surgery, Medical University of Vienna, Austria
[2] Austrian Cluster for Tissue Regeneration

Disclosure statement: The authors declare no conflicts of interest.

Keywords: extracellular vesicles, endocytosis, imaging flow cytometry

Objective
Small extracellular vesicles (EVs) are involved in a plethora of physiological and pathophysiological processes, however, many known unknowns regarding the biology of EVs remain [1, 2]. In this study, we investigate how EVs isolated from adipose tissue derived stem cells (ASCs) interact with Schwann cells (SCs), which have been ascribed an essential role in nerve repair. ASC-EVs have been shown to increase proliferation of SCs [3], making them a promising candidate for autologous therapy following injury.

Methods and Materials
While SCs and ASCs were immunophenotyped with confocal laser scanning microscopy, EVs were characterized with imaging flow cytometry (IFC), nanoparticle tracking analysis (NTA), atomic force microscopy (AFM) and both scanning- and transmission electron microscopy (SEM, TEM). Interactions between SCs and EVs were recorded by live cell imaging (LCI), and further analyzed by 3D reconstructions of confocal micrographs, as well as TEM. To quantify internalization efficiency, IFC was used following biochemical inhibition.

Results
ASC-EVs are actively internalized by SCs at their periphery. Within less than 30 minutes, the vesicles are then transported to and clustered perinuclearily. By blocking clathrin-mediated endocytosis the internalization of EVs could be significantly reduced, suggesting that in SCs, the transit of ASC-EVs through the membrane is clathrin-mediated. However, as no complete block of internalization could be achieved, additional modes of entry may supplement membrane transit upon inhibition.

Conclusion
Identifying the main internalization pathway of ASC-EVs in SCs allows future therapeutic approaches to enhance and optimize the targeted delivery of bioactive cargo via EVs directly to the desired cells of interest.

Funding Sources:
This research as funded by the Austrian Workers' Compensation Board/Austrian Social Insurance for Occupational Risk (AUVA), number FA731F0702.

References:
[1] EL Andaloussi S, Mäger I, Breakefield XO, Wood MJ. Extracellular vesicles: biology and emerging therapeutic opportunities. Nat Rev Drug Discov. 2013 May;12(5):347-57. doi: 10.1038/nrd3978. Epub 2013 Apr 15. PMID: 23584393.
[2] Margolis L, Sadovsky Y (2019) The biology of extracellular vesicles: The known unknowns. PLOS Biology 17(7): e3000363. doi: 10.1371/journal.pbio.3000363
[3] Haertinger M, Weiss T, Mann A, Tabi A, Brandel V, Radtke C. Adipose Stem Cell-Derived Extracellular Vesicles Induce Proliferation of Schwann Cells via Internalization. Cells. 2020 Jan 9;9(1):163. doi: 10.3390/cells9010163. PMID: 31936601; PMCID: PMC7016740.

eLB2 Bringing data closer to intuition: A comprehensive software for analysis, visualization, organization, and fast interaction with large microscopy recordings

Srdjan Sarikas[1], Johannes Pfabe[1], Sandra Postić[1], Marjan Slak Rupnik[1,2,3]

[1] Center for physiology and pharmacology, Medical University of Vienna, Austria
[2] Institute of Physiology, Faculty of Medicine, University of Maribor, Slovenia
[3] Alma Mater Europaea – European Center Maribor, Maribor, Slovenia

Disclosure statement: The authors declare no conflicts of interest.

Keywords: cytosolic calcium imaging, image segmentation, signal analysis

Objective

A typical recording of cytosolic calcium in pancreatic tissue slices results in dozens of gigabytes of raw data. Conventional interaction with this data is often slow, hands-on intensive, and requires the use of many different applications, and a dedicated hardware, limiting simultaneous use by more than one experimenter.

Methods and Materials

From a full recording (txy), we calculate mean (or other statistic) image, on which we detect local peaks of intensity to define regions of interest (ROIs). The traces associated with ROIs contain transients at very different timescales. We developed a signal analysis algorithm for the traces, to tag them as events at all relevant timescales. Finally, a single experiment is boiled down into only hundreds of MBs, increasing its flexibility and responsiveness. A single image of a color-coded raster of the events provides a meaningful visual representation of the whole experimental flow.

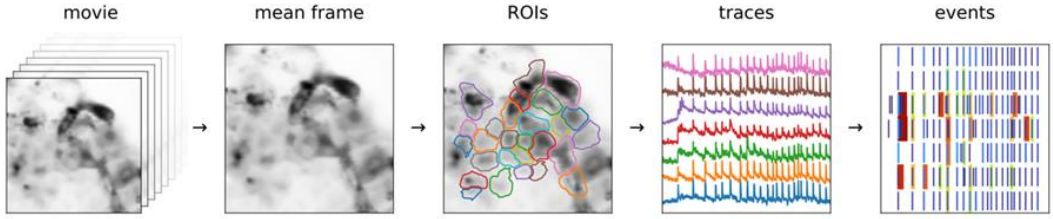

Figure 1: A representation of the analysis pipeline

We deployed our software on a jupyterhub server (1), complemented with dashboards (2) for organizing recordings and saving relevant metadata. The server also enables many concurrent users fast and simultaneous interaction with different experiments, enabling actual scientific insight.

Results

The software enabled us to see and examine transients not commonly associated with pancreatic beta cells, but characteristic of CICR discharges through IP3 and ryanodine receptors (3,4). They appear to be the actual basis of beta cell responses to physiological stimuli.

Conclusion

Large datasets require automatic analyses. Only then can the true potential of experimental setups be fully harnessed.

Funding Sources:

Austrian Science Fund (FWF): Marjan Slak Rupnik, I3562-B27; Austrian Science Fund (FWF): Marjan Slak Rupnik, I4319-B30; Javna Agencija za Raziskovalno Dejavnost RS (Slovenian Research Agency): Marjan Slak Rupnik, P3-0396

References:

1. Jupyterhub: *A multi-user version of the notebook designed for companies, classrooms and research labs*. https://jupyter.org/hub
2. ContainDS: A data science platform for teams providing simple infrastructure to share prototypes and dashboards. https://cdsdashboards.readthedocs.io
3. Sandra Postić, et al. *Intracellular Ca2+ channels initiate physiological glucose signaling in beta cells examined in situ*. bioRxiv 2021.04.14.439796; https://doi.org/10.1101/2021.04.14.439796
4. Nastja Sluga, et al. *Dual Mode of Action of Acetylcholine on Cytosolic Calcium Oscillations in Pancreatic Beta and Acinar Cells In Situ*. Cells 2021, 10, 1580. https://doi.org/10.3390/cells10071580

eLB3 Manganese Mn(II) DOTA-modified polysaccharide as alternative to gadolinium-based contrast agents for magnetic resonance imaging (MRI)

Irena Pashkunova-Martic[1,4], Joachim Friske[1], Dieter Baurecht[2], J. Ivanova-Toumbeva[3], Bernhard K. Keppler[4], Thomas H. Helbich[1]

[1] Department of Biomedical Imaging and Image-guided Therapy, Division of Molecular and Structural Preclinical Imaging, Medical University of Vienna & General Hospital of Vienna, Austria
[2] Department of Physical Chemistry, University of Vienna, Austria
[3] Faculty of Medicine, Sofia University "St. Kliment Ohridski", Sofia, Bulgaria
[4] Institute of Inorganic Chemistry, Faculty of Chemistry, University of Vienna, Austria

Disclosure statement: The authors declare no conflicts of interest.

Keywords: manganese, modified amino-dextran-DOTA, magnetic resonance imaging

Objective
Paramagnetic manganese Mn(II) chelates emerged as suitable alternatives to the routinely applied gadolinium Gd(III)-based contrast agents for Magnetic resonance imaging (MRI). Free Mn(II) ions or in labile complexes are toxic, therefore using novel macromolecular chelators may lead to improved stability and security of novel Mn(II)-based polysaccharide complexes.

Methods and Materials
1,4,7,10-Tetraazacyclododecane-1,4,7,10-tetraacetic acid mono-N-hydroxysuccinimide ester (DOTA-NHS) and 2,2′,2"-(10-(1-carboxy-4-((4-isothiocyanatobenzyl)amino)-4-oxobutyl)-1,4,7,10-tetraazacyclododecane-1,4,7-triyl)triacetic acid (p-NCS-Bz-DOTA-GA) were conjugated to lysinated (amino) dextran with 70kDa MW under mild conditions to allow introduction of the paramagnetic manganese Mn(II). ATR-FTIR of modified Mn(II)-DOTA-dextran conjugates was performed to confirm the successful coupling of the macrocyclic chelators to the polysaccharide molecule. Further characterization was made by PCS, ICP-MS and FPLC. In vitro relaxivity measurements in a high field MR scanner have been carried in order to evaluate the potential of the novel Mn(II) conjugates as MR contrast agents.

Results
Successful synthesis and characterization of Mn(II)-DOTA modified dextran, mediated through either DOTA-NHS ester or p-NCS-Bz-DOTA-GA was carried out. However, polydispersity due to possible cross-linking was observed by the DOTA-NHS-mediated coupling, where as a single peak fraction containing Mn(II)-p-NCS-Bz-DOTA-GA modified dextran could be collected. In vitro MRI relaxivity studies showed superior signal enhancement of the Mn(II) polysaccharide conjugates in comparison with the low molecular $MnCl_2$ and the cyclic Gd-HPDO3A (ProHance) gadoteridol in clinical use.

Conclusion
Novel Mn(II)-dextran compounds were successfully prepared by using two different derivatives of the more thermodynamically stable macrocyclic DOTA chelator as alternative MR CAs. A strong signal enhancement at concentrations 50 times lower than gadoteridol, used as positive control, makes them safer potential candidates for biomedical applications.

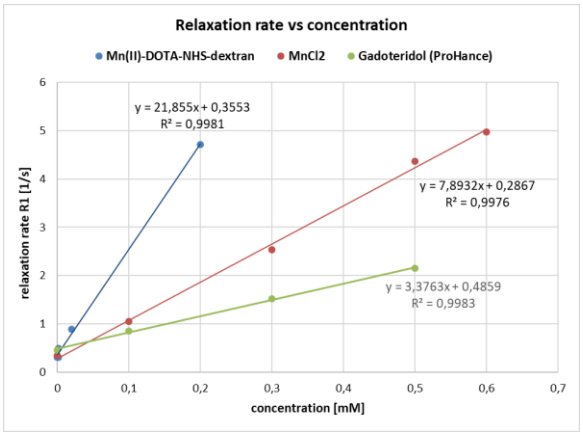

Figure 1: Plots of relaxation rate (R1, [1/s]) to concentration (mM) curves for Mn(II)-DOTA-NHS-dextran compared to low molecular weight $MnCl_2$ and clinically applied gadoteridol (ProHance, cyclic) A steep increase of the relaxation rate R1 using the Mn(II) conjugate as MR contrast agent (CA) was observed.

Funding Source:
National Science Fund of Bulgaria (grant KP-06-Austria-6/6.08.2019), the Austrian Federal Ministry of Education, Science and Research (BMBWF) (Project No: BG 07/2019) and the FWF (Austrian Science Fond: T 1145-B).

References:
[1] Devreux M, et al. *Inorg Chem*. 2021;60(6):3604-3619. doi:10.1021/acs.inorgchem.0c03120
[2] Islam MK, et al. *J Med Chem*. 2017;60(7):2993-3001. doi:10.1021/acs.jmedchem.6b01799
[3] Troughton JS, et al. *Inorg Chem*.2004;43(20):6313-6323. doi:10.1021/ic049559g
[4] Aime S, et al. *J Biol Inorg Chem*. 2002;7(1- 2):58-67. doi:10.1007/s007750100265

eLB4 Label-free multimodal nonlinear optical microscopy for intraoperative brain cancer detection

Gabriel Giardina[1], Arno Krause[1], David Reichert[1], Rainer Leitgeb[1], Wolfgang Drexler[1], Adelheid Woehrer[2], Georg Widhalm[3], Angelika Unterhuber[1], Marco Andreana[1]

[1] Center for Medical Physics and Biomedical Engineering, Medical University of Vienna, Austria
[2] Department of Neurology, Division of Neuropathology and Neurochemistry, Medical University of Vienna, Austria
[3] Department of Neurosurgery, General Hospital and Medical University of Vienna, Austria

Disclosure statement: The authors declare no conflicts of interest.

Keywords: Multimodality, Non-Linear Optics, Microscopy

Objective
Malignant brain tumours are characterized by high mortality rates and poor patient prognosis. State of the art intraoperative diagnosis for cancer is based on time consuming and labour intensive histopathological assessment of tumour biopsies[1]. The information provided is however crucial to guide surgery and optimize tumour resection to improve patient outcome. Chemical compounds such as lipids, proteins and collagen as well as the cellular metabolic state have been identified as relevant biomarkers for cancer identification and progression[2,3]. Visualizing their spatial distribution provides deeper insight for diagnosis and classification.

Methods and Materials
We have developed a multimodal label-free optical imaging benchtop platform based on a single Ti:sapphire laser featuring stimulated Raman scattering (SRS), two-photon frequency domain fluorescence lifetime (TP FD-FLIM)[4,5] and second harmonic generation (SHG) imaging. Our system acquires these imaging modalities simultaneously on the same field of view with micrometre precision. Together, they provide complementary molecular, metabolic and structural information to improve diagnosis and treatment of brain cancer[2]. Specifically, SRS visualizes the C-H bond vibration providing information about lipids and proteins content[1,6]; TP FD-FLIM measures the lifetime of enzymes involved in the cell metabolism[8,10] providing metabolic state information; SHG visualizes collagen deposition[2,10].

Results
We are acquiring multimodal images of human brain cancer biopsies and are working towards developing a multiparametric criterion to identify tumours based on quantitative textural feature analysis.

Conclusion
The proposed label-free imaging platform potentially reduces the diagnostic time by simplifying the sample preparation required compared to current histopathological methods, making it suitable for intraoperative assessment.

Funding Source:
This project has received funding from the Austrian Christian Doppler Research Association and the by the Austrian Science Fund (FWF) as part of the ERA-CVD network through project MultiFib (grant number I 4166-B).

References:
1. Hollon, T. C. et al. Near real-time intraoperative brain tumor diagnosis using stimulated Raman histology and deep neural networks. Nat Med 26, 52–58 (2020).
2. Giardina, G. et al. Morpho-Molecular Metabolic Analysis and Classification of Human Pituitary Gland and Adenoma Biopsies Based on Multimodal Optical Imaging. Cancers 13, 3234 (2021).
3. Corn, K. C., Windham, M. A. & Rafat, M. Lipids in the tumor microenvironment: From cancer progression to treatment. Progress in Lipid Research 80, 101055 (2020).
4. Gratton, E. Fluorescence lifetime imaging for the two-photon microscope: time-domain and frequency-domain methods. J. Biomed. Opt 8, 381 (2003).
5. Reichert, D. et al. Fluorescence Lifetime Imaging and Spectroscopic Co-Validation for Protoporphyrin IX-Guided Tumor Visualization in Neurosurgery. Front. Oncol. 11, 741303 (2021).
6. Andreana, M. et al. Epi-detecting label-free multimodal imaging platform using a compact diode-pumped femtosecond solid-state laser. J. Biomed. Opt 22, 1 (2017).
8. Hato, T. et al. Two-Photon Intravital Fluorescence Lifetime Imaging of the Kidney Reveals Cell-Type Specific Metabolic Signatures. JASN 28, 2420–2430 (2017).
10. Cao, R., Wallrabe, H. K. & Periasamy, A. Multiphoton FLIM imaging of NAD(P)H and FAD with one excitation wavelength. J. Biomed. Opt. 25, 1 (2020).
11. Caorsi, V. et al. Non-Linear Optical Microscopy Sheds Light on Cardiovascular Disease. PLOS ONE 8, 10 (2013).

eLB5 Image guided small-animal scanned proton and x-ray reference irradiation - dosimetry, treatment planning and workflow aspects

B. Knäusl[1,3], L. Langgartner[1], M. Clausen[1], A. Resch[1], S. Ruangchan[1], H. Fuchs[1,3], A. Ungerhofer[1], L. Zimmermann[2], V. Fröhlich[2], P. Groeger[2], S. Leitner[2], M. Zeilinger[2,3], P. Kuess[1,3], D. Georg[1,3]

[1] Department of Radiation Oncology, Medical University of Vienna, Vienna, Austria
[2] Competence Centre for Preclinical Imaging and Biomedical Engineering, Faculty of Health, University of Applied Sciences Wiener Neustadt, Austria
[3] MedAustron Ion Therapy Centre, Wiener Neustadt, Austria

Keywords: image-guided radiotherapy, pre-clinical research, workflow establishment

Objective
The aim of this project is to establish a framework for pre-clinical research in particle therapy that includes reference X-ray irradiation as well as multiparametric imaging. A precise irradiation workflow including immobilization, micro-CT imaging, treatment planning and dosimetry, as well as in-room positioning is a prerequisite. This study focuses on dose delivery aspects of X-ray and proton irradiation.

Methods and Materials
An X-ray unit (YXLON, Maxishot) with a positioning table, primary lead (collprim) (Ø 36mm) and a secondary brass (collsec) collimator (Ø 8mm) was investigated. For proton irradiation, two PMMA pre-absorbers for energy degradation, a nozzle-mounted range shifter (RaShi) and a bolus were utilized in combination with brass collimators. Dose calculation was performed in RayStation and dosimetrically validated using a micro-diamond detector (PTW-TM60019) and EBT3 films.

Results
Increasing the distance between the collprim and collsec from 5 to 15cm caused an X-ray dose rate reduction by 59%. Introducing a spacing of 8.4cm between collsec and the mouse reduced the dose rate by 1.8. Film measurements showed a transmission of 4%.
For protons, the RaShi setup was more robust to collimator misplacement and revealed a higher target dose homogeneity, while the prescribed and measured dose agreed within 3%.

Conclusion
For X-ray irradiation, a beam-collimator setup with 2cm thick brass collimators with a distance of 15cm provided optimal dosimetric characteristics. For proton irradiation, a setup with a RaShi and a nozzle mounted passive beam modifier with a collsec as close as possible to the isocenter is preferred, compared to a bolus setup.

eLB6 Phenotyping of laboratory animal models using ex vivo microDECT: exploiting the colour nature of X-rays

Stephan Handschuh [1], Ursula Reichart [1], Stefan Kummer [1], Martin Glösmann [1]

[1] VetCore Facility for Research / Imaging Unit, University of Veterinary Medicine Vienna, Veterinärplatz 1, 1210 Vienna, Austria

Keywords: microCT, µCT, microtomography

Objective
Over the last two decades, X-ray microCT gradually evolved into a routine technique for isotropic 3D imaging of non-transparent biomedical samples at micron resolutions. MicroCT image contrast is based on differences in X-ray attenuation inside a sample. Traditionally, like in medical CT, attenuation differences are displayed monochromatically as greyscale intensity information. It has been insufficiently acknowledged so far that microCT can also be utilised to exploit spectral information, thus providing knowledge about the chemical composition of a sample. While some approaches to generate 'coloured' X-ray images require the use of special energy-resolving detectors for multispectral or hyperspectral image acquisition, dual energy CT (DECT) enables X-ray colour imaging with standard commercial microCT systems.

Methods and Materials
MicroDECT is based on imaging a sample with two different energy spectra, followed by post-processing that allows the separation of two or three known material fractions.

Results
We here demonstrate that spectral microCT data can be generated using commercial equipment with spatial resolutions below 10 µm for biological samples stained with X-ray dense contrast agents containing high-Z elements. We show that microDECT can be used to image element pairs such as calcium/iodine, calcium/tungsten, calcium/ruthenium, barium/tungsten, iodine/tungsten, or iodine/osmium.

Conclusion
We showcase the potential of microDECT imaging for the simultaneous visualization of cartilage and bone in the developing mouse embryo and for vascular phenotyping in adult mice.

eLB7 Effectiveness of telemedical support during chemotherapy. Randomized controlled trial eSMART

Maguire, R. [2], McCann, L. [2], Nycz, H. [1], Krammer, K. [1], Gatterer, C. [1], Blaschke, A. [1], Riedl, J. [1], Eichinger, K. [1], Staber, P. [1], Bartsch, R. [1], Singer, C. [1], Jäger, U. [1], Gaiger, A. [1]

[1] Medical University of Vienna, Austria
[2] University of Strathclyde, Glasgow, Scotland

Objective
Our aim was to investigate whether (1) daily symptom management affects health-related quality of life of cancer patients and whether (2) eHealth technologies can offer an opportunity to be supportive for both patients and health care professionals.

Methods
We assessed the effects of telemedical support comparing intervention and control groups in a randomized, controlled pretest-posttest design and a longitudinal study. The intervention group received a smartphone-like medical device using ASyMS (Advanced Symptom Management System) consisting of daily symptom management and assessment in the active phase (P-1). The follow-up phase (P-2) was without telemedical support. This monocentric study, based on a total of 140 participants, is embedded within a larger international survey. Assessment of change was based on inferential statistical analysis using the per protocol approach. Patient-reported outcome measures (PROMs) were administered to assess health-related aspects and quality of life outcomes. To determine treatment outcome, rmANOVAs were used to obtain standardized effect sizes, with changes in the control group included as a treatment-independent trend.

Results
Within P-1, study data demonstrated significant effects of telemedical support during chemotherapy on quality of life (EQ-5D), well-being (FACT-G) and health status (VAS) (d ‘ = 0.46 - 0.55) as well as for self- efficacy (CASE-cancer) and work ability (WLQ) (d ‘ = 0.21 - 0.25).

Conclusion
The results demonstrate the effectiveness of telemedical support during chemotherapy enhancing quality of life and supporting cancer patients’ adherence through the possibility of 24/7 support, as well as providing an opportunity to reduce healthcare costs and burden on clinical staff.

Funding Source:
Seventh Framework Program (FP7): the European Union’s Research and Innovation for 2007-2013, Projekt N° 602289